ALMA MATER STUDIORUM
UNIVERSITÀ DI BOLOGNA

Dottorato di Ricerca in

Ingegneria Biomedica, Elettrica e dei Sistemi

Ciclo 37

Settore Concorsuale: 09/E2 - INGEGNERIA DELL'ENERGIA ELETTRICA

Settore Scientifico Disciplinare: IIND-08/B - SISTEMI ELETTRICI PER L'ENERGIA

Improving Renewables Integration in Distribution Networks through Real-Time Inertia Estimation and Optimal Management of Energy Community Resources

Presentata da:
Andrea Prevedi

Coordinatore Dottorato
Prof. Michele Monaci

Supervisore
Prof. Fabio Napolitano

Co-Supervisore
Prof. Carlo Alberto Nucci

Esame finale anno 2025

Acknowledgements

I dedicate this thesis to my parents and family, whose ever-present support has been invaluable.

I extend my gratitude to the Power Systems group of the University of Bologna, especially my advisors, Prof. Fabio Napolitano and Prof. Carlo Alberto Nucci, who supported me at every step of my research activities. My appreciation also goes to Prof. Alberto Borghetti, Prof. Fabio Tossani, and Prof. Stefano Lilla.

I would like to acknowledge Dr. Milan Prodanovic and Dr. Juan Diego Rios Penaloza along with the Electrical Systems group at the IMDEA Energy Institute of Móstoles-Madrid, Spain.

Special thanks also go to my former PhD colleagues, Eng. Giorgia Pulazza and Eng. Tadeo Pontecorvo.

Abstract

The thesis explores two critical aspects of renewable energy sources (RES) integration in power systems: inertia estimation in systems with many Converter-Interfaced Sources (CISs) from RES and the management of the controllable resources of Renewable Energy Communities (RECs). Unlike traditional rotating generators, CISs lack physical inertia, requiring advanced Primary Frequency Control (PFC) approaches. A two-stage online inertia estimation method is proposed, combining optimization-based PFC parameter identification with regression-based inertia estimation.

RECs are a recent means introduced in Europe to promote energy production by RES and local self-consumption. A comprehensive review of the European Union's REC regulatory framework highlights national implementation diversities, including proximity constraints, rated power limitations, and energy-sharing methods. An Energy Management System (EMS) is proposed, integrating smart meter data collection, energy price acquisition, and a rolling-horizon optimization procedure to minimize energy procurement costs. The EMS incorporates load and Photovoltaic (PV) production forecast and can be suitably adapted to account for the above-mentioned diversities. Within this context, incentive-based and four-price market models are introduced for cost minimization, compliant with national REC regulations. The impact of new asset installations, such as PV systems and Battery Energy Storage (BES), is assessed using standard load profiles obtained from measurement campaigns.

The research aimed at contributing valuable insights into the advancing landscape of power systems with substantial RES integration. In this respect, the two-stage online inertia estimation process has been proved to provide accurate inertia values by using an OPAL-RT real-time simulator and the IEEE 39-bus network model, under diverse operational scenarios including CISs presence. Finally, the proposed EMS provides practical solutions to challenges in RES management, with the EMS's adaptability to regulatory changes enhancing its potential for broader deployment in ancillary services markets.

Contents

List of Figures

List of Tables

Nomenclature

Acronyms

API	Application Programmable Interface
BES	Battery Energy Storage
BMS	Battery Management System
CEC	Citizens Energy Community
CECo	Citizens Energy Company
CEP	Clean Energy Package
CIS	Converter-Interfaced Sources
CSC	Collective Self-Consumption
CT	Current Transformer
DB	Database
DR	Demand Response
DREM	Dynamic Regression Extension and Mixing
DSO	Distribution System Operator
EMS	Energy Management System
ESCo	Energy Service Company
ESS	Energy Storage System
EU	European Union
GUI	Graphical User Interface
HIL	Hardware in the Loop
ICT	Information and Communication Technology
IEM	Internal Electricity Market
ILT	Inverse Laplace Transform
JARSC	Jointly Acting Renewable Self-Consumers
LF	Load Forecast
LSO	Least-Squares Optimization
LV	Low Voltage
MILP	Mixed-Integer Linear Programming
MS	Member State
MV	Medium Voltage
NILM	Non-Intrusive Load Monitoring
NSP	National Single Price

OF	Objective Function
P2P	Peer-to-Peer
PCC	Point of Common Coupling
PDF	Probability Distribution Function
PFC	Primary Frequency Control
PFR	Primary Frequency Response
POD	Point of Delivery
PLC	Power Line Communication
PLL	Phase-Locked Loop
PV	Photovoltaic
RAA	Renewable Acceleration Area
REC	Renewable Energy Community
RED	Renewable Energy Directive
RES	Renewable Energy Source
RoCoF	Rate of Change of Frequency
RoCoP	Rate of Change of Power
SARIMA	Seasonal Autoregressive Integrated Moving Average
SIL	Software in the Loop
SM	Smart Meter
SOC	State of Charge
TOU	Time of Use
TSO	Transmission System Operator
UD	User Device
VI	Virtual Inertia
VM	Virtual Machine
VPN	Virtual Private Network
VSM	Virtual Synchronous Machine

List of Symbols

Inertia estimation

$\tilde{f}$, f_0	Measure of system frequency and nominal frequency
$\tilde{p}_e$	Total electric power injected by generators
$\hat{H}$, $\hat{H}_c$	Estimated Inertia and estimated inertia control value
$\hat{\tau}$, $\hat{\tau}_z$, $\hat{\tau}_p$	Primary frequency control estimated parameters
ω	Angular frequency
Δp	Power unbalance
p^*	Generators' power setpoint
p_{PFC}	Primary frequency control action
p_e	Electrical power
R	Primary frequency control droop
$G(s)$	Governor and turbine dynamics in Laplace domain
$\mathcal{H}(\cdot)$	Lag operator
$\Gamma(s)$	Transfer function of frequency response to electrical power variation
$\gamma(t)$	Inverse Laplace transform of $\Gamma(s)$
λ_i	Learning rate of gradient algorithm
t_d	Time delay of lag operator
S_i	Rated power of *i*-th generator

Real-time simulator

P	Active power output of the BES at time t
Q	Reactive power output of the BES at time t
η	BES efficiency
T_s	Real-time simulator time step
E_t^{BES}	BES capacity

Load forecast

D	Number of days to be used in the base forecast profile, index d
T	Load forecast time-window, index t
$L_{t,i}^f$	Load forecast at iteration i for the time t
L_t^f	Base load forecast at iteration i for the time t
k_i	Weighting factor calculated at iteration i

$L_{t,d}$	Load measured at time *t* in the *d*-th former day of the same type
$E^{f,tot}$	Daily energy forecast to be consumed in current day
E_i^{cum}	Energy effectively consumed by the beginning of the day to current time
$E_i^{f,cum}$	Cumulated energy forecast expected to be consumed from the beginning of the day to current time

Optimization models

$P_{t,j}^{+}$, $P_{t,j}^{-}$	power injected into and withdrawn from the public grid by prosumer *j* at time *t*, respectively
$P_{t,j}^{P+}$, $P_{t,j}^{P-}$	measured power injected and withdrawn by the production meter of prosumer j at time t, respectively
$L_{t,j}^{S}$	Load forecast of prosumer *j* at time *t*
$P_{t,j}^{PV}$	PV power forecast of prosumer *j* at time *t*
$P_{t,j}^{BES+}$, $P_{t,j}^{BES-}$	BES discharge and charge power of prosumer *j* at time *t*
$E_{t,j}^{BES}$	BES energy of prosumer *j* at time *t*
Δt	Time step of optimization data
$\pi_{t,j}^{-}$, $\pi_{t,j}^{+}$	Buy and sell energy prices with energy supplier
E_t^S	Shared energy
I_E	Economic incentive for the shared energy
R_j	Correction factor for the shared energy contribution of *j*-th prosumer
N	Number of intervals adopted in the piecewise McCormick approximation
$m_{j,n}$	Binary variable for piecewise McCormick envelopes
$Z_{j,n}$, $K_{j,n}$, $W_{t,j,n}$, $X_{t,j,n}$, $G_{j,n}$, $Y_{j,n}$	auxiliary variables for piece-wise McCormick envelopes; representing $P_{t,j}^{P-}$, $P_{t,j}^{P+}$, E_t^S, $P_{t,j}^{+}$, R_j and the complement to 1 of R_j, respectively.
$n°(T)$	Number of time steps
π_t^{REC-}, π_t^{REC+}	Buy and sell energy prices for energy exchanged within the community
C_t^{PCC}	Additional cost incurred in each time interval *t* for the energy imported from or exported to the external grid

Stochastic formulation

J	Number of prosumers
N_E	Number of stochastic events (index ω)
ϕ	One-lag auto-correlation

$\varepsilon_{\omega,t}$	Random component
N_{SC}	Number of final scenarios
N_B	Number of branches in each node
N_D	Number of nodes
$d_{n,k}$	Distance of the *n*-th event from *k*-th centroid
$e_{t,j,n}$	*n*-th normalized event of *j*-th prosumer at time *t*
$c_{t,k}$	*k*-th centroid at time *t*
w_i	Probability associated to *i*-th scenario

Chapter 1. Introduction

1.1 The Role of Electric Energy in the Transition Toward Climate Neutrality

Electricity and heat generation are responsible for a significant rate of CO_2 emissions, the 44% of emissions from fuel combustion in 2021 [1], thus considerable attention has been posed in defining and implementing effective strategies to reduce emissions to mitigate the global mean surface temperature rise [2]. One of the most relevant world-wide agreements related to climate change has been achieved in 2015 during the United Nations Climate Change Conference held in Paris. The agreement, that is also called *Paris Agreement* [3], sets ambitious long-terms goal of maintaining the global temperature increase below 2°C above the pre-industrial level. In particular, the signatory nations agreed to pursue efforts to limit it to 1.5°C above pre-industrial level even financing to developing countries to mitigate climate change. In 2019 the European Union (EU) adopted the *Clean Energy Package* (CEP) a set of directives and regulations aimed to overhaul the energy policy framework to achieve the *Paris Agreement* goals. The CEP sets mid-term objectives for EU Members States (MSs) to achieve the long-term goal of carbon neutrality within 2050. The mid-term objectives to be reached within 2023 include a reduction of 40% of greenhouse gas emissions (respect to 1990), an improvement in energy efficiency (32.5% less respect the 2007 projections) and a significant renewable energy rate (40% of gross final energy consumption) [4]. More recently in 2020, the EU proposed to achieve an enhanced reduction of greenhouse gas emissions, the targeted reduction is set to 55% (again, respect to 1990) from which the climate law package takes the name: *fit for 55* [5]. The *fit for 55* package has been extended to include provisions on wide range of energy topics among which decarbonization in the shipping and transportation sector (including maritime, road and air), emissions related to land-use and forestry area and emissions trading system.

The EU with the CEP recognizes the role of citizens in the energy transition already in the first CEP draft published in 2016 [6]. According to EU provisions the consumers will be provided with better information about their electricity consumption thanks to both an easier

readability of the bill and the equipment of Smart Meters (SMs). Moreover, they will be entitled to participate in ancillary services provision as the Demand-Response (DR) program, directly or through aggregators. Several opportunities open also for producers, or customers which can both consume and produce, the so-called *prosumers*, which can generate, store and sell electricity for their own use or for the participation in the electricity market. The CEP requires that EU MSs employ rules to properly monitor vulnerable and energy poor consumers and take effective measures to protect them and avoid their disconnection.

The concept of energy efficiency can be suitably implemented within the context of *smart cities*. According to [7] a smart city is defined as "*a place where traditional services are made more efficient through the use of digital technologies – Information and Communication Technologies (ICTs) – for the benefit of its inhabitants and businesses. A smart city goes beyond the use of digital technologies for better resource usage and lower emissions. It means smarter urban transport networks, improved water supply and waste disposal systems, and more efficient ways to light and heat buildings. It also means a more interactive and responsive city administration, safer public spaces, and meeting the needs of an aging population*". The improvement of energy efficiency within the context of smart cities is of particular interest since, despite the cities cover "only" the 3% of the planet's land area, they account for more than 65% of energy consumption and they are responsible of more than 70% of global greenhouse gas emissions [8]. In the EU, 75% of citizens live in cities, the number is expected to grow up to 85% within 2050 hence cities should be considered as a key point in the path toward climate neutrality.

The EU has started an ambitious project named *100 climate-neutral cities by 2030 – by and for the citizens* whose objective is to promote and support 100 European cities to become climate-neutral within 2030. These cities will act as showcase for the other cities for the goal of net-zero emissions by 2050. The city's path toward climate-neutrality requires a multi-disciplinary and multi-objective approach including the development of a multi-level, co-creative process, formalized in a *Climate City Contract* tailored to each city's context; foster citizen empowerment through bottom-up initiatives and innovative governance models and help cities to access financing for Mission goals [9]. The *Climate City Contract* aims to express

the ambition and commitment of all parties involved in the objectives of the mission and identify gaps in implementation policies and strategies related to climate neutrality and smart city model implementation. Moreover, it should address the coordination between stakeholders and citizens around common objectives. Five priority factors are considered in the mission context: (*i*) new forms of participatory governance, (*ii*) innovative economic and financing models, (*iii*) integrated urban planning, (*iv*) digital technologies, and (*v*) innovation management. The selected candidate cities were announced on April 28, 2022, of the 100 cities (to be precise 112 as 12 additional cities from countries associated or with the potential of being associated have been considered) nine are Italian, among which the city of Bologna [10].

In the transition toward net-zero emissions electricity is going to play a key role. According to recent estimation the electric energy represents 20% of world's final consumption, this share rate is expected to increase around 50% by 2050 in the net-zero emissions scenario [11]. The consistent rise of electricity consumption is linked to the electrification of appliances and processes formerly supplied with fossil fuels. An example is the growth in electric car sales in the last years: in 2020 one car sold over 25 was electric while in 2023 the ratio increased to one over 5. In the US this ratio is expected to be 50% by 2030 [12]. Also, more and more heating systems are moving from traditional gas boilers to heat-pumps in several EU and US countries, at present they represent 10% of heating system sales. The continuously increasing of electric energy consumption requires the generation of that energy is to be from renewable origin to meet the net-zero emissions goal. Investment in clean energy has risen by 40% since 2020, the reason is not only related to emissions reduction but also to energy security issues, especially for fuel-importing countries. Among renewable resources solar photovoltaic (PV) and wind are the ones expected to sharply increase (see Figure 1.1). The solar capacity, including both rooftop and utility-scale systems, is increased of 220 GW in 2022, which corresponds to the double of the new capacity installed in 2019; the new installed capacity is almost equally shared between rooftop and utility-scale projects [11].

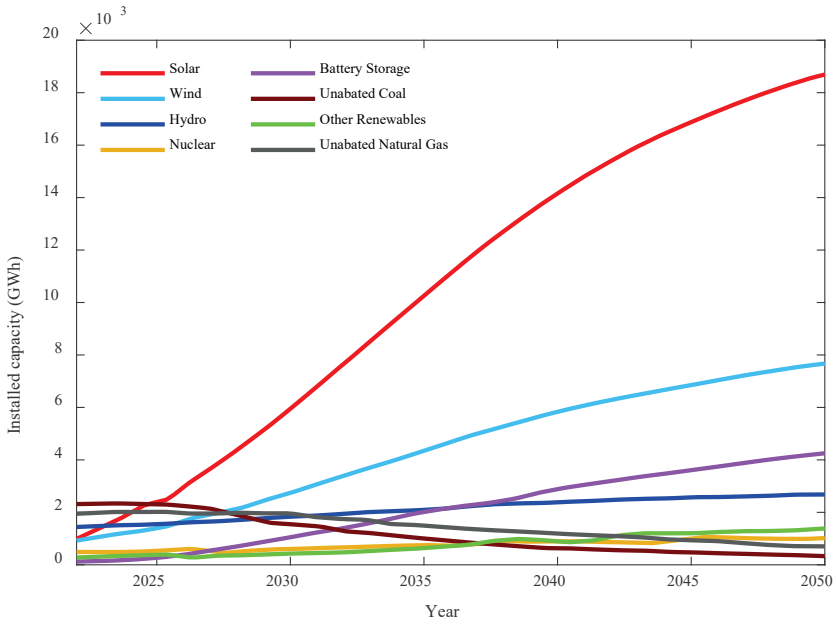

Figure 1.1 Global installed and forecasted power capacity by technology 2022-2050. Adapted from [11]

As renewable energy penetration increases, particularly with Converter Interfaced Sources (CIS) such as PV and type-3 and type-4 wind turbines [13], to ensure the resilience and proper management of power systems becomes more challenging. The issues introduced by the high penetration of renewable energy sources (RES) involve a wide range of power system aspects spanning from real-time management, dispatching process to long-term planning [14]. Among operational issues, it can be mentioned the reduction in the amount of reactive power support available in the power system, which can be mitigated by implementing voltage-control in the power converter control strategies. The displacing of traditional synchronous generators with CIS not equipped with rotating mass leads to a reduction of system inertia and Primary Frequency Response (PFR) capability. This results in a greater rate of change of frequency (RoCoF) and frequency nadir after a power disturbance due to load or generator connection or disconnection. A large frequency variation can lead to severe instabilities in the power system and cause an uncontrolled disconnection of CIS. To mitigate the inertia and PFR capability reduction, CISs can be configured to provide PFR and virtual (or synthetic) inertia. However, these services are not costless since they require the implementation of proper measures, e.g. combining RES installation with battery energy storage (BES), working in deloading conditions [15] or, only for wind turbines, exploiting the rotating inertia of wind turbine blades [16]. Another aspect to be considered is the lower short-circuit capability of

the grid, resulting from possible instabilities in the current-control-loop of the converter and from the ability to ride-through low/high voltage transient avoiding unintentional islanding scenarios [17], [18]. The aforementioned mitigation approaches necessitate the implementation of suitable power converter control strategies. While interactions among adjacent CIS can occur, these are typically case-specific challenges requiring tailored solutions [14]. For the transmission system operator (TSO) the rising penetration of non-dispatchable RES introduces some additional efforts in the dispatching process. Forecasts of day-ahead and hour-ahead wind and PV production are indeed required. A proper reserve having enough flexibility to balance the variation of non-dispatchable RES should be allocated too. Also, extreme weather conditions must be considered such as icing of blades or storms which lead to turbine shutdown for safety or fast cloud movements leading to high ramps in PV generation.

Another important issue is that the planning process for grid upgrades is significantly impacted by the increasing penetration of RES. A few decades ago, the power flow was almost entirely unidirectional, from traditional generators to transmission and distribution networks, and finally to loads. However, with the rise of distributed generation, an increasing number of generators are now connected at all network levels, possibly leading to reverse power-flow in certain hours. The simultaneity or lack thereof between RES generation and load consumption leads to significantly different scenarios to be considered in planning operation.

Although power grid expansion and flexible demand measures enhance the relocation and balancing of electricity flows, Energy Storage Systems (ESSs) can effectively equalize fluctuations and compensate for mismatches between power generation and consumption through coordinated power supply and energy time-shifting [19], thus playing a novel, smarter role, in addition to the classical arbitrage exploited by pumped hydro stations. Among ESSs technologies BESs are promising since they can provide significant advantages as the higher efficiency, the fast response time and their modularity which allows to prioritize capacity or nominal power depending on the requirements and service to provide. According to net zero emission scenario the BES global installed capacity is expected to rise from 86 GWh in 2023 to 1200 GWh in 2050 [20]. BESs are good candidates to provide short-term power system

flexibility and by 2030 are expected to provide about 50% of flexibility services. A study by Fitzgerald et al. [21] claims that the closer BESs are to the final customers, the more services they can provide to the system. This implies that behind-the-meter storage could offer services to the transmission grid, potentially through aggregation. Certain services relevant to prosumers, such as increasing self-consumption, can only be performed by behind-the-meter storage. BESs are capable to provide a wide range of ancillary services to facilitate RES integration among which voltage regulation, to avoid under/over voltages due to high load/generation conditions [22]. Another service is congestion relief which allows to limit the power below line capacity. The frequency regulation market aims to provide additional PFR from RES or even inertial response if a fast frequency response service is implemented. Storage allows also to exploit the energy price variations to perform energy arbitrage [23]. The EU fosters the participation of prosumers in energy markets, including the ancillary services ones. Within the ancillary services context storage plays a fundamental role, with prosumer-owned BES systems expected to contribute significantly [24].

Concerning the participation of prosumers in energy markets, it is worth noting that within the CEP two directives are aimed at empowering the role of citizens in the energy markets and transition toward climate neutrality, namely the Directive 2018/2001 also known as Renewable Energy Directive (RED) II [25] and the Internal Electricity Market (IEM) Directive 2019/944 [26]. The aim of these two directives is to enable the participation of citizens, through aggregation, in the electricity market sector from which they were excluded or not competitive.

More specifically, RED II introduces the concepts of *Jointly Acting Renewable Self-Consumers* (JARSC) and *Renewable Energy Community* (REC). The first one identifies a group of at least two *renewable self-consumers*, i.e. a final customer who generates renewable energy for its own consumption and may store or sell the self-generated electricity. However, these activities must not constitute their primary commercial or professional activity. The REC is a legal entity based on open and voluntary participation aimed at developing renewable energy projects. The primary purpose of REC is to provide environmental and economic or social benefits to REC members or in the area in which the community operates. It should be noted

that RED II introduces provisions for energy of renewable origin, encompassing not only electrical energy but also thermal energy. In contrast, the IEM directive introduces the concept of Citizen Energy Community (CEC) which establishes provisions exclusively for electrical energy, without limiting it to renewable sources. Similarities and differences between the two different types of communities and from JARSC will be discussed next.

The economic rationale for establishing an energy community is closely linked to the remuneration scheme designed for such communities. However, it is crucial to consider the difference between the price of energy supplied by an external provider and the price at which the community sells energy to the main grid. This difference can be substantial, due to the costs applied by the energy provider or transmission, distribution and balancing costs by the TSO and Distribution System Operator (DSO) [27]. Therefore, aggregating prosumers into collective schemes which allow energy sharing could be advantageous. Moreover, the community as an aggregator entity enables the participation of prosumers in ancillary services market which typically requires power or energy capacity not available at single-customer level. The transposition of the EU directives into national regulations has been affected by the previous experience of each EU MSs in collective schemes [28]. Thus, in EU Member States, the maturity of the RED II and IED is not uniform, and remuneration schemes differ across countries.

1.2 Contributions

This dissertation addresses two key aspects of the energy transition towards climate neutrality and the increasing of RES penetration in power networks. The first is real-time inertia estimation. As mentioned in the introduction the increasing penetration of CIS, typically associated with new RES installation, results in the replacement of conventional rotating masses, sources of 'physical' inertia, with CIS having no-inertia or 'virtual' inertia provided if a proper control algorithm is employed. The second main issue is the optimal management of energy communities, considered here as a tool to facilitate the deployment of RES at 'local' level fostering citizen participation in the energy transition.

More specifically, Chapter 2 presents a novel online inertia estimation algorithm consisting of two stages: an optimization-based parameter identification and a regression-based inertia estimation. The optimization stage estimates the parameters that characterize the dynamics of the primary frequency control (PFC). These parameters are then used by the regression stage to track the inertia constant of the system. Inertia estimation based on dynamic regression extension and mixing (DREM) method has already been explored in the literature. However, such a method requires the knowledge of dynamic parameters of the PFC, which are typically unknown. To overcome this problem, the integration of a parameter identification stage, employing a least square optimization (LSO), is here proposed. Furthermore, a criterion for determining when to update the PFC parameters is proposed, ensuring accuracy over time. The proposed method is validated using the IEEE 39-bus benchmark network, demonstrating its effectiveness under various conditions, including normal load variations, large disturbances, and CIS operating in both grid-following and grid-forming modes.

Then, the thesis explores the multi-faced aspect of RECs optimal management. Firstly, in Chapter 3 a review of the European Union's regulatory framework for energy communities is presented, followed by a discussion of how different EU member states have transposed these regulations into national law. The review highlights commonalities and differences in REC

implementation and locally produced renewable energy sharing, which are critical considerations for optimal REC management.

In Chapter 4 an approach to evaluate the impact of new assets installation, i.e. PV system and BESs, within RECs is proposed to facilitate the REC sizing process. The second part of the chapter illustrates the developed EMS to be employed for the optimal operation of RECs. The proposed EMS architecture encompasses a metering system infrastructure, proper data storage, and an optimization process. The system employs forecasts for load, and PV generation as well as energy prices acquisition from day-ahead market, to minimize energy procurement costs. The optimization procedure is performed in a rolling-horizon fashion to incorporate continuously updated consequently more accurate forecasts. The proposed EMS is validated by using a real-time simulator.

Chapter 5 proposes standard consumption profiles for different user types, developed through measurement campaigns and tailored to specific customer segments such as schools, offices, residential, and industrial customers. Standard profiles for different user types are used in the sizing phase of RECs. The chapter discusses how variations in user profiles (e.g., working days versus Saturdays or holidays) are accounted for. The last part of Chapter 5 is devoted to forecasting techniques, employing both historical data and the latest available measurements, to generate load forecasts for the REC's EMS. Simplified forecasting methods, such as those based on average values or autoregressive integrated moving average models, are proposed for inclusion in the EMS.

In Chapter 6 two optimization models to minimize the community energy procurement costs are proposed. The first model leads to cost minimization assuming a regulatory framework in which an economic incentive applies to shared energy. While the second model leads to cost minimization assuming a legal framework in which price agreement of the locally produced renewable energy is established by consumers and producers. The effectiveness of these optimization models is demonstrated by comparing their outcomes to those of two benchmark, non-optimized algorithms. Furthermore, a stochastic formulation is proposed to address uncertainties in load consumption and PV production. A scenario reduction technique

based on K-means clustering is applied to manage the computational effort of solving a large stochastic problem.

Chapter 2. Two-Stage Online Inertia Estimation

Introduction

The last decade has seen a significant increase in the deployment of renewable energy sources and energy storage systems, most of which are connected to the grid through power electronic converters [29]. As the number of these CIS increases, the overall system inertia decreases, affecting the stability of the power system. To mitigate these effects, the use of storage systems controlled to provide Virtual Inertia (VI) has been proposed [30], [31], usually mimicking the behavior of synchronous generators. As a consequence, inertia has become a parameter strongly dependent on the number of CISs connected to the system and the characteristics of their controllers.

In this context, the effective inertia estimation becomes a critical issue. The main aspects are the following:

- Inertia is no longer solely dependent on a physical parameter as in conventional generation but can also depend on the characteristics of the power converters. It depends on the converter control mode (e.g., grid-following, grid-forming), the implemented strategy (e.g., droop control, virtual synchronous machine), and the control parameters [32]. Commercial inverters mostly function as grid-following sources, adjusting their power output based on the grid voltage angle measured via a phase-locked loop. Consequently, these inverters simply track the grid angle and frequency without exerting active control over their own frequency output. Conversely, grid-forming sources actively regulate both frequency and voltage output, thereby enhancing the frequency dynamics and stability of power systems dominated by CISs [33].

- The amount of inertia in the system varies significantly over time due to the variability of the CISs connected to the system. The unpredictability of renewable energy increases the impact of this variability.

- System operators can use information on the effective inertia trend to take preventive measures to increase the stability and resilience of the system. Such measures may include the use of synchronous condensers or increasing frequency regulation reserves.

- In addition, system operators may require generators to provide certain levels of inertia to ensure stability margins, even if they are inverter-based [34]. Inertia estimation algorithms can help to verify compliance with such requirements.

There are several ways to classify inertia estimation methods according to their characteristics [35]–[39] : state (static or dynamic); time horizon of interest (online, offline, forecast); type of data (large disturbance data, ambient data, micro disturbance data); method employed (model-based, measurement-based).

Static methods [40], [41] rely on operating schedules or full system monitoring, often dependent on the availability of synchronous generator data. However, they may not be suitable for power systems with limited observability and a high penetration of distributed resources providing inertial response. Dynamic methods, on the other hand, overcome the disadvantages of static methods by directly analyzing the dynamic behavior of the system. This allows for a more accurate and up-to-date characterization of inertia. For this reason, most of the methods proposed in recent literature are dynamic.

Offline methods [42], [43], also known as post-mortem, typically analyze large disturbance events and are based on historical data, whereas online methods monitor inertia in real time using readily available measurements. A key advantage of offline methods is the ability to perform data processing and inertia estimation without concern for computational time. Online methods [44]–[56] offer the advantage of real-time (or close to real-time) awareness of the system state, allowing system operators to make adaptive adjustments based on current conditions. Another useful resource comes from predictive methods [41], [57]–[59]. By using such methods, operators can take preventive actions to maintain system stability margins based on expected future conditions.

In terms of data type, large disturbance-based methods [42]–[47] rely on events that produce large frequency variations, such as faults, connection/disconnection of large generators or loads, etc. The accuracy of these methods typically depends on precise knowledge of the disturbance characteristics (size, timing). Moreover, the inertia information cannot be updated in real time. In contrast, ambient data-based estimation methods [48]–[54] use measurements obtained under normal operating conditions, taking advantage of the normal fluctuations of load and generation in the system. This feature makes them more flexible to adapt to changes in the network topology. Typically, methods based on ambient measurements also work with large perturbations, but not vice versa. Microperturbation-based methods [55], [56] use a probe signal with known characteristics. This approach requires additional equipment, which increases the complexity of the implementation.

Considering the above characteristics, continuous awareness of the system inertia level is provided by dynamic online methods based on field data. This paper focuses on an inertia estimation method with these characteristics. In terms of the method employed, model-based methods [44], [45], [48], [49], [55] use dynamic models of varying complexity and adopt optimization algorithms, Kalman filters, state-space models, and transfer functions to estimate inertia and other parameters. These methods suffer from parameter uncertainties and the accuracy of the estimation depends on the models used. In contrast, measurement-based methods [46], [50]–[53], [56] do not require complex model representations and often use only the swing equation. However, they are susceptible to measure noise.

The methods proposed in [47], [54] are difficult to categorize as purely measurement based. Both methods are based on the swing equation but do not require the definition of model parameters. The method proposed in [47] is capable of tracking inertia with high accuracy. However, it depends on the accurate estimation of the rate of change of power (RoCoP) and frequency. In particular, the frequency is estimated using the frequency divider formula, which is based on the augmented matrix of the network and the knowledge of the generator impedances. In [54], a regression model is constructed from the swing equation, based on the DREM. The model includes a transfer function that represents the dynamics of the PFC. The method is tested during small disturbances associated with rescheduling events and shows

good performance. However, the main drawback lies in the assumption that the parameters characterizing the PFC dynamics are known. To overcome this limitation, an extension of the method has been preliminarily proposed in [60]. The extension consisted of the introduction of a least-squares optimization (LSO) to obtain the PFC parameters. The optimization was based on an iterative procedure using a dynamic Simulink model, which made the process slow.

The inertia estimation technique proposed in [60] is improved with the following features:

- The PFC dynamics are represented using an analytical formulation. This allows the optimization phase of the algorithm to be significantly accelerated.
- A sensitivity analysis is performed to evaluate the influence of the DREM algorithm on the performance of the estimator. The results made it possible to establish a criterion indicating the need to update the PFC parameters. This improvement allows the entire estimation process to be automated, making it suitable for practical use. It also provides useful insights into the DREM characteristics for this application.

The proposed LSO-DREM procedure is tested on the IEEE 39-bus system model. The tests consider load variations under normal operating conditions, load and generation steps in different inertia conditions, and the impact of CISs controlled in both grid-following and grid-forming modes. The performance of the LSO-DREM procedure is compared with the results obtained using the algorithm proposed in [47]. Real-time simulations are performed to validate the implementation.

2.1 Mathematical Formulation

Figure 2.1 shows the inertia estimation process. The inputs to the algorithm are measurements of system frequency $\tilde{f}$ and total electric power injected by generators $\tilde{p}_e$, and the output is the estimated inertia of the power system, denoted as $\hat{H}$. Throughout the paper, the tilde ($\tilde{u}$) refers to measured quantities, while the hat ($\hat{u}$) refers to estimated quantities.

The optimization stage identifies the parameters of the PFC dynamic and the regression stage tracks the inertia value in real time. A control block checks the PFC parameters are up to date. Whenever it detects a change in the dynamic, a request to update the parameters is sent to the optimizer. The main contributions are those marked in the orange blocks, and the details of the algorithm are shown in Figure 2.2.

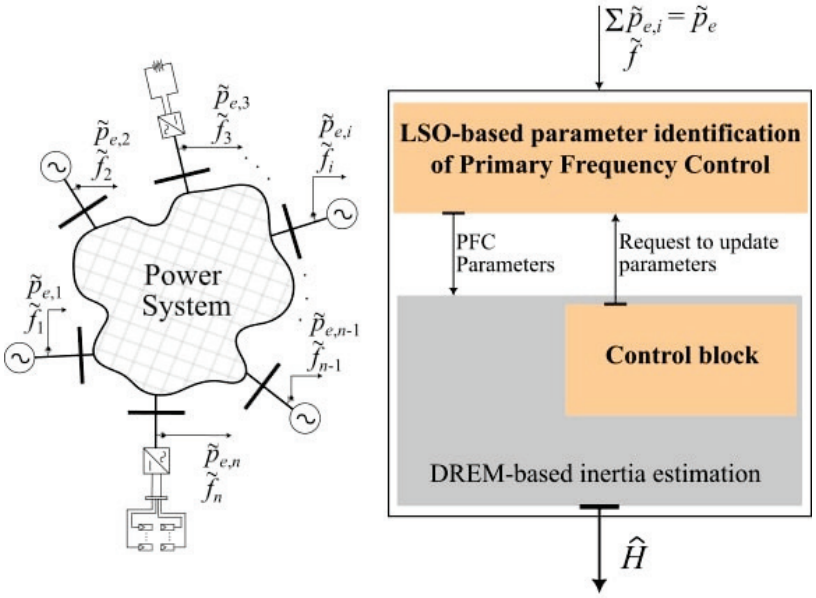

Figure 2.1 Scheme of the inertia estimation for a generic power system.

The DREM method uses a regression and gradient algorithm to estimate inertia. However, as mentioned above, the parameters of the PFC are needed to construct the regression model. To solve this problem, the optimization stage estimates these parameters ($\hat{\tau}$, $\hat{\tau}_z$, $\hat{\tau}_p$). The dynamic behavior of the PFC is represented by an analytical form, in which the frequency variation is expressed as a function of the electrical power variation and the PFC parameters.

Optimization-based PFC identification follows the following steps:

i. frequency variation $\Delta\tilde{f}$ and electrical power variation $\Delta\tilde{p}_e$ are measured over time window t_w when a disturbance occurs;

ii. frequency variation Δf is evaluated by using the analytical expression;

iii. the difference between $\Delta\tilde{f}$ and Δf is minimized and the PFC parameters are obtained.

The DREM stage constantly tracks the inertia, while the optimization stage is started only when it is necessary to update the PFC parameters, which are determined by the following conditions:

- Δ*H* condition: a control value ($\hat{H}_c$) is estimated by a parallel gradient algorithm with different regression parameters. Estimated inertia $\hat{H}$ and control value $\hat{H}_c$ diverge only if the PFC parameters do not correspond to the real dynamics of the system (details are given in section 2.2.2). If the difference between these two values exceeds a threshold (ε_H), the optimization stage must be performed to estimate new PFC parameters. To prevent this condition from being activated during the transient state of the estimator, the threshold must be exceeded for a specified time interval (t_H).

- Δ*p* condition: to ensure the accuracy of the PFC parameters, the optimization is performed when a significant disturbance occurs. The LSO is therefore executed when Δ*p* is greater than the tolerance ε_P.

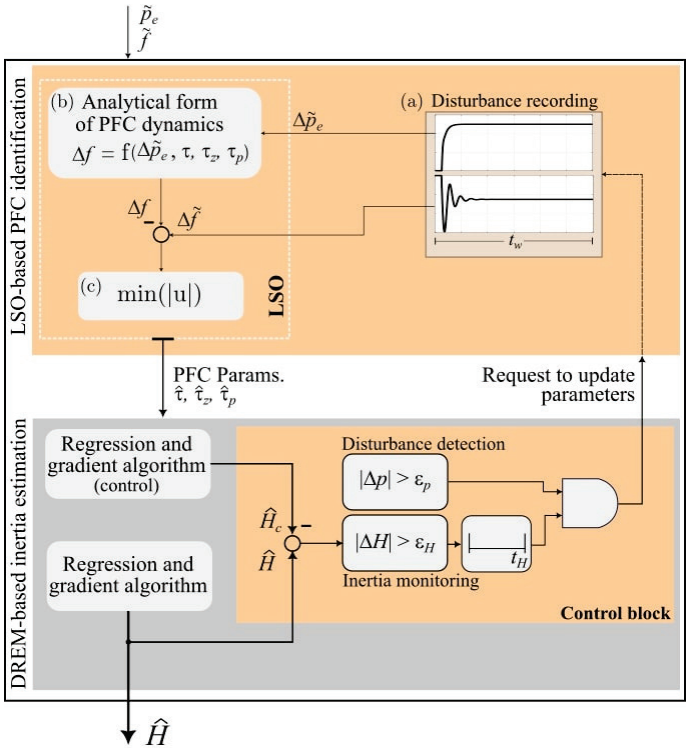

Figure 2.2 Block diagram of the proposed LSO-DREM inertia estimation algorithm.

Section 2.1.1 briefly recalls the swing equation and introduces the general representation of the primary frequency control. Section 2.1.2 derives the analytical expression of the PFC dynamics and illustrates the optimization procedure. Section 2.1.3 constructs the regression model from the swing equation based on the DREM procedure.

2.1.1. Swing equation

The swing equation of a generator expressed in per unit (pu) is given by [61]:

$$2H\dot{\omega} = \frac{\Delta p}{\omega} \qquad (2.1)$$

where the damping can be neglected [36], [37]; ω is the angular frequency and $\dot{\omega}$ its time derivative; and Δp is the power unbalance. The power unbalance can be expressed as:

$$\Delta p = p^* + p_{PFC} - p_e \qquad (2.2)$$

where p^* is the power setpoint; p_{PFC} is the mechanical power resulting from primary frequency control action; and p_e is the electric power. Equation (2.2) represents the actual unbalance between the load and the mechanical power, which accounts for the deviation from the set point due to the action of the governor. The whole power system's behavior can be represented by the aggregated swing equation ($\omega=f$ in pu):

$$\dot{f} = \frac{1}{2H}\frac{p^* + p_{PFC} - p_e}{f} \qquad (2.3)$$

While p_e and f can be measured, direct measurement of p^* and p_{PFC} is not possible. If the aggregated droop constant is known, the steady-state value of p_{PFC} can be derived. However, in the case of synchronous generators, the dynamic behavior of p_{PFC} depends on that of the turbine-governor system, which is often unknown to the system operator. Similarly, for CISs, the dynamics of p_{PFC} depend on the characteristics of the source and the control system, which are also unknown.

2.1.2. Identification of PFC dynamic parameters

This section outlines the process implemented to determine the dynamics of the PFC. This is one of the main contributions of the thesis. In general, p_{PFC} can be represented in the Laplace domain as:

$$p_{PFC}(s) = -\frac{1}{R}G(s)\left(f - f_0\right) \qquad (2.4)$$

where R is the droop constant and f_0 is the nominal frequency. $G(s)$ is the transfer function of the turbine and of PFC of the equivalent aggregated system represents the dynamics of the PFC. $G(s)$ tends to 1 when s goes to zero, therefore the steady-state contribution of the PFC is equal to $-\Delta f/R$.

For small disturbances the frequency is close enough to its nominal value. Hence, (2.3) can be expressed as

$$s\Delta f(s) = \frac{1}{2H}\left(\Delta p_{PFC} - \Delta p_e\right) \qquad (2.5)$$

The dynamic model used for the PFC dynamic identification can be derived from (2.4) and (2.5) as

$$\Delta f(s) = \Delta p_e(s) \cdot \frac{-1}{2Hs + \frac{1}{R}G(s)} \qquad (2.6)$$

To represent $G(s)$, a low-order model with one pole and one zero is introduced in [62]. This model allows to focus on the power system frequency dynamics [63]. In this paper, an additional pole is used to represent the aggregated PFC dynamics of the entire system. A second-order representation gives more flexibility with respect to the single-pole representation of [62], and allows to represent the dynamics of different units and their governors [61]. Thus, $G(s)$ is expressed as

$$G(s) = \frac{1}{1+\tau s} \cdot \frac{1+\tau_z s}{1+\tau_p s} \qquad (2.7)$$

where τ, τ_z and τ_p are the corresponding time constants and represent the PFC parameters to be estimated. $G(s)$ represents both governor and turbine dynamics. Then (2.6) can be rewritten as

$$\Delta f(s) = \Gamma(s) \cdot \Delta p_e(s) \qquad (2.8)$$

where the transfer function $\Gamma(s)$ is defined as:

$$\Gamma(s) = -\frac{1}{2Hs + \frac{1}{R} \cdot \frac{1}{1+\tau s} \cdot \frac{1+\tau_z s}{1+\tau_p s}} \qquad (2.9)$$

This transfer function represents the dynamic relationship between frequency and electrical power. However, in order to use the frequency and power measurements, it is necessary to

express the relationship in the time domain. This is achieved by applying the convolution theorem to (8):

$$\Delta f(t) = \gamma(t) \otimes \Delta p_e(t) \qquad (2.10)$$

where $\otimes$ is the convolution operator and $\gamma(t)$ is the inverse Laplace transform of $\Gamma(s)$. It characterizes the time domain representation of the PFC dynamics. The derivation of $\gamma(t)$ is detailed in Appendix A, and its final form is

$$\gamma(t) = -R \cdot \left(k_1 e^{-r_1 t} + k_2 e^{-r_2 t} + k_3 e^{-r_3 t} \right) \qquad (2.11)$$

where k_1, k_2, k_3 and r_1, r_2, r_3 are functions of H, R, τ, τ_z and τ_p.

To estimate τ, τ_z and τ_p, a parameter identification process is performed based on a least-squares optimization technique. The objective function to be minimized is the difference between the measured frequency variation and the analytical formulation resulting from (2.10)–(2.11):

$$J = min \left\| \Delta \tilde{f} - \Delta f \right\|_2 \qquad (2.12)$$

The optimization is performed over a time window t_w that is appropriately sized to include the entire PFC action. For the implementation, the equations must be discretized. If Ts is the sampling period of the measurements, then (2.10)-(2.12) are expressed as

$$\Delta f(k) = \Delta \tilde{p}_e(k) \otimes \gamma(k) \qquad (2.13)$$

$$\gamma(k) = -R \cdot \left(k_1 e^{-r_1 k T_s} + k_2 e^{-r_2 k T_s} + k_3 e^{-r_3 k T_s} \right) \qquad (2.14)$$

$$\mathcal{J} = min \sum_{k=1}^{N} \left(\Delta \tilde{f}(k) - \Delta f(k) \right)^2 \qquad (2.15)$$

where k is the discrete time step and N is the number of samples within the time window t_w. An estimated frequency deviation, denoted in the following as $\hat{\Delta f}_{LSO}$, is obtained from the solution of the optimization problem.

The LSO procedure is illustrated in Figure 2.3. In addition to estimating $\hat{\tau}$, $\hat{\tau}_z$ and $\hat{\tau}_p$, the optimization also estimates the inertia ($\hat{H}_{LSO}$). Since (2.11) is a linear combination of exponential functions, (2.12) is evaluated using a recursive convolution scheme, which drastically reduces the computation time. However, real-time tracking of inertia is not efficient using this method alone, as the optimization requires a significant disturbance to obtain accurate results. The minimization procedure is terminated when the function tolerance is met, i.e. when the values of the objective function, in two subsequent iterations differ by less than the chosen threshold, assumed to be 1e-9.

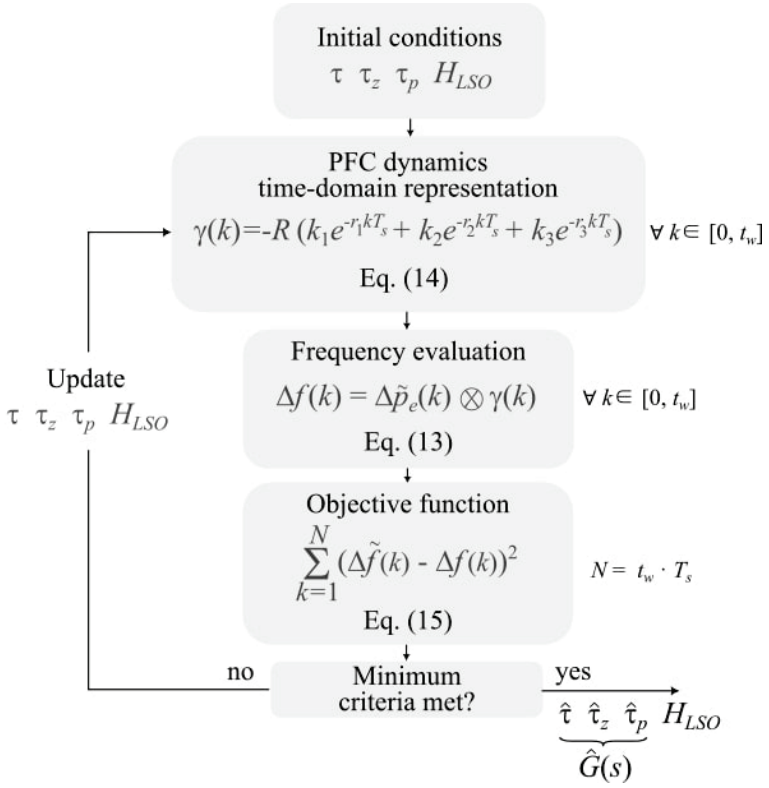

Figure 2.3 Flowchart of the least-squares optimization

2.1.3. Dynamic regression extension and mixing

To achieve real-time inertia tracking, the method used in this chapter is based on the DREM procedure. To keep the chapter self-contained, the mathematical formulation of the DREM is

given in Appendix A. In this section, only those aspects relevant to the LSO-DREM algorithm are presented.

The DREM constructs a linear regression based on (2.3), which can be rewritten as

$$\dot{f} = \frac{1}{H}\left(\frac{1}{2}\frac{p_{PFC} - p_e}{f}\right) + \frac{p^*}{H}\left(\frac{1}{2f}\right) \qquad (2.16)$$

Once p_{PFC} is known, the unknown parameters are H and p^*. To match the number of equations to the number of unknown parameters, the regression is extended by applying a dynamic operator to the original regressor. The extension is obtained by applying the lag operator $\mathcal{H}$:

$$\left[\mathcal{H}(\cdot)\right](t) = (\cdot)(t - t_d) \qquad (2.17)$$

where t_d is the time delay. This operation gives a second regression equation:

$$\mathcal{H}(\dot{f}) = \frac{1}{H}\cdot\mathcal{H}\left(\frac{1}{2}\frac{p_{PFC} - p_e}{f}\right) + \frac{p^*}{H}\cdot\mathcal{H}\left(\frac{1}{2f}\right) \qquad (2.18)$$

For the practical implementation of the regression equations (2.16) and (2.18), a filter is used to avoid the derivative operator applied to the frequency. Further details are given in Appendix A. Combining the two regression equations (2.16) and (2.18) gives a regression of general form:

$$\mathbf{A} = \mathbf{B}\,\mathbf{x} \qquad (2.19)$$

where **A** is a 2x1 vector and **B** is a 2x2 matrix, both composed of known quantities; **x=[**x_1,x_2**]** is the vector of variables to be estimated, i.e. $x_1 = 1/H$ and $x_2 = p^*/H$ in (2.18).

The mixing procedure then decouples the regressions, allowing the two unknown parameters to be estimated independently. The final form of the regression is:

$$\mathbf{Z} = \partial \cdot \mathbf{x} \qquad (2.20)$$

where **Z** is a 2x1 vector and ∂ is a scalar, both of which are known quantities.

Parameters $\hat{x}_1$ and $\hat{x}_2$ can be estimated from (2.20) using the gradient algorithm [64]. The discretized law describing the update of $\hat{x}_1$ and $\hat{x}_2$ is

$$\Delta\hat{x}_i(k+1) = \lambda_i \partial \left[Z_i - \partial \hat{x}_i(k) \right] T_s \quad i = 1,2 \quad (2.21)$$

where λ_i is the learning rate of the gradient algorithm for each process. For simplicity, the same value of λ is used for all processes.

The variables of interest are derived from the estimated parameters as

$$\begin{aligned} \hat{H} &= \left(\hat{x}_1\right)^{-1} \\ \hat{p}^* &= \hat{H} \cdot \hat{x}_2 \end{aligned} \qquad (2.22)$$

The DREM procedure is shown in Figure 2.4. The focus is on inertia, so the estimation of p^* is not considered. To reduce the effects of transients during the estimation, the DREM output is saturated (H_{max} and H_{min}) and filtered. The purpose of the saturation is only to avoid unrealistic values and it has no effect on the performance of the algorithm.

The two parameters that determine the behavior of the DREM are time delay t_d, and learning rate λ. In Section 2.2 a sensitivity analysis is performed to assess their impact.

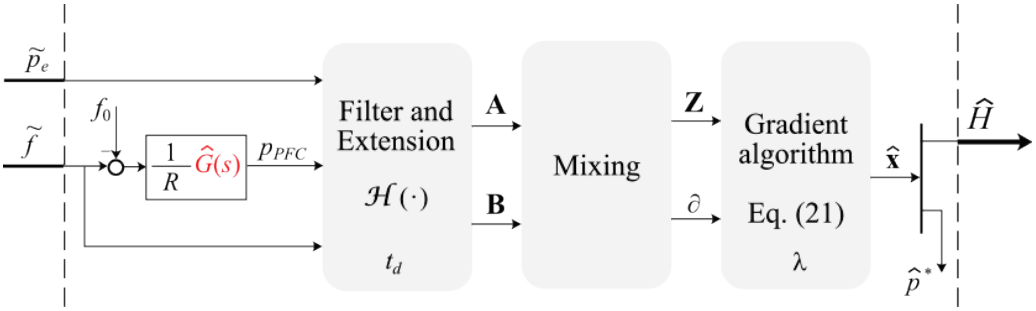

Figure 2.4 Scheme of the dynamic regression extension and mixing procedure

2.2 Sensitivity Analysis

2.2.1. Preliminary results

The performance of the LSO and the DREM procedures is first tested separately on the simplified system of Figure 2.5. The equivalent system is simulated using a 10 GW synchronous generator driven by a steam turbine (as in [65]). The nameplate inertia constant (H_n) is 6 s and the droop is 5%.

To test the optimization performance, a 200 MW (0.02 pu) load step is simulated. The LSO is performed over a 60 s time window to account for the PFC dynamics. The estimated parameters of $\hat{G}(s)$ are given in Table 2.1 and the correspondence between $\Delta\tilde{f}$ and $\Delta\hat{f}_{LSO}$ is shown in Figure 2.6. The real-time tracking of the inertia performed by the DREM is shown in Figure 2.7, and the results are given in Table 2.2 along with the LSO estimated inertia. After the initial transient following the disturbance, the estimation algorithm stabilizes at a constant value.

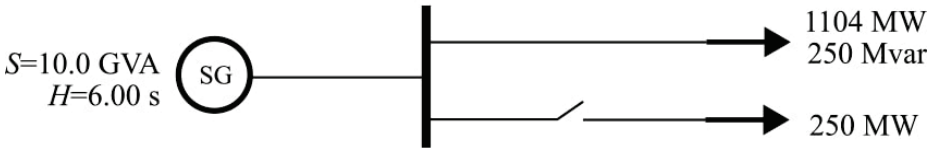

Figure 2.5 Simplified test system for the sensitivity analysis of regression-based estimation.

Table 2.1 LSO and DREM Parameters

LSO	τ	τ_z	τ_p
Value	0.288	1.650	10.149
DREM	λ		t_d
Value	10^9		2 s

Table 2.2 Estimated inertia by LSO and DREM

	$\hat{H}$ (s)	error
LSO	5.940	1.00%
DREM	6.008	0.13%

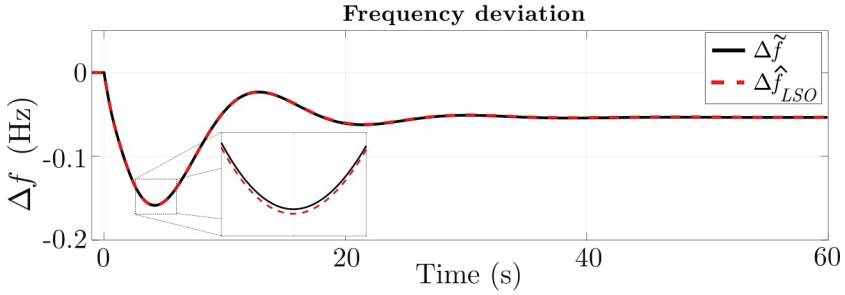

Figure 2.6 Comparison between frequency measured $(\Delta\tilde{f})$ and estimated by the LSO $(\Delta\hat{f}_{LSO})$

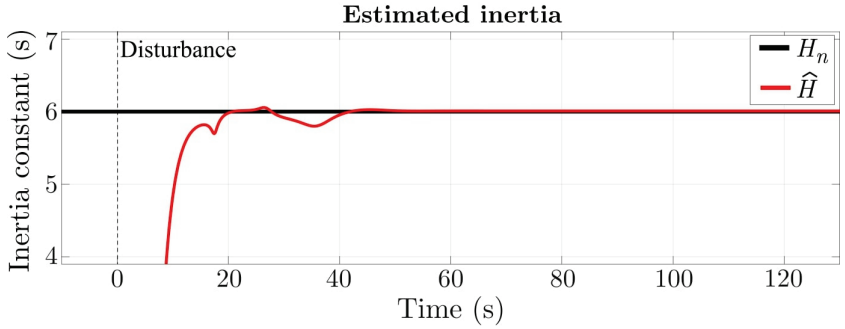

Figure 2.7 Real-time inertia tracking with the DREM procedure

2.2.2. Sensitivity analysis

A sensitivity analysis of the DREM procedure is carried out to propose a criterion to determine when the PFC parameters must be updated (e.g., due to the connection of other sources that modify the PFC dynamic characteristics of the system). This allows the integration between the two algorithms, which is the second main contribution of the paper.

Firstly, it is of interest to evaluate the performance of the DREM when either the inertia or the PFC dynamics change. Two scenarios are defined:

- Scenario A – Variation of the inertia constant: the inertia of the equivalent system is changed to 5 s. The PFC dynamics are the same as in the base case.
- Scenario B – Variation of the PFC dynamics: the PFC dynamics are changed by varying the time constants of the governor. The inertia is the same as in the base case (i.e., 6 s).

The performance of the DREM is assessed for both cases using the parameters from Table 2.1. A 200 MW load step at t=0 s is introduced and the estimated inertia for both scenarios is shown in Figure 2.8. For scenario A, the estimated inertia is 4.928 s (1.44% error), and for scenario B it is 6.537 s (7.72% error). These results show that the DREM is accurate when the PFC dynamic parameters are updated. However, its accuracy decreases when these dynamics change without the parameters being updated.

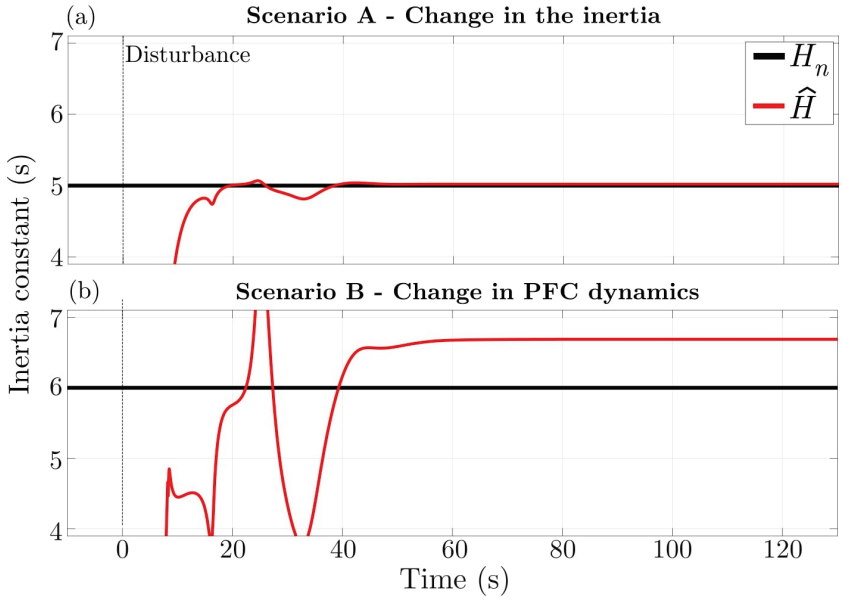

Figure 2.8 Estimated inertia for scenarios (a) A and (b) B

To further explore the characteristics of DREM, the influence of time delay t_d and learning rate λ are examined, considering the base case and the two scenarios previously described. To

avoid the numerical divergence of $\hat{H}$, H_{min} and H_{max} are set to 0 and 10 s. These limits do not affect the performance of the algorithm.

A. Influence of the time delay

The time delay should be within the inertial response window of the system. Figure 2.9 illustrates the effect of t_d on the estimated inertia. The shaded area indicates a ±5% error margin. The blue dots indicate those estimates where parametric error $\hat{e}$ is large, making the estimate unreliable.

In both the base case and Scenario A (PFC dynamics have not changed since the optimization), the estimated inertia is not significantly affected by the choice of t_d. However, in Scenario B the effect is significant. For values of t_d greater than 2 s, the error is significant. This dependence of the estimated inertia for different t_d values when the PFC dynamics change is used as a criterion to determine the need to update the PFC parameters. For this purpose, a parallel gradient algorithm with different t_d is used to estimate the control inertia $\hat{H}_c$ (see Figure 2.2).

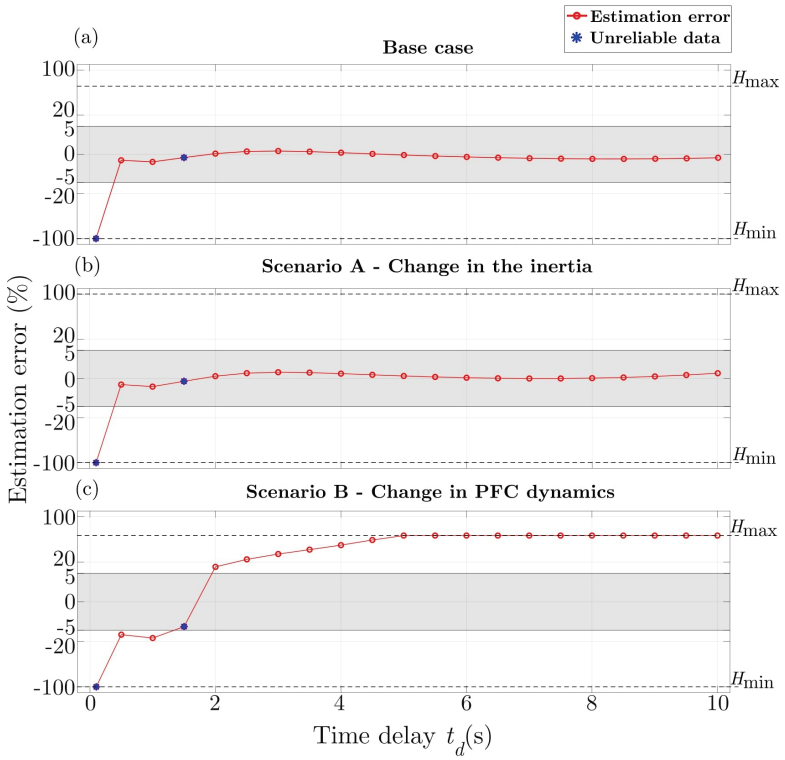

Figure 2.9 Effect of time delay on estimated inertia. Estimation errors for different values of t_d for (a) the base case; (b) Scenario A; (c) Scenario B.

B. Influence of the learning rate

The learning rate determines the convergence speed of the gradient algorithm. Large values make the estimation procedure faster, but too large values can cause overshooting and increase the sensitivity to noise. Figure 2.10 illustrates the effect of λ on the estimated inertia.

For the base case and Scenario A the estimation error is minimal for a wide range of λ values ($5 \cdot 10^4$–10^{15}). However, for scenario B, the influence of λ becomes significant. The errors are large for several values of λ, making the estimation unreliable in these conditions.

The algorithm is stable for a wide range of λ values as long as the PFC parameters are updated. This dependence could also be used as a criterion for updating the PFC parameters.

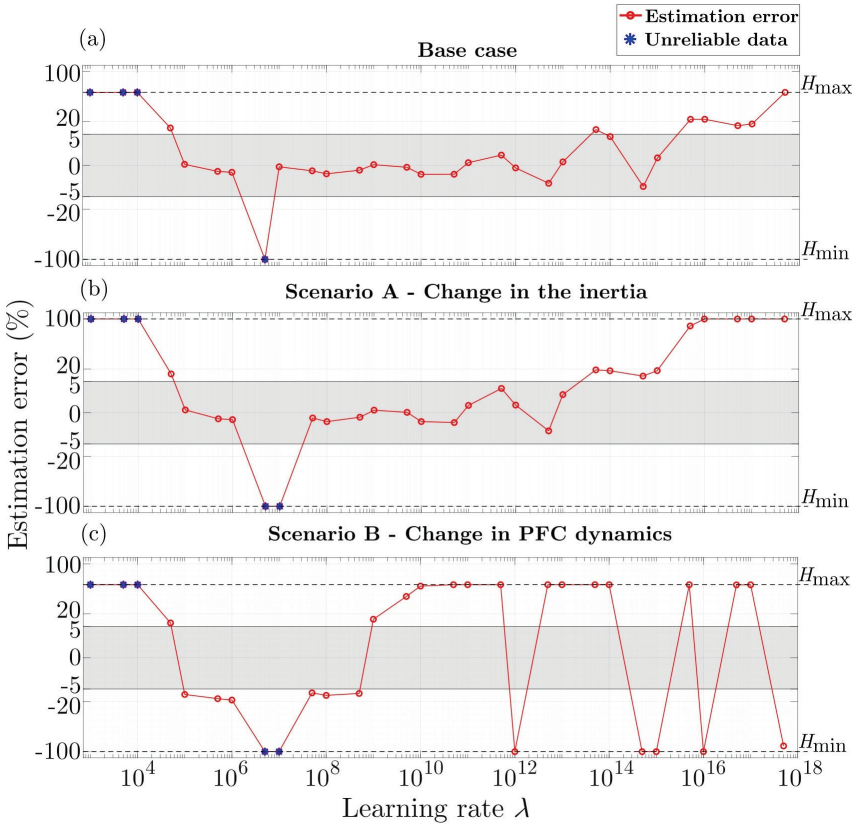

Figure 2.10 Effect of the learning rate on the estimated inertia. Estimation errors for different values of λ for (a) the base case; (b) Scenario A; (c) Scenario B.

2.3 Test Cases

To evaluate the algorithm performance, the 10-generator, 39-bus IEEE system shown in Figure 2.11 is implemented in Matlab/Simulink [65]. The injected active power is measured for each generator and the frequency is obtained from a phase-locked loop (PLL) module connected to the bus of generator 1.

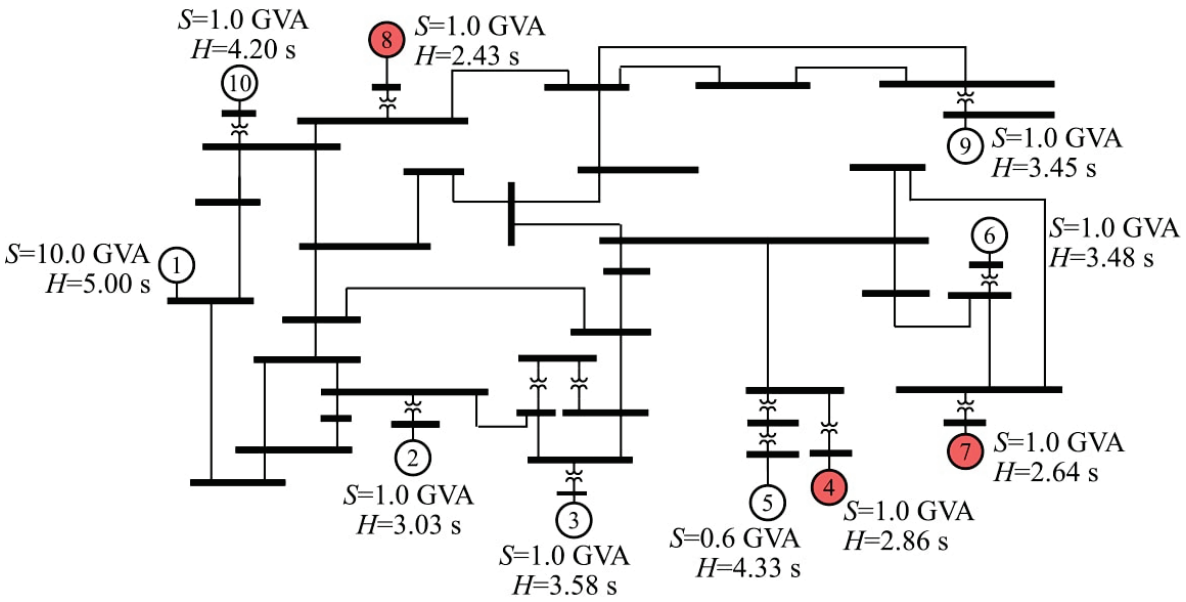

Figure 2.11 IEEE 39-bus test system.

The system inertia constant H_n is calculated using:

$$\sum_i H_i \cdot S_i / \sum_i S_i \qquad (2.23)$$

for all *i*-th generators effectively connected to the grid. When all synchronous generators are connected to the system, this value is 4.208 s. The PFC and LSO-DREM parameters are given in Table 2.3.

Table 2.3 LSO-DREM parameters

LSO					
Parameter		τ	τ_z	τ_p	t_w
Value	①	0.356	1.564	9.738	60 s
	②	0.363	1.590	9.842	
DREM					
Parameter		λ		t_d	
Value		10^9		1 s	
Control					
Parameter		t_d	ε_H	t_H	ε_P
Value		3 s	0.25 s	60 s	15 MW

①: Base case; ②: After the generation disconnection.

For the performance tests, generators n° 4, 7, and 8 of Figure 2.11 (marked in red) are operated to vary the dynamics of the system. In the first case, these generators are disconnected. In the second case, they are replaced by CISs with power converters controlled in either grid-following or grid-forming mode. In the grid-following mode, the inverter controls the active and reactive power to follow a reference. In the grid-forming mode, the frequency is controlled by implementing a virtual synchronous machine (VSM) technique with damping [66], and the voltage is controlled with a droop control strategy. The LSO-DREM algorithm is also tested under normal operating conditions, considering load and frequency variations.

2.3.1. Disconnection of synchronous generators

This scenario simulates a sequence of disturbances and the disconnection of the three generators 4, 7, and 8. This test illustrates the algorithm operation. The result provided by the algorithm is compared to the estimated inertia based on the method proposed in [47] (designed as $\hat{H}_{dP}$ as it is a by-product of the RoCoP estimation).

The estimated values of the inertia constant and the control variables of interest are shown in Figure 2.12 including the control value $\hat{H}_c$. The inertia is first estimated after a disturbance at t=5 s. At t=100 s, the three generators are disconnected, causing the change in the PFC dynamics. The algorithm detects the change in inertia and the ΔH condition is activated due to the change in the PFC dynamics. At t=300 s, a disturbance is detected and recorded for the

time window t_w. Optimization is then triggered, and the PFC parameters are updated. Finally, after a disturbance at t=550 s, the inertia is estimated with the new PFC parameters. The accuracy of the algorithm is tested at three times, as shown in Figure 2.12:

A) before the generators are disconnected;

B) after the disconnection but before updating the PFC parameters;

C) after updating the PFC parameters.

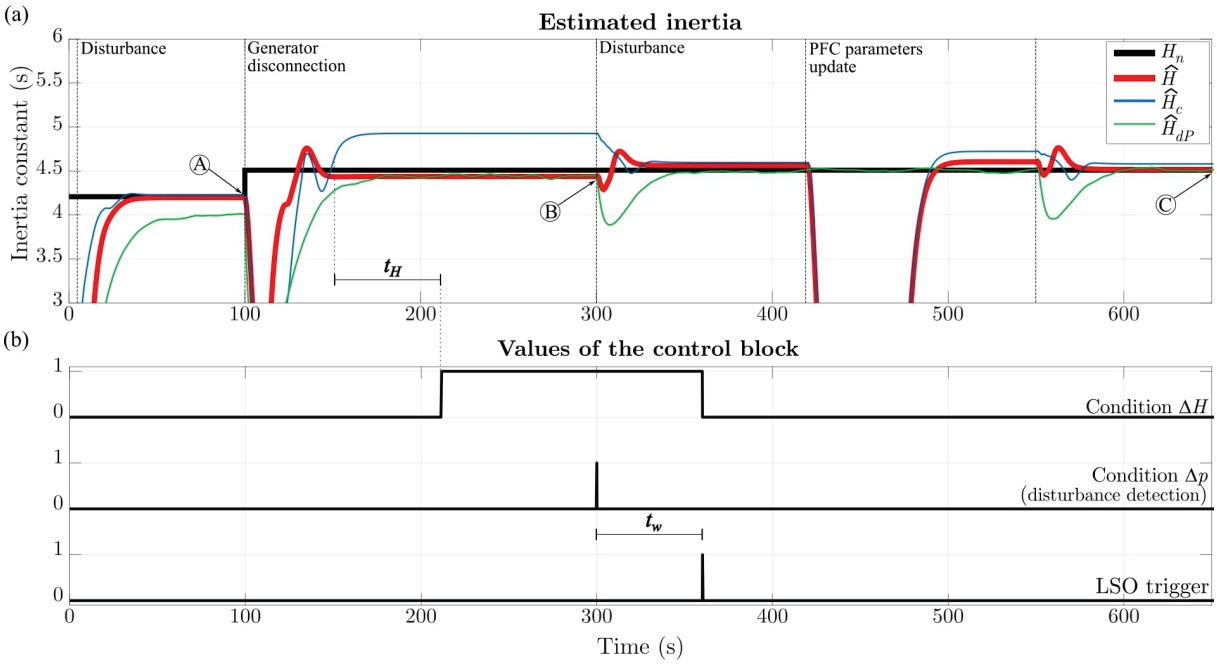

Figure 2.12 Performance of the LSO-DREM algorithm in the case of synchronous generator disconnection: (a) estimated inertia and (b) control block values

When the generators are disconnected the system inertia constant H_n increases to 4.509 s, even though the total moment of inertia decreases, as shown in Table 2.4. This increase occurs because the base power, which acts as the denominator in (2.23), decreases.

Table 2.4 compares the inertia constants estimated by using the different methods and their corresponding relative errors. It shows that the considered methods are sufficiently accurate in estimating the inertia. The RoCoP-based method has the important advantage of working without the need for parameter updates. However, this method relies on the accurate estimation of the rotor frequency of each generator due to its dependence on the second

derivative of the frequency. For the calculation of the inertia constants given in Table 2.4 the rotor frequency values were assumed to be known. However, the RoCoP-based method did not work correctly using the PLL measurement; instead, the LSO-DREM works well with the frequency measured at a single point in the system, which is a major advantage.

Table 2.4 Estimated inertia constant

	H_n	LSO		LSO-DREM		RoCoP	
		$\hat{H}_{LSO}$	error	$\hat{H}$	error	$\hat{H}_{dP}$	error
A	4.208 (S_b=18.6 GVA) J = 1.586 MJ s^2	4.231	0.55 %	4.197	0.26 %	4.011	4.68 %
B	4.509 (S_b=15.6 GVA) J = 1.425 MJ s^2		6.17 %	4.438	1.58 %	4.449	1.32 %
C		4.491	0.40 %	4.517	0.18 %	4.516	0.16 %

2.3.2. Normal operating conditions

The algorithm is tested under normal operating conditions. Figure 2.13(a) shows the system frequency caused by the load variation. Figure 2.13(b) shows the comparison between the estimated inertia and H_n. The mean value of the estimated inertia in the last 200 s (to neglect the initial transient) is 4.267 s, giving an error of 1.41%.

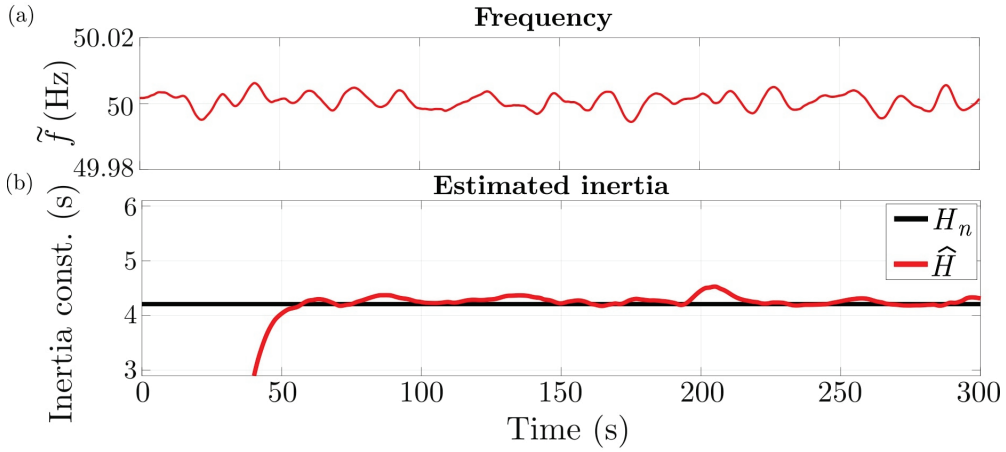

Figure 2.13 (a) Frequency variation and (b) estimated inertia under normal operating conditions

2.3.3. Algorithm performance with unchanged PFC dynamics

Although the DREM does not use the value of $\hat{H}_{LSO}$ directly in the estimation process, it is correlated with the values of $\hat{\tau}$, $\hat{\tau}_z$ and $\hat{\tau}_p$. To evaluate such dependency, the algorithm is

tested in the presence of a highly variable load. The three generators are disconnected at *t*=160 s changing the PFC dynamics. The results are shown in Figure 2.14. In this scenario, the difference between $\hat{H}$ and $\hat{H}_c$ is small and not persistent. Therefore, the condition Δ*H* is not satisfied and the optimizer is not triggered. Nevertheless, the DREM is able to track the change in system inertia.

As long as $\hat{H}$ and $\hat{H}_c$ do not diverge, the accuracy of the inertia estimated by the proposed algorithm is adequate. However, a periodic estimation of the PFC parameters could be performed independently of the activation of the Δ*H* condition.

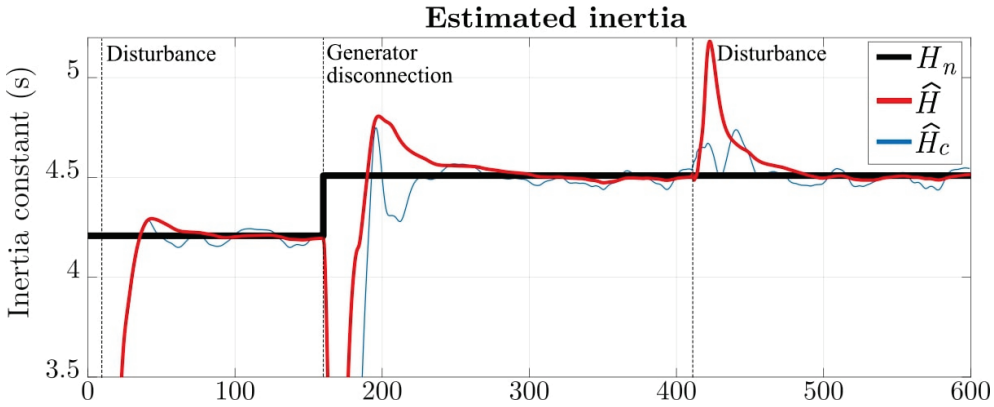

Figure 2.14 Estimated inertia when the PFC dynamics are not updated after generator disconnection

2.3.4. Converter interfaced sources

To evaluate the impact of DERs, the three generators n° 4, 7, and 8 of Figure 2.11 are replaced by CISs controlled in either grid-following or grid-forming mode. A 250 MW load step is introduced at *t*=0 s. The frequency of the system and the estimated inertias are shown in Figure 2.15 and in Table 2.5.

For the grid-following case the inertia is $H_{n,GFL}$=3.782 s, considering the contribution of the CIS zero in (2.23). The estimated value is 3.781 s, resulting in a negligible error.

The grid-forming inverters are designed to provide the same inertia constant as the synchronous generators they replace. However, the primary response of the grid-forming inverters is faster than that of the synchronous generators [47], [67], resulting in a lower

frequency deviation and a lower rate of frequency change compared to the case without CIS. The droop effect of the GFM converters results in a higher effective inertia [68]–[70], as shown in Figure 2.15. In this case, the nominal inertia is $H_{n,GFM}$=4.209 s as for the base case. However, this nominal value does not consider the inertia due to the above-mentioned droop action. An error for this would not be relevant for the present analysis and, therefore, it is not shown in Table 2.5.

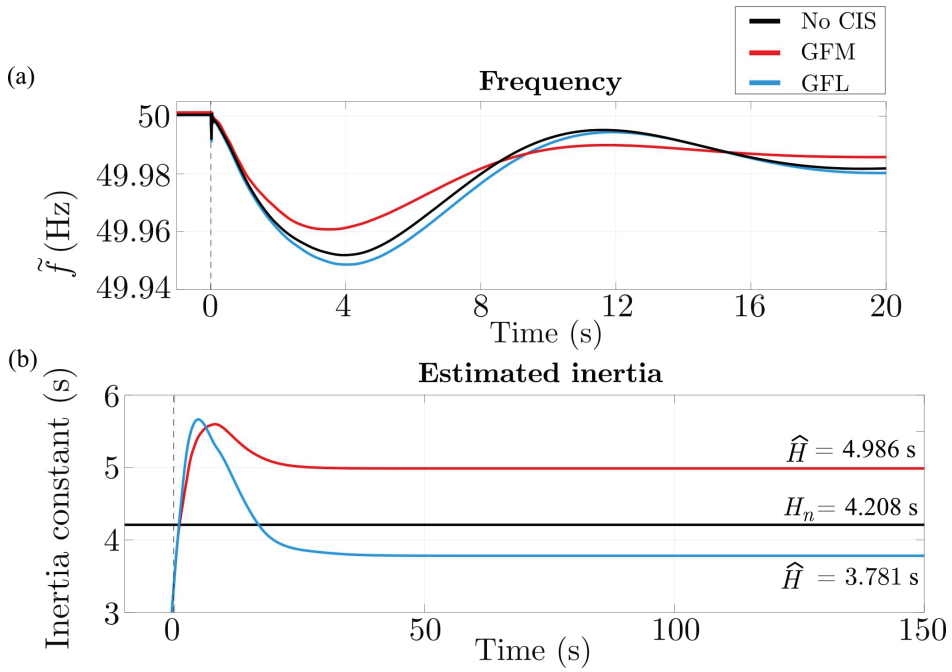

Figure 2.15 Effect of CIS on (a) frequency and (b) system inertia. CIS are controlled in grid-following (GFL) or grid-forming (GFM) mode

Table 2.5 Estimated inertia constant with converter-interfaced sources

	H_n	LSO		LSO-DREM	
		$\hat{H}_{LSO}$	error	$\hat{H}$	error
GFL	3.782	3.765	0.45 %	3.781	0.00 %
GFM	4.209[†]	5.055	--	4.986	--

[†]This value does not consider the inertia effect provided by the droop action of GFM converters. Therefore, the error is not reported in this case.

2.3.5. Real-time implementation

A real-time test was performed using an Opal-RT 4510 simulator. The aim of this simulation is to validate the approach and confirm that the LSO-DREM algorithm can handle real-time computational tasks.

The implementation is shown in Figure 2.16. In the proposed algorithm, the regression must run continuously while the optimization is triggered only when required. For the real-time simulation, the optimization is built into an executable file. The optimization stage is executed asynchronously on the development computer (host). When executed, it writes the estimated PFC parameters into a text file. The regression algorithm then reads this file periodically (e.g., every 60 s). Similarly, the disturbance data required for the optimization is written into a text file, which is read by the optimizer when it runs.

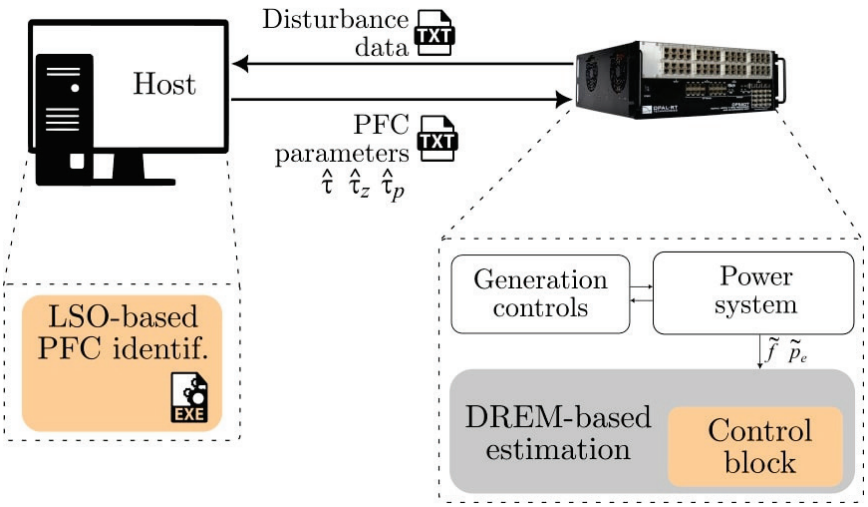

Figure 2.16 Test of the LSO-DREM approach using a real-time simulator

For the real-time simulation the system was divided into three subsystems: the power system (generators, transformers, lines, loads); the generator controls (governors and exciters); and the inertia estimation algorithm. A scenario similar to that described in Section 2.3.1 is simulated and the real-time results are shown in Fig. 17. The behavior of the DREM without the output filter is also shown.

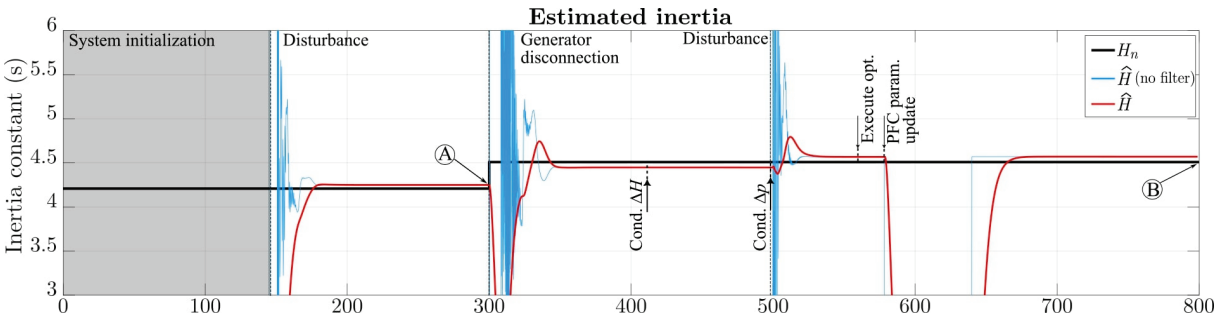

Figure 2.17 Estimated inertia - Real-time results

The estimated inertia values and the computation times required for a simulation of 800 s are given in Table 2.6. The time step is 2 ms. The main computation burden at each step of the simulation is the power system computation (an average time of 1.84 ms). The inertia estimation subsystem takes about 91.5 µs. This shows that the algorithm is well suited for real-time implementation. Moreover, since the LSO-DREM algorithm relies solely on frequency and active power measurements, its resource consumption is not affected by the complexity or size of the system, making it scalable.

Table 2.6 Real-time results

Computational times				
Subsystem	**Resource usage**	**Step-time**		
		Minimum	**Maximum**	**Average**
Power system	91.83 %	1831.55 µs	1846.49 µs	1836.63 µs
Generation controls	0.16 %	2.93 µs	3.68 µs	3.21 µs
DREM	4.57 %	91.23 µs	92.04 µs	91.50 µs
Inertia estimation				
	H_n	$\hat{H}$	**Error**	
A	4.208 s	4.250 s	1.00 %	
B	4.509 s	4.570 s	1.35 %	

Chapter 3. European Regulatory Framework and State of the Art of Energy Communities Implementation

Introduction

This chapter provides a comprehensive overview of the European regulatory framework designed to facilitate the transition towards climate neutrality by promoting the development of renewable energy projects and improving energy efficiency. It focuses on key elements of the CEP, with particular attention to the RED and IEM Directive, aiming to highlight the foundational concepts for the implementation of RECs and CECs.

One of the primary objectives of energy communities is to facilitate energy sharing among community members. A critical aspect explored in this chapter is how energy sharing is assessed as the computation can be different from the physical power flow. The calculation varies depending on the scheme employed. The two commonly used schemes are analyzed in detail, with a focus on their respective advantages and disadvantages, as well as the measures necessary to ensure the rights and obligations of consumers.

The chapter concludes with a review of the national transpositions of the RED across different European countries. The goal is to identify the most prevalent approaches used to foster the development of RECs, the energy sharing schemes adopted, and the benefits that REC members can gain from participating in such communities. The findings from this comparative analysis will serve as the basis for the development of an optimization model, presented further in the thesis, designed to approximate the diverse national transpositions effectively.

3.1 European Regulations on Energy Communities

As mentioned in the introduction the CEP is a set of rules whose aim is to pave the transition from a fossil fuel-based economy toward a carbon-neutral one. The CEP comprises four directives and four regulations. The CEP provisions cover a widespread number of topics and areas, each contributing to achieving the climate neutrality objective. The set of rules encompasses topics such as buildings and transports efficiency, as well as their integration, energy generation, consumption and storage, energy safety and diversification, citizen empowerment, smart systems integration, harmonization of regulations among EU MSs and research coordination. The RED and IEM directive, discussed in section 3.1.1 and 3.1.2, respectively, are of particular interest to energy communities, JARSC and prosumers. It should be highlighted that an EU regulation "*is a binding legislative act. It must be applied in its entirety across the EU*" [71]. In contrast, a directive "*is a legislative act that sets out a goal that EU countries must achieve*" [71]. Thus, each MS has to approve a law to transpose the directive. In the implementing decrees, adaptation to existing regulatory frameworks often takes place, which poses some differences in the practical applications of the directive in the different MSs. In section 3.3 the characteristics of the transposition in some EU MSs are presented. Hereafter a brief description of each directive and regulation belonging to the CEP is provided.

Energy Performance in Buildings Directive 2018/844 [72]: the Directive establishes specific provisions aimed at promoting better and more energy-efficient buildings. The EU buildings are responsible for about 40% of energy consumption and 36% of CO_2 emissions. The directive encourages building automation to create smarter buildings that operate more efficiently and adapt to the needs of consumers. The directive contains also provisions for the integration of electric mobility with the building system. About 35% of EU buildings are more than 50 years old and 75% are also considered energy inefficient. Thus, the directives encourage the implementation by MSs of incentivizing schemes to promote building renovations.

Renewable Energy Directives 2018/2001 [25] *and 2023/2413* [73]: the directives focus on promoting the use of energy from renewable sources. They aim to engage citizens in

environmental and energy issues to boost the diffusion of renewable energy and advance system digitalization. Further aspects of the REDs are discussed next in section 3.1.1.

Energy Efficiency Directive 2023/1791 [74]: firstly adopted in 2012 the directive has been recently revised with the introduction of stronger objectives and requirements on energy efficiency to achieve the goals set by the *fit for 55* package. Changes with respect to the previous version of energy efficiency directive are the reduction of EU's consumption by 11.7% by 2030 (relative to the 2020 reference scenario) and a requirement to achieve an average of 1.49% in new annual energy savings for the period from 2024 to 2030. In addition, MSs are now obligated to prioritize vulnerable customers and social housing within their energy savings measures. The public sector is also targeted with a new 1.9% annual energy consumption reduction goal. Whereas, businesses will need to adopt a different approach, based on energy consumption, either through implementing EMS or conducting energy audits. Lastly, the directive promotes the development of local heating and cooling plans in larger municipalities and progressively increases the efficiency of energy consumption in heat or cold supply, particularly in district heating systems.

Governance of the Energy Union Regulation 2018/1999 [75]: the regulation establishes a robust governance framework for the energy union, requiring each MS to develop an integrated ten-year *National Energy and Climate Plan*, encompassing the 2021-2030 period, while maintaining a longer-term perspective extending to 2050. The EU MSs should achieve the targets for all the five dimensions [76], i.e.

i. security, solidarity and trust: the EU's energy security strategy focuses on reducing dependency on specific energy sources and routes by diversifying supplies, enhancing cooperation among MSs, and improving energy market integration. It emphasizes the need for stronger global partnerships, increased domestic energy production, and greater transparency in energy agreements to ensure a secure and resilient energy system;

ii. fully integrated internal energy market: to ensure a well-functioning internal energy market, a robust regulatory framework that promotes effective cooperation among

TSOs (both electricity and gas) and regulators should be employed. Furthermore, to achieve an effective integration of RES into the market requires flexibility on both the supply and demand sides, across and beyond national borders;

iii. energy efficiency: buildings and transportation are responsible of a large part of energy consumption. Thus, the EU promotes new schemes to improve the buildings' energy efficiency at local level and it also supports initiatives like Smart Cities. While in the transport sector, the focus is on tightening CO_2 standards and improving fuel efficiency;

iv. climate action, decarbonizing the economy: The EU's climate policy employs an emissions trading system to drive low-carbon investments and reduce greenhouse gas emissions. The EU also aims to become the global leader in renewable energy, integrating RES with alternative sustainable fuels. Also, the environmental impacts, public acceptance and infrastructure needs such as land-use and food production are considered;

v. research, innovation and competitiveness: the EU aims to be one of the world leaders in RES thus, it should also lead the next generation of renewable technologies such as smart grid and smart home technology as well as storage solutions. To achieve this objective, it is necessary to fully coordinate the EU research around common goals and deliverables alongside with industries that can ground the research outcome.

Electricity Regulation 2019/943 [77]: outlines principles for the internal EU electricity market, primarily focusing on the wholesale market and network operations. To align with these principles, the regulation incorporates provisions that amend specific articles within the existing electricity network codes and guidelines.

Internal Electricity Market Directive 2019/944 [26]: contains provisions electricity generation, transmission, distribution, supply, and storage, while also addressing consumer empowerment and protection. Additionally, provisions for the procurement of flexibility by distribution system operators are provided. Further details on the IEM directive are provided next in section 3.1.2

Risk Preparedness Regulation 2019/941 [78]: requires the development of plans addressing potential electricity crises by MSs. These plans employ standardized methodologies to identify potential crisis scenarios at both national and regional levels.

Agency for the Cooperation of Energy Regulators Regulation 2019/942 [79]: redefines the role and operations of the European Union Agency for the Cooperation of Energy Regulators enhancing its authority in cross-border cooperation. Agency for the cooperation of energy regulators is tasked to monitor and analyze the performance of regional coordination centers in close collaboration with national regulatory authorities and the European TSO for electricity. Moreover, the agency is responsible for the revisions of grid code drafts, for the oversight of generation adequacy and risk preparedness and it is responsible for taking a decision when competent authorities do not agree in the implementation of new grid codes.

3.1.1. Renewable Energy Directive

The RED establishes a European policy framework conceived to stimulate the integration of RES into the energy mix. By actively engaging citizens in environmental and energy matters, RED seeks to accelerate the adoption of renewable energy technologies and advance the digitalization of energy systems. Additionally, RED draw up guidelines for financial support mechanisms to promote renewable energy generation, encourages the self-consumption of renewable electricity, and outlines strategies for integrating renewable energy into the heating, cooling, and transportation sectors.

The second edition of RED, entered into force in 2018, has the target to reach a share of 32% of consumption by renewable energy by 2030. The target rate has been risen to 40% in the revised version of RED entered into force in November 2023 and it should be transposed within 18 months. Moreover, to facilitate the phase out of fossil fuels, bioenergy, i.e. energy from biomass or biofuels, has been included in the list of recognized renewable energy sources. This is particularly relevant as the International Energy Agency [80] predicts that the use of bioenergy is expected to double by 2050, given its potential to serve as a direct drop-in alternative to fossil fuels. According to the directive, renewable non-fossil energy sources include wind, solar (both thermal and photovoltaic), geothermal energy, osmotic energy,

ambient energy, tide, wave and other ocean energy, hydropower, biomass, landfill gas, sewage treatment facility gas and biogas.

RED III, namely directive 2023/2413 aims to simplify and expedite the permitting procedures for renewable energy projects and if necessary their relevant distribution network to improve the exploitation of RES. Moreover, the Directive requires that MSs conduct a mapping procedure having two primary objectives: first, to identify areas with high renewable energy potential to meet renewable energy share targets, and second, to ensure expedited approval processes for renewable energy projects within those areas. The mapping process is expected to be performed in two stages [81]. The first stages consist in the identification of the areas, encompassing land, surface, sub-surface and sea or inland water, with a significant renewable energy potential. The potential is assessed considering the estimated energy production, the projected energy demand (taking into account demand-response flexibility, expected efficiency gains and energy system integration) and the availability of relevant energy infrastructure, including grids, storage and other flexibility tools. The first mapping stage can be performed regardless of environmental impact constraints, and it is expected to be completed by May 2025. The second stage consist in the identification of the *Renewable Acceleration Areas* (RAAs), in these areas the renewable projects are not expected to have significant environmental impact thus, they can benefit of shorter and potentially simplified permitting procedures. The RAA identification is expected to be completed by February 2026.

Table 3.1 Permit-granting procedure time-limits provided by RED III for RES installations

	Inside RAA		**Outside RAA**	
Rated power	**<150 kW**	**≥150 kW**	**<150 kW**	**≥150 kW**
Other RES	6 months	1 year	1 year	2 years
Wind	1 year	2 years	2 years	3 years
Rated power	**<100 kW**			
PV	1 month			
Rated power	**<50 kW**			
Heat Pump	1 month			

To pave the path toward the goal of 40% share of renewable energy the RED II outlines the concept of JARSC and REC. The primary objectives of these entities are to enhance public acceptance of RESs at the decentralized level, promote energy efficiency, and facilitate market participation for users who may otherwise be excluded. Additionally, these entities aim to ensure the provision of electricity at accessible prices while combating energy poverty by reducing both supply costs and energy consumption through improved efficiency.

According to the Directive a renewable self-consumer is entitled to generate, store and eventually sell the exceeding energy. MSs must ensure the energy fed into the grid is subject to fair network charges and receives a remuneration which reflects the market value. The renewable self-consumer maintains rights and obligations as final user, this aspect is crucial for the choice of the energy sharing schemes that are discussed in section 3.2. The assets belonging to the self-consumer may be owned and managed by a third party such as an Energy Service Company (ESCo) provided that the control is held by the self-consumer (the third party is not considered a self-consumer). Additionally, MSs should guarantee that renewable self-consumers have the possibility to engage energy sharing, provided that they are located within the same building. The principles established for the renewable self-consumers are extended to JARSC although non-discriminatory differences between the two configurations can be implemented by MSs.

A REC is a legal entity entitled to produce, consume, store and sell renewable energy. The renewable energy generated by REC's assets can be shared among its members. Moreover, REC can access energy markets directly or through aggregation. As for the renewable self-consumer, REC should not be subject to unfair network charges or administrative barriers, and the REC members should maintain their rights and obligation as final customers. The Directive requires a proximity between the REC and its assets, or the renewable energy project developed, this proximity limit is linked to the REC purpose of providing environmental, economic or social community benefits for its shareholders or members or for the local areas where it operates. However, the proximity constraints must be defined by each MS in its national transposition.

RED is not constrained to electric energy, but it also includes thermal energy, encompassing both heating and cooling, provided that it has to come from a renewable source. The Directive also opens the possibility of Peer-to-Peer (P2P) energy trading, i.e. the sale of renewable energy between market participants through a contract with pre-determined conditions. The right to engage in P2P trading shall not compromise the existing rights and obligations of the parties involved, whether they are end-users, producers, suppliers, or aggregators.

3.1.2. Internal Electricity Market Directive

The IEM directive entered into force in 2019 establishes provisions for a wide range of aspects related to the rights and obligations of customers, energy providers and grid operators. The Directive allows for the possibility that consumers and producers, either individually or jointly, can exchange electricity using direct lines, as long as these lines are confined within their own premises. Moreover, the Directive aims to increase consumer awareness of their energy consumption and the potential benefits of adopting different tariff schemes. To achieve this, the IEM mandates that providers must offer time-varying energy prices and enhance the role of SMs in supporting these pricing models. Consumers will also be able to switch energy providers more quickly: the maximum time limit is set at three weeks, with the goal of reducing this to one day by 2026.

The regulation introduces the definition of *active customer* and *citizen energy community (CEC):*

- An active customer is an individual final customer or a group of jointly acting final customers who consume and potentially store energy produced within their premises. If permitted, this energy can also be sold or used to participate in ancillary services markets. This activity must not constitute the primary commercial activity. An active customer can operate in the aforementioned activities directly or through aggregation. Each final customer should be capable of behaving as an active customer without being charged for not cost-reflective grid-fees or disproportionate administrative requirements/procedures. The assets can be operated and maintained by a third party, however the third party is not considered an active customer. It should be noted that

the active customers are financially responsible for the imbalance generated in the power system. The role of storage is emphasized: the regulation provides that the grid connection time should be reasonably short, and the energy remaining in the active customer premises or used to provide ancillary services should not be subject to double network charges. Additionally, more than one ancillary service at a time (if technically feasible) can be provided.

- The CEC is a legal entity based on voluntary and open participation, effectively controlled by members or shareholders that can include natural person, local authorities, including municipalities, or small enterprises. The primary purpose is to provide environmental, economic or social community benefits to its members, shareholders or to the local areas where it operates rather than to generate financial profit. Members maintain their rights and obligations as final customers. The CEC can engage in the entire electric energy chain, from generation to consumption, including distribution, storage, aggregation, providing services for energy efficiency and for electric vehicle integration. Additionally, CEC can own, establish, purchase or lease distribution networks and autonomously manage them. An operational agreement can be established with the relevant DSO or TSO to which the network is connected. Appropriate network charges should be determined by differentiating the energy exchanged within the CEC network from that which is fed into or withdrawn from the public grid. Additionally, customers who remain connected to the public grid should not face any discriminatory charges. As active customers, CECs are financially responsible for the imbalances generated in the electric grid and are entitled to access to the electricity market either individually or through aggregation. The CEC deals only with electric energy, including but not limited to the renewable one.

Table 3.2 outlines the key differences between REC and based on various criteria, including membership and control, the types of energy sources that can be utilized, the range of activities they can engage in, and the geographical areas within which they are permitted to operate. The key differences between the two community' type emerge from the directives which defines them: CEC is formally recognized as a market actor whereas REC has the main purpose of promote the RES growth [82].

Table 3.2 Differences between REC and CEC. Adapted from [83]

Criteria	REC	CEC
Energy source	Limited to RES	Limited to electricity, not necessarily from renewable sources
Proximity constraint	Members and shareholders must be located in the proximity of renewable energy projects	No geographical limitation, cross-border activities may be allowed by MSs
Purpose	Encouraging the development of community ownership models to increase the share of RES while providing environmental, economic or social benefits	A new energy market actor capable of participating across the electricity market as well as able to provide environmental, economic or social benefits.
Activity	Production, consumption, storage and selling of renewable energy	Generation, including from renewable sources, distribution, supply, consumption, aggregation, energy storage, energy efficiency services or charging services for electric vehicles or provide other energy services to its members or shareholders
Membership	Natural persons, small-medium enterprises, local authorities, including municipalities	No limitation
Effective control	Members and shareholders located in proximity of the RE projects owned by the community	Members or shareholders that are natural person, local authorities, including municipalities, or small enterprises. Medium and large enterprises can participate but are excluded from effective control.

3.2 Energy Sharing Schemes

At present, the most common configuration of an electricity supply contract involves having one energy provider for the energy withdrawn from the grid and another (which can be the same provider but is not required to be) for the energy fed into the grid. The introduction of energy sharing concept by RED II and IEM directive pave the way for distributing the locally generated energy among community members without the need for an energy supplier [84].

The RED II does not provide a strict definition of shared energy to leave a degree of freedom at MSs to harmonize the concept of shared energy with their existing regulation, if present [84]. A general definition of shared energy, which aligns with most national transpositions, is energy that is locally produced by the community and consumed by its members within a specific timeframe (defined by national regulations), this is often referred as *netting period* [85]. The netting period typically is less than one hour thus it should not be compared with the concept of *net-metering* which usually refers to a longer time period (e.g. a month or a year) and consists in a deduction of the energy fed into the grid from the amount of the energy withdrawn from the grid.

The way on how this energy can be shared from both technical and economical points of view have to be defined by each MS in its national transposition also based on previous energy-sharing projects experience. According to [86] two energy sharing models can be identified based on how the energy shared is transferred: the physical model requires the adoption of a dedicated physical network to share energy, as opposite to the virtual model which employs the public grid to share the energy. Within these two main containers several approaches can be employed to administratively and economically allocate the energy shared. The approaches are influenced by national regulation as well as by the regulation employed by the community. Details on physical and virtual models are given hereafter, whilst how they are employed in different national transpositions is discussed in section 3.3.

3.2.1. Physical model

The physical model employs a private connection among the community members. The instantaneous shared energy within the community remains confined within the private network without affecting the DSO meter. The private grid is interfaced with the public grid acting as a slack bus to compensate for the energy surplus or deficit of the community. At the point of coupling with the public grid, i.e. the Point of Delivery (POD), a fiscal meter is installed, responsible for measuring the energy withdrawn from or fed into the public grid to properly bill the community. To properly allocate the cost for the energy consumed and fed by each customer an internal metering is required.

Figure 3.1 shows an example of the physical model applied to an apartment building in which there is a single prosumer equipped with a PV system and three consumers. The four customers are connected at the apartment building private grid. Each one is equipped with an energy meter which is monitored by the manager of the community and allocates the costs/revenues according to the internal agreement. The private grid is connected to the public grid through a DSO meter which is used to bill the apartment building for the energy bought or sold.

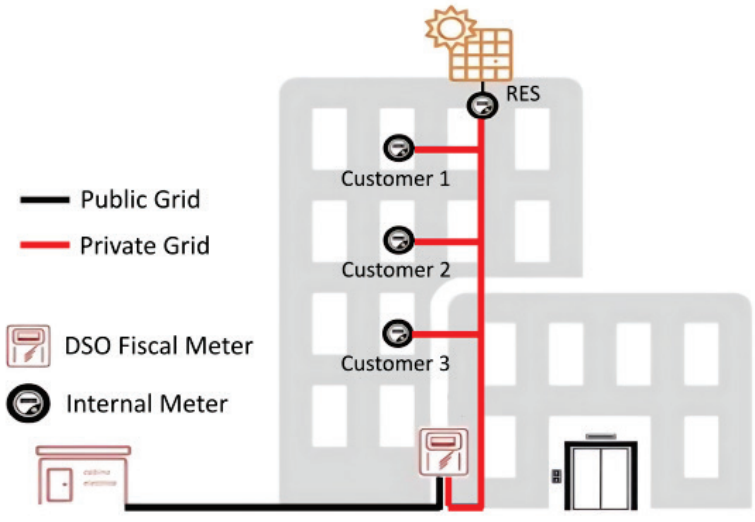

Figure 3.1 Energy share physical model. Adapted from [86]

The physical model can be suitable for community concentrated in a small area, where customers are in close proximity to one another as in an apartment building or area that may

operate islanded. Otherwise, the costs associated with the installation, operation, and maintenance of a private distribution grid may render it economically unfeasible [85].

The physical connection employed by this model introduces some regulatory issues to be properly considered. Firstly, the community has a single POD and therefore a unique energy provider for all the community members [86]. This contradicts the principle established by the RED, which allows individual REC members to freely choose their energy supplier. Additionally, also freedom of joining or leaving the community is hindered due to costs related to the connection switching from the private grid to the public one [87]. Finally, from a network charges and fees point of view having a single POD means that all the fixed components of the bill are paid only once, rather than by each individual customer. This approach is unfair because all community members benefit from the ancillary services provided by the DSO and TSO through the community POD.

3.2.2. Virtual model

The virtual model employs the DSO grid to share energy among community members. In this configuration each customer has his own POD managed by the DSO as shown in Figure 3.2. Thus, the right to freely choose an energy supplier is respected [86]. Energy procurement is provided by the local prosumers as well as by the chosen retailer responsible for covering the lack or absorbing the exceeding energy. Both supplies use the users' unique PCC with the distribution grid and the meter installed there.

The possibility of joining or leaving the community is facilitated since no physical modifications to the grid connection are required; only contractual matters need to be managed. In this configuration the energy shared is not 'confined' within a private grid as other customers outside the community may also be connected to the public grid. Consequently, the concept of consuming locally generated energy within the community becomes more of an administrative notion, disregarding the actual power flow within the grid [88]. Due to the use of a portion of public grid to share energy it is expected that network charges, or a part of them, have to be paid also for the shared energy.

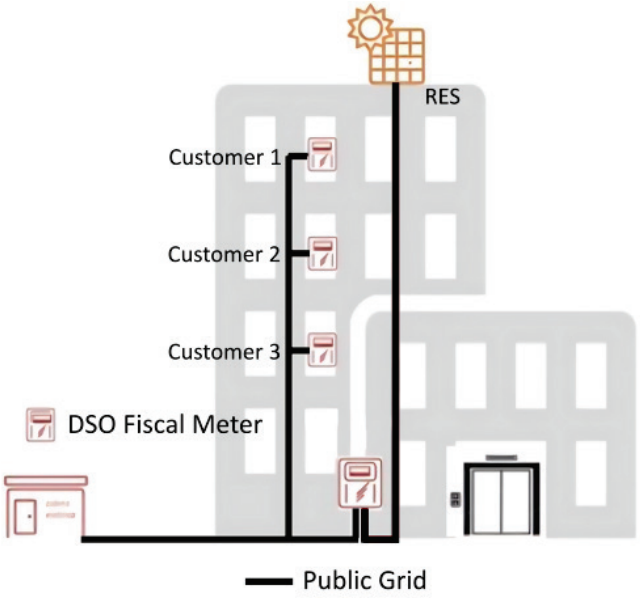

Figure 3.2 Energy share virtual model. Adapted from [86]

Additionally, the netting time period is a crucial factor. DSO meters do not continuously transmit instantaneous production and consumption values; instead, they aggregate energy consumption over a specific timeframe, typically 15 minutes. As a result, the DSO receives quarter-hourly measurements of energy production and consumption. Consequently, the calculation of shared energy must be based on this timeframe (typically 15 minutes or 1 hour) [85]. This introduces a degree of non-contemporaneity between consumption and production resulting in certain indeterminacy in the allocation of the energy exchanges [89]. Hence, virtual schemes necessitate pre-established allocation criteria and sharing keys to ensure a fair and efficient distribution of energy.

The allocation procedure for shared energy quotas depends on the national regulation. It can be managed internally by the community's manager according to pre-established agreements, or it can be handled by the energy provider based on the measurements provided by the DSO and the allocation criteria communicated by the community. These aspects are further discussed in the section hereafter.

3.3 National Transpositions

As mentioned in section 3.1, EU MSs have different levels of integration of the RED II into national regulations depending on the electricity market size and maturity [90]. Almost all the national regulations assume that each final customer maintains the supply contract with the freely chosen energy provider and that the energy sharing is performed by employing the virtual model, thus via the public distribution network. The virtual model is employed in Italy [91], Spain [89], France [92]. In Germany, the physical configuration is permitted as the local production can be shared also via a private distribution network [87]. This setup employs specific measures, discussed in section 3.3.4, to comply with the RED requirements, ensuring that members maintain the freedom to choose their energy supplier and the right to join or leave the community.

In recent years, incentive schemes for RES production have evolved to better align production with consumption. Earlier net billing schemes allowed complete decoupling, whereas current incentive mechanisms emphasize simultaneity between generation and consumption [93], [94]. This simultaneously applied to the virtual scheme should reduce power flows in transformers and lines, thereby decreasing losses and potentially mitigating dispatching issues. The choice of distribution keys for locally produced energy or economic incentives share employed in the virtual model can significantly affect the profitability of the participation in the community. The literature presents various distribution keys, and their impact on profitability has been analyzed under specific scenarios, as discussed in [95]–[97]. The flexibility guaranteed by the choice of distribution key allows for a better alignment with the different socio-economic goals established by each REC.

3.3.1. Italy

Italy transposed the articles 21 and 22 of RED II, i.e. the ones related to JARSC and REC, in 2019 through Decree Law n°162 of 30th December 2019. This Decree, along with the technical regulations published by the ARERA (the Italian Regulatory Authority for Energy, Networks and the Environment the DCO 112/2020/R/EEL [98] of April 2020 and its recast, the resolution 318/2020/R/EEL [99] published in August of the same year, establish the regulatory

framework for RECs and JARSC. It is important to note that in literature, the JARSC configuration is commonly referred to as Collective Self-Consumption (CSC). In 2021, the decree 199/2021 [100] has fully transposed the RED II.

The Italian regulation adopts a virtual scheme for REC and CSC configurations. However, members of the REC or CSC are not allowed to choose an additional energy supplier from within the community; instead, they maintain their existing supply contracts with their current energy providers. This choice might seem to offer no economic benefit for participating in the community. Nevertheless, the government provides an economic incentive to the community, which is proportional to the amount of energy shared among its members. The economic incentive is provided for 20 years. Moreover, a refund of a grid charges quota applies to consider the reduced grid use of locally shared energy.

The shared energy is expressed as the minimum, in each hour, between the overall energy absorbed by the REC's members and the energy of renewable source produced by the REC's prosumers. As the incentive is only recognized for energy produced from RESs a penalization factor is applied in presence of storage systems that can be charged withdrawing energy from the grid instead from the RES. This is the case when the storage systems employ bidirectional converters. This factor is calculated on a monthly basis [101]. Further details on the penalization factor are provided in section 6.3 which discuss the optimization procedure in the scenario of energy shared rewarded through incentives with a particular reference to the Italian scenario.

The members of a CSC scheme must be located within the same building, as provided by the RED II. The proximity constraint chosen for the REC has been initially set as customers belonging to the same secondary substation, i.e. customers belonging to the same LV network. However, this limit has been extended in 2021 through a new regulation, to customers belonging to the same primary substation [100], thus customers connected to different medium voltage (MV) feeders may be members of the same REC.

The RES production systems installed with the regulation of 2019, and participating in a REC or a CSC scheme, are eligible to contribute at the incentivized shared energy only if the rated power is lower than 200 kW, the allowed limit has been increased to 1 MW in 2021 (values referring to the single production facility, not to the overall community). Systems not compliant with the rated power can anyway join the community, nevertheless they do not contribute economic incentive calculation. The same applies to systems installed before the regulation entered into force.

According to the regulation established in 2019 the economic incentive for the shared energy is set to 100 €/MWh for CSC and to 110 €/MWh for REC. The overall incentive is assigned to the REC or to the CSC manager, and how it is allocated to each member has to be defined in the contract. The members are free to choose their own energy seller. The prosumers receive the remuneration for the energy sold and the buyer is almost always the Italian Energy Services Manager - GSE; the possible assigned incentive quota adds to the remuneration. In the new regulation a variable component is introduced to account for energy price fluctuations. The revised economic incentive fixed tariff depends on the nominal power of RES system and, in case of PV installation also on the geographical position.

Table 3.3 reports the economic incentive established by the two subsequent regulations, differentiated for type of energy sharing scheme. The tariffs in force between 2019 and 2021 consisted solely of fixed components. In contrast, the current tariff structure includes both a fixed component, representing the minimum incentive, and a variable component [102]. The sum of these components is capped at a maximum value, which ranges from 100 €/MWh to 120 €/MWh, depending on the rated power of the installation. Additionally, a geographical component is added when applicable. In the price-dependent component Pz is the hourly zonal price.

Table 3.3 Incentive tariffs for CSC and REC in Italy

Power (kW)	2019-2021		From 2021			
	CSC	REC	All			
	Fixed Component (€/MWh)	**Fixed Component** (€/MWh)	**Fixed Component** (€/MWh)	**Price-dependent Component** (€/MWh)	**Max. tariff allowed**	**Geographical component (PV only)** (€/MWh)
P≤200	100	110	80	$max(0; 180 - Pz)$	120	*South* 0
200<P≤600	-	-	70		110	*Centre* 4
600<P≤1000	-	-	60		100	*North* 10

The refund of grid charges differs from REC and CSC due to the diverse grid-use involved in energy sharing. For RECs the monthly refunds C_{AC}, see equation (3.1), is equal to the product between of the shared energy E_s and the monthly flat-rate unit fee $CU_{Af,m}$. The last one is given by the sum of the transmission fee variable part for LV consumer $TRAS_E$ and the higher value of the distribution variable component for LV consumer $BTAU$, these values are defined by the Italian authority ARERA.

$$C_{AC} = CU_{Af,m} \times E_s \qquad (3.1)$$

For CSC, which typically involves a reduced use of public grid with respect to REC, as it requires members belonging the same building, at the refunds of REC is added an additional term which is a function of energy price and voltage level (MV or LV).The additional term is given by the sum, for the voltage level *'i'* and for the hour *'h'*, of the product between the shared energy at voltage level *'i'* $E_{s,h,i}$, the grid avoided losses coefficient $C_{Pr,h}$ corresponding to the voltage level *'i'* and the hourly zonal price Pz_h. The overall refund is calculated according to (3.2).

$$C_{AC} = CU_{Af,m} \times E_s + \sum_{i,h} E_{s,h,i} \times C_{Pr,h} \times Pz_h \qquad (3.2)$$

3.3.2. France

In 2016 France introduced provisions for CSC [103] in advance to the RED II publication. According to French regulation to create a CSC scheme the following must be satisfied:

i. members of the CSC scheme should belong to the same legal entity;

ii. members should be located within a limited area. The geographical limit is set to customers belonging the same distribution network and having a maximum distance between the production and consumption PCCs equal to 2 km [104] (extended to 20-km for low population density area [105]);

iii. for each CSC scheme the maximum allowed aggregated power is 3 MW.

The definition of the French CSC aligns with the requirements and characteristics of REC as outlined in RED II as well its transposition implemented in Italy. In contrast, the Italian definition of CSC (see section 3.3.1) is consistent with the concept of JARSC. A significant difference in the maximum rated power for production systems can be observed between the French CSC and the Italian REC: In France, the aggregated power is capped at 3 MW, whereas in Italy, each production system is limited to 1 MW, with no restriction on the total aggregated power.

As Italy and Spain also, France has adopted a virtual scheme, therefore energy shared within the community uses a portion of public power grid: even so, this energy can benefit of advantageous network tariff [106]. The legal entity is entitled to supply the customers belonging to the CSC scheme with the electric energy fed into the grid by the prosumers, i.e. the difference between energy produced and behind the meter self-consumption; consumers still maintain an energy supply contract with the licensed supplier which is responsible to cover the lack of energy [94]. The legal entity acts as an interface between the community players and the DSO, however it is not responsible for contracts between prosumer and consumers. The price for the energy fed by prosumers and consumed locally is exchanged at the price agreed between the producer and the consumer [92], which is typically lower than the tariff charged by external suppliers.

The produced energy is allocated to each consumer based on either default or personalized key; the first case considers the power injected by the prosumer shared proportionally to the customers' consumption, while in the second case the entity defines ad-hoc rules [97]. This allocation key should be communicated to the DSO, which is responsible for calculating the shared energy quote and the energy provided by the external supplier. The shared energy is computed on a 30-minute basis until January 2025, then on 15-minute one.

The licensed supplier bills the consumer for residual energy and the grid tariff associated with both the residual energy and the customer's quote of energy shared. Other taxes, such as the VAT, are collected by the entity billing the shared energy, typically the prosumer [92].

The French definition of the energy shared in a CSC scheme (energy collectively self-consumed) is similar to the Italian one except for the direct allocation of a production quote: it cannot exceed the sum of the production of each participating facility in the operation, nor the sum of the consumption of the final consumers participating in the operation; moreover the quantity of production allocated to each final consumer, calculated as the product of energy produced and a distribution coefficient, cannot exceed the measured consumption. In the presence of a storage system, it acts as a consumer when withdrawing energy and as a producer otherwise [107].

In 2021, with the Ordinance 2021-236 [108] the French Government transposed the RED II and the IEM directive into national regulation; the transposed definition of REC as well as the respective rights and obligations reflect the ones expressed in the RED II. Despite the enabling framework established with [108] the decree to implement the law has not yet been published [92].

3.3.3. Spain

In Spain, self-consumption of locally produced energy was not permitted until the Royal Decree 900/2015 [109], came into force; prior this decree came into force the energy produced could be only sold to the grid. Hence the Royal Decree 900/2015 made it possible to consume the self-generated electric energy without buying it from the grid, i.e. employing

a net-metering configuration. On the other hand, the Royal Decree 900/2015 introduced administrative procedures, financial barriers [110] and fees on self-consumed energy from PV installations (the so-called “solar tax” [111]). Residential customers were not receiving a remuneration for their energy surplus, i.e. the energy fed into the grid. Moreover, industrial and commercial customers had to pay a fee on the self-consumed energy [112]. Recently Spain introduced new provisions for energy sharing with the Royal Decree 244/2019 [113] and Royal Decree-Law 23/2020 [114]. Concurrently, the solar tax introduced in 2015 with the Royal Decree 900/2015 has been removed.

Installations having capacity greater than 100 kW cannot be classified either as prosumers or participate in CSC schemes. For smaller facilities, simplified procedures have been introduced: no permission is required for rated power below 15 kW, though no remuneration for energy surplus is provided; for systems between 15 kW and 100 kW bill compensation mechanism can be applied [115]. The bill compensation mechanism consists of a monthly net billing approach in which the energy surplus is evaluated at the wholesale market price if the supplier belongs to regulated retailers or at the agreed price in the case of market retailer. The bill compensation cannot be negative: if the energy surplus compensation exceeds the cost of the imported electricity, resulting in a zero balance, the prosumer is not maximizing the profits. The benefits of the net billing simplified approach are multiple: reduced administrative requirements, no grid-access charge for the energy surplus as well as no generation taxes. Prosumers who do not want to apply the net billing scheme can configure themselves as producers and directly sell the energy; however, the legal and administrative requirements are stronger. Additionally, the electricity surplus is subject to the generation tax and grid-access fee [112].

The energy surplus can be shared in a CSC scheme if the customers belong to the same secondary substation and have the same first 14 digits of registry number [116], alternatively to the latter requirement the geographical distance should be lower than 2 km (the previous range of 500 m has been recently extended with the introduction of Royal Decree-Law 18/2022 [117] and Royal Decree-Law 20/2022 [118]) [119]. The energy surplus is allocated to

each member according to distribution coefficients similarly to the French case; however, the energy shared is computed on an hourly basis.

The distribution coefficient can be static, i.e. fixed for all the time periods or dynamic, i.e. a different value can be assigned to the user in each hour [120].

3.3.4. Germany

The relevant regulation for self-consumption, energy sharing schemes and renewable energy is the Renewable Energy Sources Act (*Erneuerbare-Energien-Gesetz*); in the 2017 enactment [121] self-supply and energy community provisions have been introduced. Prosumers can benefit from several remuneration possibilities of energy surplus: direct sell, market premium, feed-in tariff depending on system size or tenant electricity supplement [115].

The possibility of implementing a CSC scheme, also known as *Mieterstrom*, introduced in the EEG 2017 for the same multi-apartment building, has been extended to the neighborhood scale in the EEG 2021 [122]; the power limit has been enlarged from 100 kW of aggregated nominal power to 100 kW per single installation [123]. The energy exchange is restricted to private network thus, in Germany a physical model is employed.

According to *Mieterstrom* the prosumer acts as licensed supplier, thus is responsible also for providing the energy required by consumers not coming from the production installation, i.e. the energy imported from the public grid. To comply with the RED II requirement of free choice of energy supplier, the German regulation has implemented specific provisions to safeguard the tenants: the energy supply contract cannot be incorporated in the rental contract (except for specific cases), it must be renewed each year, and in case of relocation the contract terminates automatically [94]. The energy price for tenants must be less or equal to 90% of the external electricity supply tariff [124].

The supplier is responsible for billing the tenants, therefore a proper metering system should be employed. There are three possible metering schemes for the CSC: double busbar model,

totalizer model with conventional meters, and totalizer with smart meters. Hereafter details and characteristics of each metering system are provided:

i. The double busbar model requires the adoption of two different busbars, one for the CSC scheme and the other one for the connection to the public grid of customers not participating in the CSC scheme. This method is rarely used due to the costs of switching from one busbar to the other when moving in/out the CSC scheme.

ii. In the totalizer models, all customers are connected to the same busbar, regardless of their participation in the CSC scheme. A bidirectional meter is installed at the grid PCC and a production meter measures the energy generated from each PV system. Additionally, all consumers are equipped with sub-meters. To properly separate the consumption of CSC members from the customers' consumption who have an external supplier, the consumption of the latter is virtually moved outside the CSC scheme: the consumption of non-CSC members is subtracted from the measurement performed by the PCC's meter. If the difference is positive, the residual consumption is allocated to the CSC members; otherwise, the resulting value represents energy virtually fed into the grid.

iii. In the totalizer models the use of conventional meter does not accurately reflect the real power flows of the CSC scheme, this can be mitigated by adopting smart-meters and performing the calculations every 15-minute [87] resulting in the totalizer model with smart meters.

At present the energy shared can benefit of a subsidy, the so called Tenant Electricity Surcharge, variable according to the system size: 3.79 c€/kWh for system lower than 10 kW, 3.52 c€/kWh for system between 10 kW and 40 kW and 2.37 c€/kWh for installation up to 750kW; the subsidy is guaranteed for a maximum capacity of new PV installation of 500 MW [122].

The Citizens Energy Company (CECo), introduced in the Renewable Energy Sources Act 2017, are mainly focused on the renewable energy from PV and wind sources. The creation of a CECo is subject to the following constraints: at least 10 individual members eligible to vote, natural

person hold a minimum of 51% of the voting rights and no member holds more than 10% of voting rights. CECos can submit bids for up to six onshore wind installations having a global capacity of 18 MW; moreover, CECos can benefit from financial security deposit [123]. The CECo can participate directly in the energy market (registration as energy supplier is required) or through aggregators/energy provider.

Chapter 4. Optimal Management of Energy Communities

Introduction

The optimal configuration and management of a REC is a multifaceted process that can be assessed during both the sizing and operational phases. In the sizing phase, the community's candidate members are carefully analyzed based on their energy consumption pattern and renewable energy production, if present. Consumption patterns can be accurately estimated when a metering infrastructure is in place and has gathered sufficient data over time. In the absence of such infrastructure, an estimation can be made by combining consumption data from utility bills, or in some cases from the DSO's website, with typical load profiles for that customer category. The objective is to determine the optimal sizes of both PV installations and BESs [125]. By analyzing how the self-consumption and energy-sharing rates evolve with different configurations, the sizing process seeks to maximize local energy use and optimize energy-sharing within the community. This ensures that PVs and BESs are tailored to the community's collective and individual needs, enhancing both economic and energy efficiency.

Once the system is properly sized, the operational phase comes into play where an EMS controls the BES units to achieve predefined objectives, such as minimizing energy procurement cost. The role of the EMS is different by the function provided by the Battery Management System (BMS). The BMS of single prosumers typically relies on local measurements only and can solely pursue the self-consumption of the single user, this might not allow the minimization of the overall energy procurement cost of the REC, if not suitably coordinated. Moreover, the legal framework could introduce some limitations on the possibility of using production and storage units of different final users. Therefore, the management of the distributed BESs in RECs must account for the billing schemes and regulatory framework of RECs can be very different even for EU member states, as illustrated

in section 3.3, even if all are introduced in force of the same UE Directive [28], [126], [127]. The EMS has the role of providing a high-level control of BES to achieve the objective ensuring compliance with the regulation. It utilizes not only local measurements from prosumers but also community-wide data and forecasts.

The EMS continuously monitors real-time or quasi-real-time data, such as load consumption, PV generation, SOC value and market prices, to control output power of the BESs. The optimal power output is obtained by periodically executing an optimization procedure. By optimizing the use of BES during operation, the REC can further enhance its community self-consumption, by increasing energy sharing among members, and even engage in energy trading or demand response services, thereby providing economic benefits and grid support.

Data availability is fundamental for the effective implementation of RECs, both in the design and operational phases [125]. Therefore, part of this work is devoted to data collection and storage to develop standard profiles to be used in absence of specific-customer data, including the available instruments to perform measurements.

4.1 Renewable Energy Community Projects

This section is devoted to the description of the Climate-KIC pilot project *Green Energy COmmunity*, hereafter referred to as GECO, and of the *Self-User* project. The activities carried out within the framework of these projects have significantly contributed to the material presented in this thesis. To appropriately credit these projects, a dedicated section is provided.

4.1.1. Green Energy Community

GECO (see www.gecocommunity.it) is a pilot project supporting the development of an energy community in the Pilastro–Roveri districts located in the Italian city of Bologna. The project addresses the social, technical, and economic dimensions necessary for creating a REC. GECO aims to support the transposition of the CEP into national legislation, enhance sustainability, reduce energy poverty, and foster a low-carbon economy through the integration of digitalization and IoT, data collection, smart optimization algorithms and blockchain technologies. The community aims not only to provide renewable energy but also to climate change mitigation, fostering neighbors' cooperation, and adding value to the local economy. Citizens are expected to have a crucial role in the project having the opportunity to become prosumers and actively participating in renewable electricity generation and sharing.

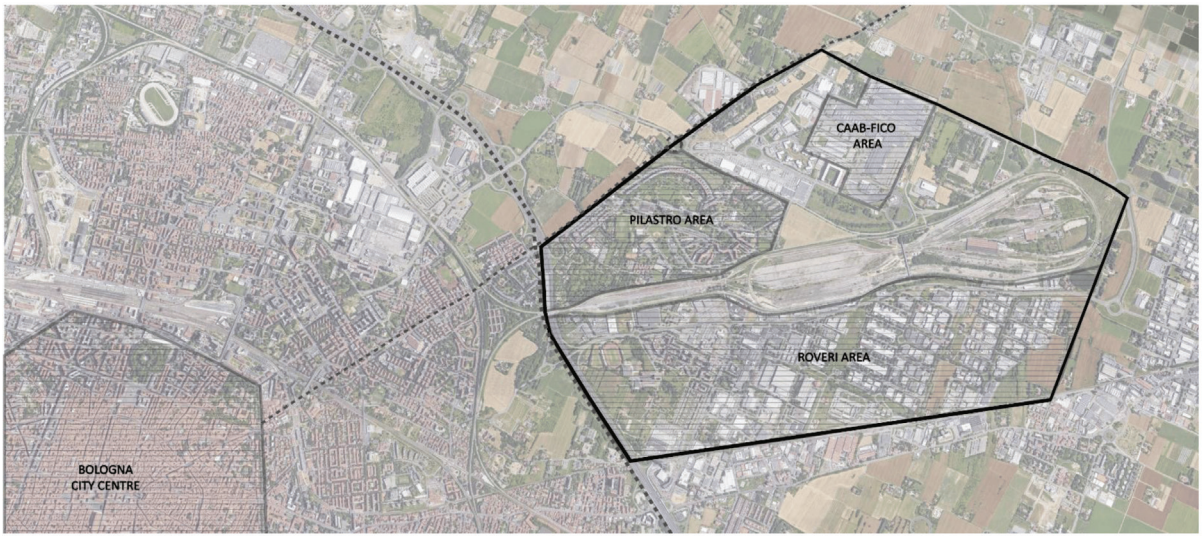

Figure 4.1 Pilastro and Roveri districts located in the outskirt of Bologna, Italy. Adapted from [128]

Both private and public actors are involved. The main stakeholders of the project are: 'AESS – Agenzia per l'Energia e lo Sviluppo Sostenibile', 'ENEA – Agenzia nazionale per le nuove tecnologie, l'energia e lo sviluppo economico sostenibile' and the University of Bologna. Local parties collaborating in the project are 'CAAB – Centro AgroAlimentare di Bologna' and the 'Agenzia locale di sviluppo Pilastro/Distretto Nord-Est'. Moreover, it is supported by 'GSE – Gestore Servizi Energetici', 'RSE – Ricerca sul Sistema Energetico', Emilia-Romagna region and the city of Bologna.

A comprehensive systems approach has been employed during GECO development. The employed approach encompasses technical, legal, administrative, financial, and social considerations and aims to implement the best cost-benefit to exploit the available resources. Hereafter the project outlooks for the aspects considered are provided:

i. From a technical perspective, the project aims to explore novel smart solutions for real-time state estimation in RECs distribution network. This is fundamental for the optimal operation and management of distributed RES and storage systems. The optimal management aims for maximizing the energies self-consumed and shared while minimizing the energy procurement cost through an effective control of storage and decentralized energy resources. Moreover, it attempts to enhance system flexibility through real-time monitoring and predictive analysis.

ii. In the social, cultural, and behavioral outlook, the project emphasizes the citizen role and its empowerment employing a community-based approach. It seeks to engage and raise awareness of citizens and local businesses about climate issues while providing the community with opportunities to take action in mitigating climate change. The establishment of a REC in the district is expected to reduce electricity costs for social housing, enhance local businesses, optimize power flow in local substations, increase self-consumption of renewable energy, and reduce demand peaks.

iii. Legal and administrative aspects encompass the establishment of REC legal entity, the development of smart contracts and blockchain applications. The project

experience can support national stakeholders in the recasting process of national regulation.

In the framework of this project several SMs were installed in Pilastro and Roveri districts, to measure the consumption of residential buildings, and within the CAAB area (see Figure 4.1) to measure consumption of offices and industrial cold storages as well as the production of PV systems. The CAAB area is particularly interesting since on the building's roof several PV facilities are installed (see Figure 4.2) for an overall power exceeding 6 MWp.

Figure 4.2 CAAB area top view

The data collected from SMs are used to create datasets of consumption and production. These datasets can be employed in the planning phase of a REC as well as in the operational phase to optimally-manage the REC assets. A description of SMs installed is provided in section 4.3.2.A and the resulting datasets are illustrated in section 5.1.

In the project's context, also information of the secondary substations, the customer connected as well as the power measurement of the MV feeders feeding those substations were provided by the DSO *E-Distribuzione* thanks to a memorandum of understanding signed by the DSO and the project's partners. This information is used to investigate the

characteristics of a certain area, for example whether it is more industrial or residential, the relevance of generation already installed and the potential consumption that could be covered with new RESs. The geographical information of the secondary substations was used in the developed feasibility studies to identify at which community a customer could belong previously to the publication of the on-line tool by the GSE [129].

4.1.2. Self-User

The Self-User project (see www.selfuser.it) aims to promote energy transition boosting the exploitation of RES. Achieving this objective requires a transformation in the configurations of the socio-economic system, both technologically and socially. This transformation aims to address ongoing climate change through intentional processes that generate benefits in terms of environmental sustainability, as well as community development and social justice.

The project is founded by the Emilia-Romagna Region while the project partners are: 'ART-ER – Attrattività Ricerca e Territorio Emilia-Romagna', University of Bologna, 'ACER – Azienda Casa Emilia-Romagna Reggio Emilia', 'Enel X' and 'ENEA – Agenzia nazionale per le nuove tecnologie, l'energia e lo sviluppo economico sostenibile'.

Self-user is focused on the implementation of a CSC scheme; it aims to analyze different CSC suitable for apartment buildings and establish appropriate planning criteria for CSC implementation. The resulting business model must be both sustainable and scalable, defining clear criteria for sharing incentives among prosumers. To be developed the business model requires the knowledge of key parameters such as the rated power of the PV system, number of apartments and common services appliances, average consumption profile and battery capacity and power, if present. Additionally, the project aims to contribute to regulatory recasts in the context of energy sharing schemes.

During the project development 56 SMs have been installed in an apartment-building located in Scandiano (Italy) municipality. The SMs monitor both common areas and private PODs. These devices have collected data for more than 2 years contributing, together with the GECO project, to the creation of data sets for the planning and operation of REC and CSC schemes.

Additionally, a meteorological station has been installed to record the irradiance and temperature values in the apartment-building area.

4.2 Sizing of a Renewable Energy Community

The process of estimating the optimal size of PV installations and BES systems for energy communities begins with identifying customer consumption patterns. It is assumed that the annual consumption and the consumption type are known for each customer. Customers are grouped into categories such as schools, offices, residential, or industrial, and their respective load profiles are applied (see section 5.1). This assumption is based on the minimal available information. However, if more detailed customer data is available, such as from a metering system, more precise consumption patterns can be used.

The estimation of PV production is based on historical data available on PVGIS [130], using hourly profiles from the year 2016, which closely matches the average yearly production from the 2005-2020 dataset. The production data assumes a roof-mounted PV system located in Bologna, with a slope of 20° and southward orientation. The overall system losses are assumed to be 14%. In the proposed scenario, the PV systems are sized according to the available roof surface on each building.

For each prosumer the energy produced, self-consumed and fed into the grid is calculated. In the proposed scenario different storage system sizes are tested. A normalized value, corresponding to 1 p.u., defined as the minimum between the average daily net energy production, i.e. the PV production decurted by the self-consumption that corresponds to the energy fed into the grid measured by the exchange meter, and the average daily energy net consumption, i.e. the energy withdrawn from the grid measured by the exchange meter, is used. BESs ranging from zero, i.e. no BES installed, and twice of the proposed normalized value are tested. The final BES size is selected based on the closest available commercial option to the calculated value.

Table 4.1 shows the data of the customers aiming at the creation of a REC, most of them are schools, two are offices and only one is residential. Two schools and one office have available surfaces to install PV systems for an overall rated power of 265 kWp and a yearly production of more than 300 MWh. Additionally, the comparison between the scenario without BES and

a 0.8 p.u. BES is proposed. This value of BESs leads to a considerable increase in the self-consumption rate, calculated as the ratio between the energy self-consumed and the PV production.

Table 4.1 Prosumers type, yearly consumption, PV rated power, yearly production and self-consumption.

Customer	Yearly Consumption (MWh)	PV (kWp)	Yearly Production (MWh)	Self-Consumption (MWh/year)		Net Production (MWh/year)	
				Without BES	With BES	Without BES	With BES
School 1	43.00	40	48.30	19.27 (40%)	26.59 (55%)	29.03 (60%)	21.70 (45%)
Office 1	30.30	115	138.86	14.73 (11%)	24.42 (18%)	124.13 (89%)	114.44 (82%)
School 2	13.00	-	-	-	-	-	-
School 3	20.00	-	-	-	-	-	-
School 4	74.50	110	132.82	38.25 (29%)	53.20 (40%)	94.57 (71%)	79.62 (60%)
School 5	39.00	-	-	-	-	-	-
Office 2	79.00	-	-	-	-	-	-
Residential	30.40	-	-	-	-	-	-
Total	**329.20**	**265**	**319.98**	**72.25**	**104.24**	**247.73**	**215.76**

Figure 4.3 illustrates the variation of the energy self-consumed as a function of the p.u. BES size, the curves face saturation as the BES size increases, meaning that an excessive BES size may not be properly exploited.

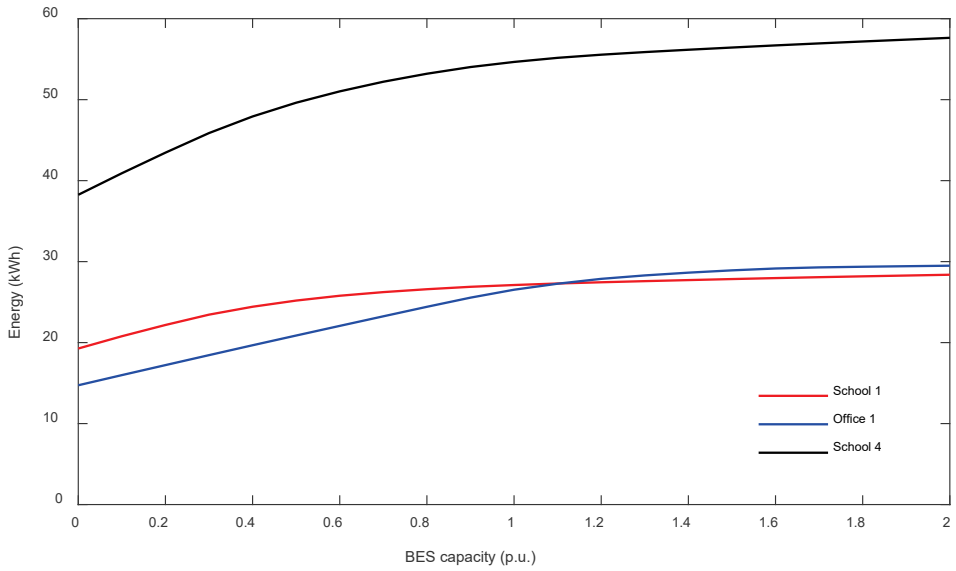

Figure 4.3 Energy self-consumed by prosumers as function of BES size (p.u.)

Figure 4.4 illustrates the cost for energy bought the revenues from energy sold and the savings in the bill related to the energy self-consumed as function of the BES size (expressed in p.u.) for A) school-1 and B) office-1. Revenues and costs are calculated employing hourly values of National Single Price (NSP) of the year 2023. NSP is applied to revenues for energy sold, while NSP plus a spread of 150 €/MWh is applied to both energy bought and savings in the bill derived from self-consumption. The spread is the difference between the price for energy bought and the price for the energy sold, this difference is linked to energy retailer profit and grid fees proportional to energy consumption. The spread value of 150 €/MWh is inspired to values derived from Italian customers' bills. Values for other EU countries can be obtained from [131]. The energy prices and the respective taxes for some EU countries in the first semester of 2024 are illustrated in Figure 4.5.

Similarly, to the self-consumption plot (see Figure 4.3) also the revenues plots (see Figure 4.4) exhibit a saturation.

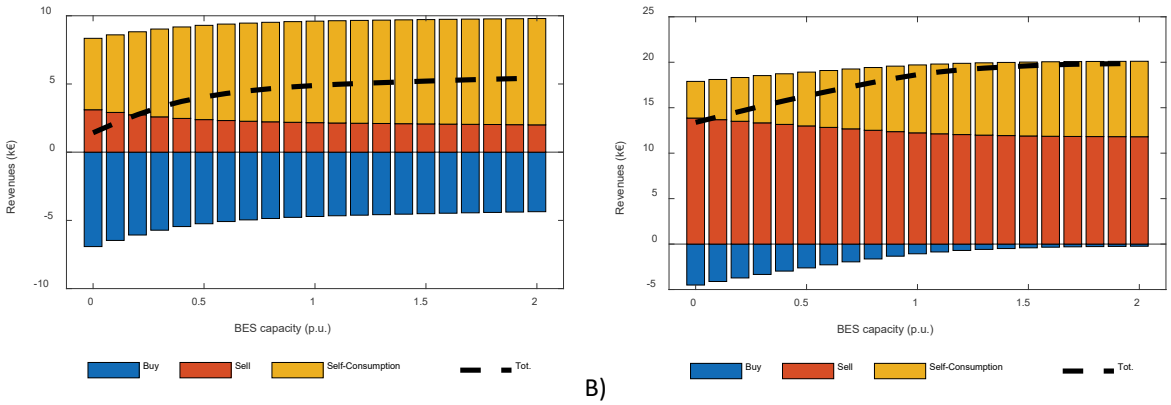

Figure 4.4 Revenues as function of the BES size (in p.u.) of A) School 1, B) Office 1

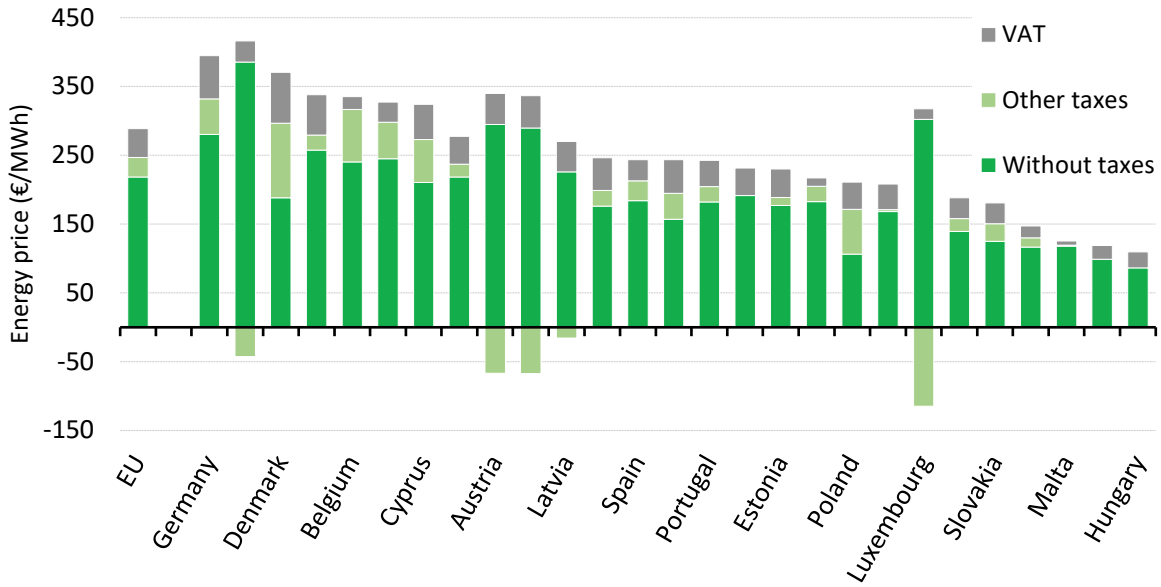

Figure 4.5 Electricity price in EU countries (first semester of 2024), adapted from [131].

From the REC point of view, as it is made up of only three prosumers while the other members are pure consumers, the increase of the prosumers' self-consumption leads to a reduction of shared energy. Figure 4.6 illustrates REC's revenues as function of the BES size including the incentive received from the shared energy. The incentive is assumed to be constant and equal to 110 €/MWh, a realistic value inspired to the Italian regulation. As pure consumers cannot provide flexibility they would contribute with a negative constant value, related to energy bought, not affected by BES size, that constant cost is not reported for figure clarity. The black dash line represents the overall REC revenues (excluding the fixed cost of pure consumers).

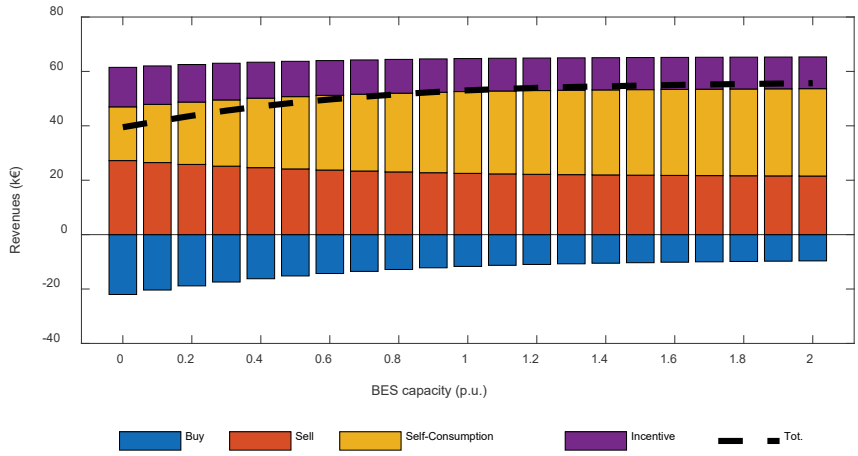

Figure 4.6 REC's revenues as function of the BES size (in p.u.)

4.3 Energy Management System for Renewable Energy Community

The optimal scheduling of the controllable resources of an energy community usually pursues the objective function of minimizing the overall energy procurement cost of the set of users belonging to the community on a daily time horizon, as in [126], [132]. In distributed approaches (see [132] and reference therein), the information that each prosumer has to communicate is limited. The uncertainties in load forecasts can be managed by means of stochastic approaches [133] or intra-day corrections to the day-ahead scheduler decisions [134]. Robust optimizations [126], [135] as well as three stages of scheduling are also proposed to cope with uncertainties, namely day-ahead, intra-day and real-time stage [136]. Short-term load forecasting is used to forecast REC's members load profile, despite the difficulties due to their small size and high randomness, as shown in [137] concerning microgrids. Robust optimization, stochastic models and complex load forecast methods like artificial neural networks [138], usually require a computational burden that is not compliant with real-time schedulers.

The scheduling performed by EMS is structured as a centralized optimization problem, in which the control unit collects and keeps updated all the relevant data of the prosumers' equipment, e.g., battery State of Charge (SOC), actual power flows, as well as load and PV production forecasts. The proposed EMS consists of a one stage layer optimization, that is the real-time scheduler executed with a rolling horizon time window. In order to benefit from up-to-date PV and load forecasts, and known day-after energy prices, the optimization time window is set to a 48-hour time period. Due to the time constraint of the real-time scheduler, simplified load forecast methods are implemented.

4.3.1. Energy management system architecture

The optimal operation of RECs requires the implementation of an EMS to ensure the proper management of the resources of generation and load, including BES systems. As shown in Figure 4.7 the proposed EMS system schedules the prosumers' BESs as a centralized optimization problem, able to cope with forecast uncertainties and to manage the information provided by an advanced metering infrastructure, and in particular the power and energy

measurements provided by devices capable of Smart Meter (SM) reading and Non-Intrusive Load Monitoring (NILM) devices installed in an urban district in the framework of the GECO project [139], [140].

In the proposed scheme an advanced metering infrastructure is employed to collect data on the status of the community' assets, i.e. the values of production, consumption and BES' SOC. Different metering devices can be used to collect data, as discussed further in section 4.3.2.A. Additionally, many inverter manufacturers provide Application Programming Interfaces (APIs) for direct data retrieval from inverters, typically with a time resolution of 5 minutes. The collected data are stored in the database (DB) employing APIs. The aim of the DB extends the data collection and storage as it is employed to standardize measurement: gathered data may come in different units such as W, kW or even kWh as some meters provide energy information rather than power. The DB makes the measurement available to both the optimization algorithm, via APIs, and customers through a Graphical User Interface (GUI).

The EMS' optimization procedure aims to calculate the optimal power profile of BESs to minimize (or maximize) a specified Objective Function (OF). Two possible OFs are outlined in Chapter 6. To properly execute the optimization procedure data the optimizer requires the knowledge of data as load consumption forecast, PV production forecast, current SOCs and energy prices.

The EMS acquires the historical data necessary to forecast the loads from the DB (how the forecast is generated from historical data is discussed in section 5.2), the PVs generation forecast from meteorological service, and the NSP profile from the website of the day-ahead Italian electricity market. The aforementioned elements are discussed in section 4.3.2. The optimization problem is solved at regular intervals of 15 minutes, following a rolling-horizon approach [133]. This allows taking advantage of the updated forecasts of PV generation and load demand, facilitating precise adjustments to the battery setpoint values according to the current operational conditions of the community resources.

To test the capability of the EMS to cope with real-time operation and data exchange with the database collecting available measurements, an Opal-RT digital simulator is used. The real-time simulator allows the evaluation of different scenarios and enabling the safe testing and selection of new equipment and strategies.

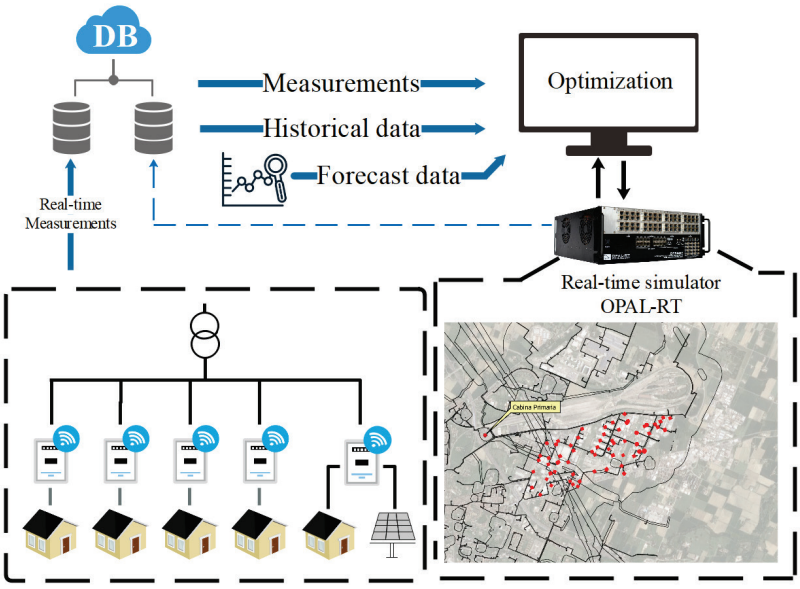

Figure 4.7 EMS validation

4.3.2. Input data acquisition

A. Load and production measure

As mentioned, data availability is essential for the effective implementation of RECs, both in the design and operational phases [125]. The most crucial element of this is the advanced metering infrastructure, which enables the measure of energy consumption and generation in real-time or quasi-real-time, facilitating the monitoring and optimization of REC operation [141]. Hereafter three types of meters capable to monitor load consumption or PV generation, along with their main functionalities are presented.

Non-Intrusive Load Monitoring

NILM meters are gaining popularity alongside the development of SMs in the smart grid framework. These meters provide real-time information on energy consumption (or

production), which can be employed in optimization procedures, load scheduling, and demand-response programs [142].

NILM meters are involved in the direct measuring of the electrical quantities, i.e. voltages and currents. According to the cable cross section two solutions can be employed: for cables up to 35 mm^2 a passthrough meter can be installed, this means that the line to be measured, if already existent may be cut to be connected in series with the meter. In contrast, for large cross-section or to avoid the cable cut, Current Transformer (CT) can be employed. The NILM employed in the GECO project are provided by *Eastron* (see www.eastroneurope.com), the provided meters are Measuring Instruments Directive [143] compliant and the installed devices have less than 1% error. During the installation the proper system configuration (e.g. single-phase, three-phase three-wires or three-phase four-wires) as well as the correct ratio of CT have to be selected to avoid bad measurements.

The main drawback of these devices is the installation: modification to the electrical system must be executed by a qualified technician and it may require the interruption of the electrical supply during the installation. NILM devices are suitable only for LV connection.

To remotely acquire the measurement the NILM meter needs to be interfaced with a gateway device capable of receiving the measurements from the SMs and forwarding them to the desired destination which in our case is the DB. The interface between the NILM and the gateway device is performed using the Modbus communication protocol. In the GECO project two solutions have been tested:

i. the first one consists of using a commercial service that manage the data routing. Typically, this service is provided by a third-party company that requires a subscription fee or is included in a larger energy management service package. In this case the third party manages the data collection and storage in a proprietary database. In the framework of GECO project the service provided by Regalgrid (see www.regalgrid.com) is used. The gateway device is called '*Smart Node Control Unit-SNOCU'* and in our application it is connected to the internet through Ethernet cable to guarantee a more stable and efficient connection. The data collected by the SNOCU

are transmitted to Regalgrid's server, where they are made accessible via an API. Real-time data can be requested with a frequency of up to 5 seconds. Alternatively, historical data can be accessed, though in this case, the time resolution of the measurements is reduced to 5 minutes. The available data are described in Table 4.2

Table 4.2 Power and energy data available via API request

Name	Description
Device ID	SNOCU unique ID
Last Update UTC	Date/time (in UTC format) of last data read from SNOCU.
Status	SNOCU current status (Online/NoData/Offline).
PV Energy Total	Lifetime Photovoltaic energy (Wh), if available from inverter.
Load Energy Total	Lifetime Loads (Wh).
Battery Energy In Total	Lifetime Battery Energy In (Wh), if available from inverter.
Battery Energy Out Total	Lifetime Battery Energy Out (Wh), if available from inverter.
Exported Energy Total	Lifetime energy exported to grid (Wh).
Imported Energy Total	Lifetime energy imported from grid (Wh).
Inverter Energy Out Total	Lifetime energy produced by inverter (Wh), if available from inverter.
Inverter Energy IN Total	Lifetime energy imported by inverter (Wh), if available from inverter.
Name	Description
Active Command	Inverter's current active command issued by SNOCU (SelfMode/BatteryCharge/BatteryDischarge/BatteryStop/SleepMode).
Power PV	Photovoltaic real time power (W).
Power Load	Loads real time power (W).
Power Battery	Real time battery power (W). Positive means charging, negative means discharging.
Power Grid	Realtime grid exchange (W). Positive means export, negative means import.
Battery SOC	Battery State of Charge (%).

ii. The second method consists in the own development of the gateway interface. This solution allows to overcome the necessity of a subscription as well as limits imposed by the commercial provider. The hardware chosen for the gateway development is an ESP32 microcontroller. The ESP32 board has enough computational power to perform data acquisition, logging and transmission to the database. It is used also to elaborate data if necessary. A RS495-RS232 converter is used to interface the meter and the ESP32. Moreover, The ESP32 is equipped with an integrated Wi-Fi module which enables the connection to local area network or internet, if necessary.

The code developed for the ESP32 can be roughly summarized as follows:

- The initialization, executed at board start-up, enables serial communication with the meter, defines all the necessary variables and connects the ESP32 board to the Wi-Fi network.

- The measurements acquisition code section continuously acquires the measurements from the NILM meter, i.e. currents, voltages, power factors (PFs) and frequency; every time period Δt it performs the average value of the above quantities, assemble a string according to the JSON format requested by the database and execute the HTTP request to log the measurements in the database.

- The code has been equipped with a webserver functionality that allows to remotely change the time period Δt through a webpage. To access the ESP32's webserver the user should be connected to the same LAN of the ESP32, either physically or through a Virtual Private Network (VPN). The access is password protected.

Details on communication between the NILM meters, in both configurations, and the database are provided in Appendix B.

The information about the meters installed in the CAAB area is provided in Table 4.3, the name of the involved customers is anonymized to preserve their privacy: they are represented through the device ID used in the API request. Figure 4.8 shows the measures of the prosumer with ID 348, two of the curves are obtained from measures, i.e. the PV production in red and the consumption in black (load is represented with negative sign), the blue curve corresponding to the power at the PCC is obtained as the sum of the formers.

Table 4.3 Device ID, meter and customer information of the installed devices.

Device ID	Meter installed	Description
348	CT 200/5 A	Prosumer equipped with a 94 kWp PV system.
335	Passthrough	Consumer, the main load is constituted by forklifts charging stations.
519	CT 150/5 A	Consumer with cold storage.
2080	CT 300/5 A	Consumer equipped with cold storage; contractual power: 82 kW
2517	CT 150/5 A	Consumer, the main loads are constituted by PCs, HVAC system, servers and instrumentation for fruit and vegetables quality analysis; contractual power: 50 kW.

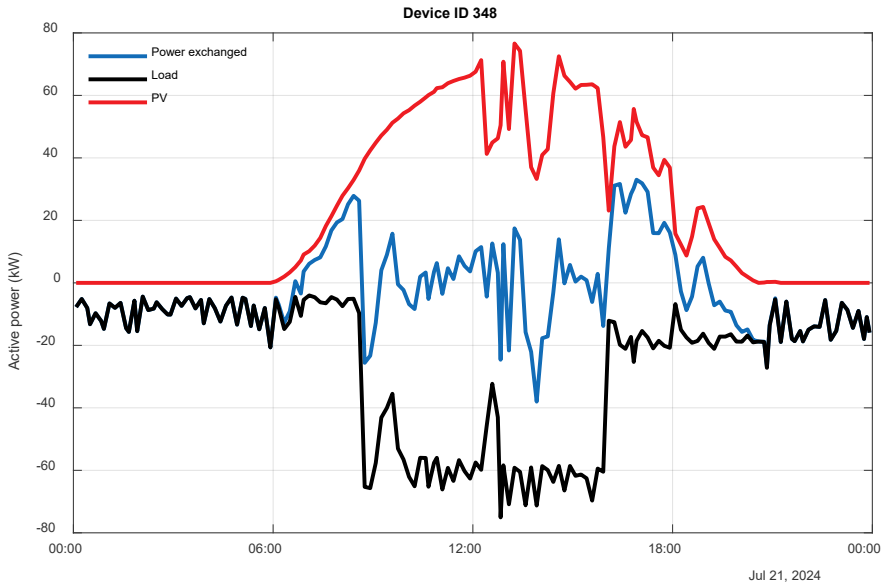

Figure 4.8 PV production, load consumption and power exchanged of prosumer 348

User Device

User Devices (UDs) are monitoring instruments capable of establishing communication with the new generation of DSO's fiscal meter installed at the user PCC. The UD SMs do not directly measure power and energy production and consumption. Instead, they acquire these measurements from the DSO's fiscal meter via the Power Line Communication (PLC) Chain 2 interface (see figure hereafter).

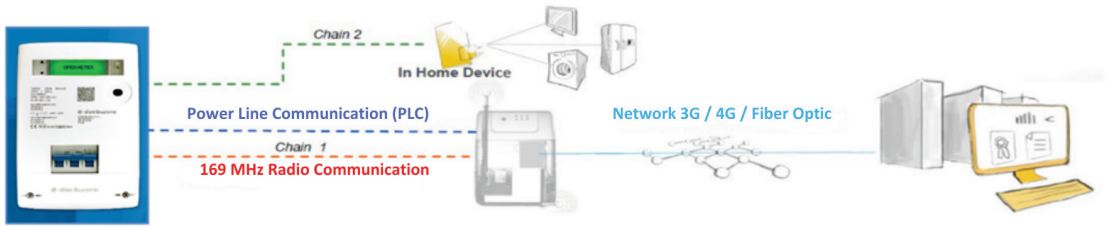

Figure 4.9 Communication chain employed by smart DSO meter. Adapted from [144]

PLC consists in injecting a signal into the electrical system at a frequency within the C-band (125 kHz – 140 kHz), distinct from the 50 Hz power frequency, to establish communication between the fiscal meter and UD. To be eligible for interfacing with the DSO meter, the UD must comply with regulations CEI 13-82, CEI 13-83, and CEI 13-84, and successfully pass a certification procedure. To interface smart meters with fiscal meters, preliminary steps by the manufacturer are required. Specifically, a binding process is necessary between a UD meter (identified by its serial number) and a customer (identified by its POD) through the DSO's business portal, which configures the PLC-chain2 communication. The communication chain between the fiscal meter and the UD is secured by design, as these devices are linked using a secure pair of cryptographic keys. This setup prevents external entities with malicious intent from injecting unauthorized messages into the user device. Similarly, communication between the UD and the producer's gateway is secured by encrypting all messages using a public-private key pair, ensuring that all messages are digitally signed.

Once the preliminary binding procedure between the DSO meter and the UD is concluded, to start measurement acquiring the UD should be plugged in an electric socket to establish the PLC chain-2 communication with the DSO meter. In the case of a three-phase system, typically the DSO's meter sends the PLC signal only in one of the three phases, thus a socket fed by the right phase should be used. Moreover, if the distance (intended as wire path) between the UD and the DSO meter is significant the communication may experience interruptions or instabilities due to signal attenuation or disturbances presence, i.e. a low signal-to-noise ratio.

The data transmitted through the PLC-chain 2 is limited, the DSO's meter transmits the following information:

i. Instantaneous power: thresholds at each 10% of the contractual power are established, each time that the measured power crosses one of these thresholds the measure of the instantaneous power in that specific time is sent to the UD. Thus, the frequency of the information depends on the load variability.

ii. Consumption above limit: if the measured consumption overcomes the maximum allowed power consumption a message is sent. It indicates that the system may be disconnected remotely by the DSO if the power absorbed is not decreased.

iii. Average power every 15 minutes. This information is the only one which has a fixed periodicity.

Figure 4.10 shows the data received from a domestic consumer, the blue bars represent the average power received every 15 minutes, while the red circles represent the instantaneous power measured at each threshold passthrough. The asynchronous information on instantaneous power is capable of detect short duration load spikes, that are either lost or smoothed out in the 15 minutes average. On the other hand, a data loss in the average values is easy to detect, as it results in a missing time slot, whereas the loss of instantaneous power information is more challenging to detect.

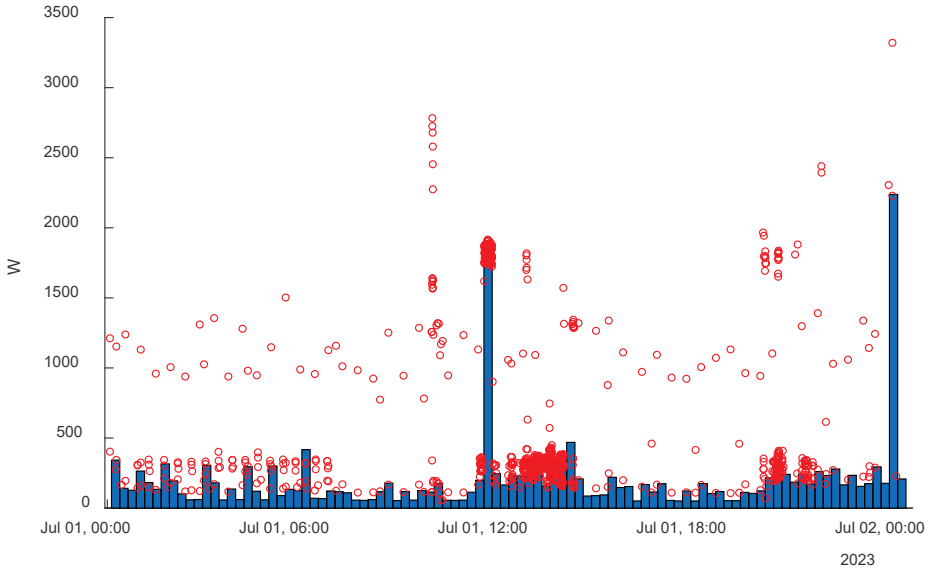

Figure 4.10 Active power measurement adopting UD meter. In blue, average power received every 15 minutes, in red instantaneous power measure at the threshold crossing.

In the framework of GECO project UD from two manufacturers have been tested. Devices manufactured by Tera (see https://www.terasrl.it/it) have been installed in the CAAB area while devices manufactured by Urmet (see https://www.urmet.com/it-it/) have been installed in households located in the Pilastro district in Bologna. The list of devices and their location is provided in Table 3.1.

Table 4.4 UDs installed in the GECO project

Device ID	Manufacturer	User	Description
0001	Urmet	House 1	Residential
0002	Urmet	House 2	Residential
0003	Urmet	House 3	Residential
0004	Urmet	House 4	Residential
0005	Urmet	House 5	Residential
0006	Urmet	House 6	Residential
0007	Urmet	House 7	Residential
0009	Urmet	House 8	Residential
000B	Urmet	House 9	Residential
1058	Tera	Cenerini	Consumer, the relevant loads are the cold storages; also, PCs, heat pump/climatization are present.
1098	Tera	Agribologna	Consumer, the main loads are constituted by PCs, HVAC system, servers and instrumentation for fruit and vegetables quality analysis; contractual power: 50 kW. (Note that this is the same user monitored with NILM in previous section. Monitor a user with the two technologies allows to compare them)
1115	Tera	CAAB	Prosumer equipped with a 96 kWp PV system. The relevant loads are constituted by server and network apparatus and motorized entrance bar

UDs provided by Tera involve the use of two devices: the *Beeta Reader*, which is the UD responsible for establishing the communication with DSO's meter and the *Beetabox* which is a gateway capable to use wi-fi or ethernet connection to forward the information. The gateway allows also to interface several types of sensors such as humidity, light, etc. and actuators as switches and smart plugs that have not been employed in the project deployment. While UD provided by Urmet embed the routing capability since they are equipped with an integrated wi-fi module (in this case the ethernet port is not available) or with a modem module that allows internet connection through a SIM.

Pulse Counter

An intermediate solution to NILM, which directly performs the measure of electric quantities, and UD, which acquire the measures of the DSO's meter but the sampling time cannot be controlled, is the use of pulse counter. Typically, energy meters are equipped with a LED and a light pulse is emitted after a specific amount of energy consumption or production. Similar to the previously described approach, a custom energy meter has been developed using an ESP32 board. A photoresistor is connected to the ESP32, and through a voltage divider circuit, the resistance and consequently the voltage variation of the photoresistor is detected by the ESP32 at each light pulse. This setup enables the measurement of energy consumption by detecting the pulses generated by the existing meter, a similar procedure has been proposed in [145].

This solution allows for measuring the incremental value of energy, however, to calculate power, the time information must be introduced in the ESP32 adopting a timer. Two methods can be applied to calculate the average power:

i. Pulse-based averaging: this method waits for a specific number of pulses before calculating the average power. The timing between pulses is tracked by the timer, ensuring precise average power calculation. However, this method leads to asynchronous power data since the time interval between average calculation depends on the amount of energy consumption or production.

ii. Fixed time interval averaging: in this approach, average power is calculated at fixed time intervals. However, energy consumed or produced between the last detected pulse and the end of the interval is excluded from the current period and carried over to the next. This introduces errors in average power calculation and is emphasized when the consumption or production are low (few pulses in the averaging period).

B. Database

A key aspect for the successful implementation of an EMS is the availability of historical power and energy data, which are essential for generating load forecasts used in optimization algorithms. A comprehensive historical dataset has been established and is regularly updated

using measurements from SMs installed during the GECO project. To effectively manage this continuous data influx, an online database has been implemented. This database, designed for remote access, acts as a central repository for all power and energy measurements, ensuring secure storage and easy access for analysis and integration into the EMS.

To create the DB the open-source web application *Emoncms* has been used. Emoncms enables the logging, processing, and visualization of energy data. The software can be either accessed in online versions or downloaded and installed on a computer or in a virtual environment. The online option requires a subscription which cost is related to the number of inputs to be received by the platform [146]. The self-hosted option can be installed in systems as Linux (Ubuntu or Debian), Windows or Raspberry-PI.

According to our goal of exploiting the maximum scalability and flexibility though the full control guaranteed by the administrative privileges, the self-hosted version is used. The DB software has been installed in a virtual machine (VM) running Ubuntu 20.04 (long-term support version). The VM is hosted in a VPN belonging to the University of Bologna network.

To properly work Emoncms requires the presence of additional components as:

i. *Apache* to provide HTTP server capabilities;

ii. *PHP* to process hypertext;

iii. *MariaDB* as relational database management system. Alternatively, MySQL can be employed;

iv. *Redis* (REmote DIctionary Server) is a database management system designed for high-speed data access, as it stores information directly in RAM. This enables rapid data retrieval and processing. Data is written to non-volatile storage at a later stage, ensuring persistence while prioritizing fast access times.

To enhance the safety of data stored in the DB as well as of the VM hosting the DB, the access to the VPN is secured through a personal certificate generated by OpenVPN (see

https://openvpn.net/). To each certificate a specific IP address is bonded, thus no simultaneous connection from devices using the same certificate is allowed. It is suggested that each device aiming to access the VPN has its own certificate.

The access to the Emoncms's GUI is performed using the DB's URL (in our specific case it corresponds to the IP address of the VM). The login credentials allow the administrator to manage the set of inputs belonging to the community. The possibility to register multiple administrators allows to manage and to store data from multiple communities with the same hardware setup.

Once the user is successfully logged into the DB, the GUI that appears is showed in Figure 4.11. The left column shows the main tabs, thus the main functionalities exploitable from the DB. The main functionalities related to data logging are contained in tabs *inputs* and *feeds*, respectively.

The *inputs* tab contains a list of all the nodes used in the DB, along with the corresponding inputs for each node. Each node, represented by either an integer number or a word, identifies a set of inputs (e.g., measurements associated with a meter or a consumer/prosumer). Several inputs may be linked to each node, including power consumption, power production, voltage and current measurements from loads and PV systems, BESs power, and their SOC. In the input panel the last value received by each input is shown along with the elapsed time since the information was received. The *inputs* tab is not responsible for the data storage, it keeps only the last value received. To store the data for later use, it is necessary to create a feed.

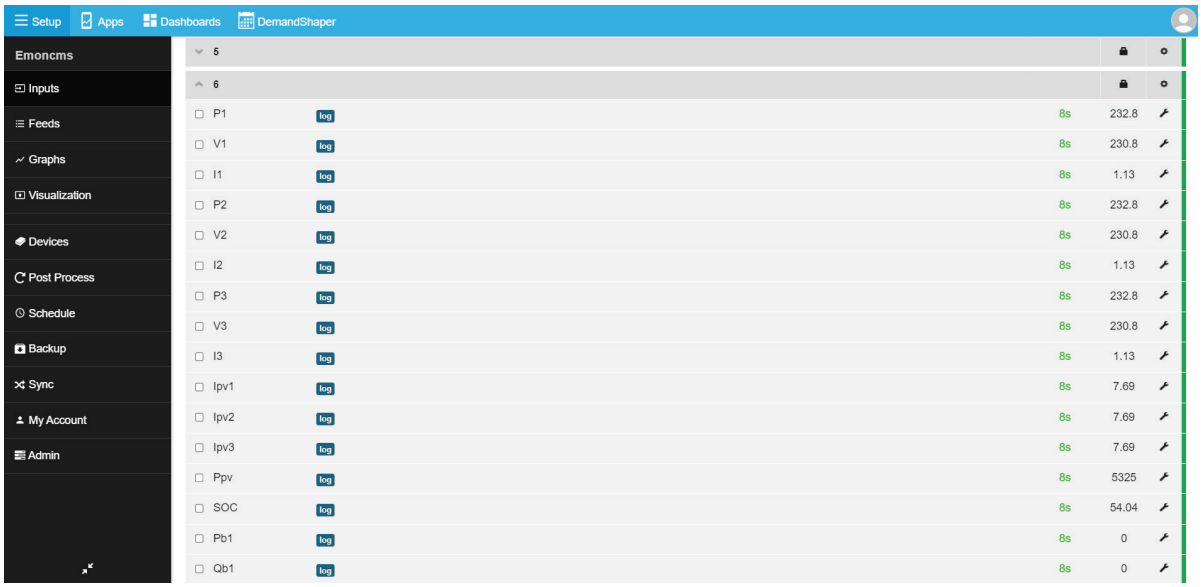

Figure 4.11 Inputs tab of Emoncms

The *feeds* tab lists the feeds created in the database, provides options to create new feeds or edit existing ones. Feeds enable logging, as well as mathematical and conditional operations on the inputs. Multiple feeds can be created for each input. For instance, for a power measurement input, both its value and its time integral (i.e., energy) can be stored by creating a logging feed for power measurements and a power-to-kWh feed for energy data. Next to each feed, the memory usage, the most recent recorded value, and the time elapsed since the last update are displayed. Additionally, "virtual feeds" can be created, which allow mathematical or logical operations using data from one or more traditional feeds. The key advantage of virtual feeds is that they do not consume storage memory.

The APIs list used to enable the data logging in the DB is reported in Appendix B.

The Emoncms application offers also other features as visualization capability through the *Graphs* section or a light post-process of the data which allows to perform simple operations on the data collected. These functionalities are used to create users' dashboards to make available the information collected in a straightforward way not only to the optimization algorithm but also to the REC members. This is a key point in improving customer awareness of its consumption.

Three types of members have been considered in the design of dashboards: community managers, prosumers, and consumers. For privacy reasons, each member can access only their own data, while the community manager can view the overall status of the entire community.

The default dashboard for consumers (see Figure 4.12) displays instantaneous power consumption in the top left corner, while the remaining three graphs present the consumer's historical data. Users can adjust the timespan of the plotted data. The bottom left graph shows the profile of power absorbed from the grid, while the two bar graphs on the right indicate energy consumption by hour (upper graph) and by day (lower graph).

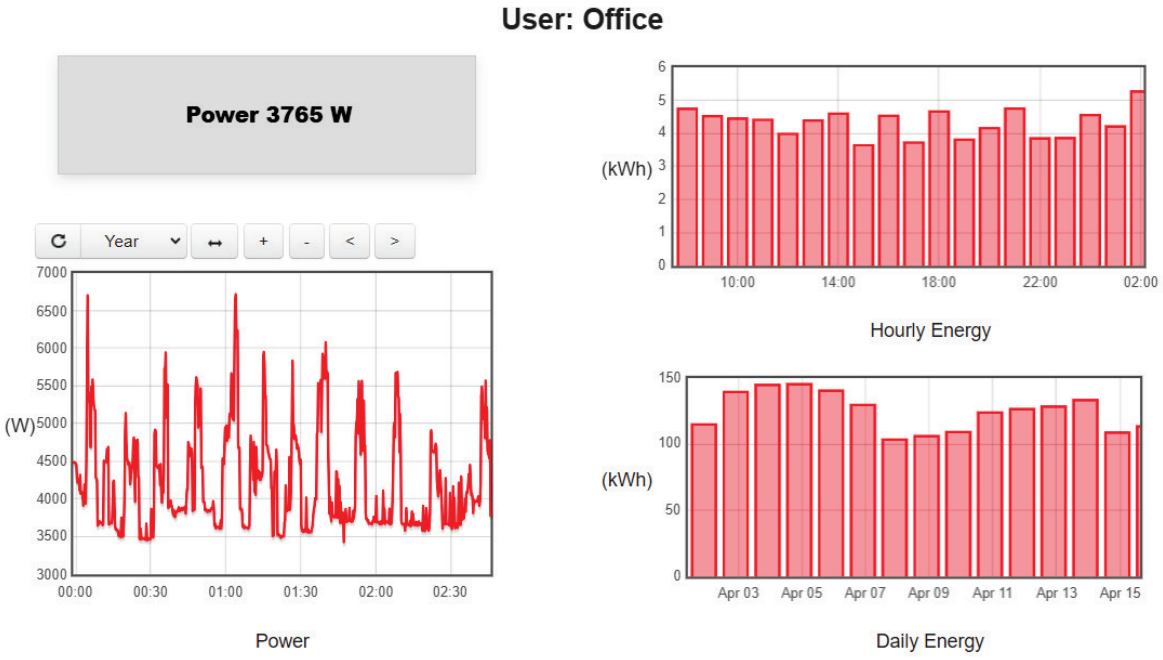

Figure 4.12 Dashboard for consumers created in Emoncms.

Energy data can also be aggregated by month instead of hourly or daily aggregation, the resulting plot is shown in Figure 4.13.

The dashboard can be an effective tool to identify which activity and home appliances consume more energy. Being aware of this information the consumer can adopt a behavior to

reduce its own consumption or evaluate the modernization of appliances/machineries with low energy efficiency.

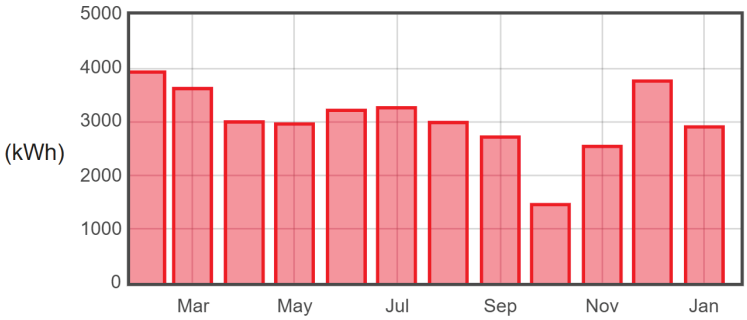

Figure 4.13 Customer monthly energy consumption.

The dashboard for prosumers (see Figure 4.14) includes additional information compared to the consumer dashboard, in this specific case a PV system and a BES are considered. In addition to consumption information, data on production and battery power and the SOC are displayed. The profile of PV generation has been overlapped to the consumption one and, at its right side, a plot contains the historical profiles of battery power (negative values means charging while positive values discharging the battery) and SOC (ranging from 0 to 100% of the right vertical axis) is added. On the right side of the page the two bar graphs show the hourly energy generated and consumed respectively. As in the consumer case, the time window can be time shifted and the energy can be varied from kWh per hour to kWh per day, month or year.

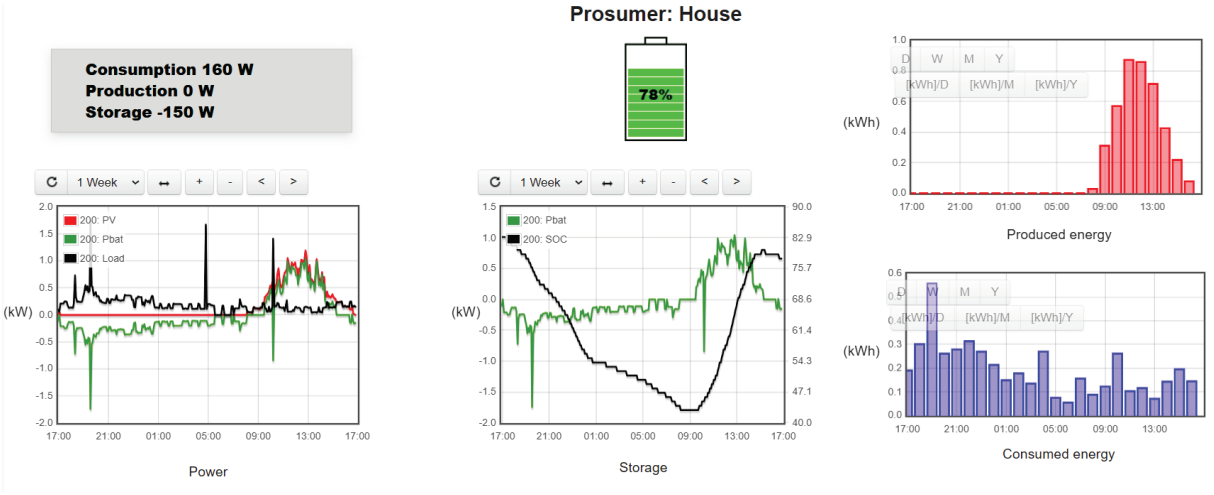

Figure 4.14 Dashboard for prosumers created in Emoncms.

The dashboard designed for the energy community manager (Figure 4.15) shows a simplified scheme of the REC configuration and assets. In the proposed example two prosumers, equipped with PV and BES, are considered. Arrows provide information of the real time power-flow obtained by the SMs. Moreover, a community PV and BES are considered to maximize the community self-consumption. The scenario reported in the figure hereafter is acquired during the afternoon: the solar irradiation is decreasing, however is still sufficient to cover the load requirements of the two prosumers. Community storage is covering the energy deficit of the community.

The overall power absorbed by REC members is reported in blue, i.e. the sum of absorptions measured by the DSO meters belonging to the REC. While the overall power fed into the grid by the REC members is reported in red, i.e. the sum of injections measured by the DSO meters belonging to the REC. The corresponding energy shared within the REC is represented in green. Even if an automatic EMS is not employed to optimize energy sharing, the community manager can still offer recommendations to members on optimal time slots in which shift their loads, thereby enhancing energy sharing within the community.

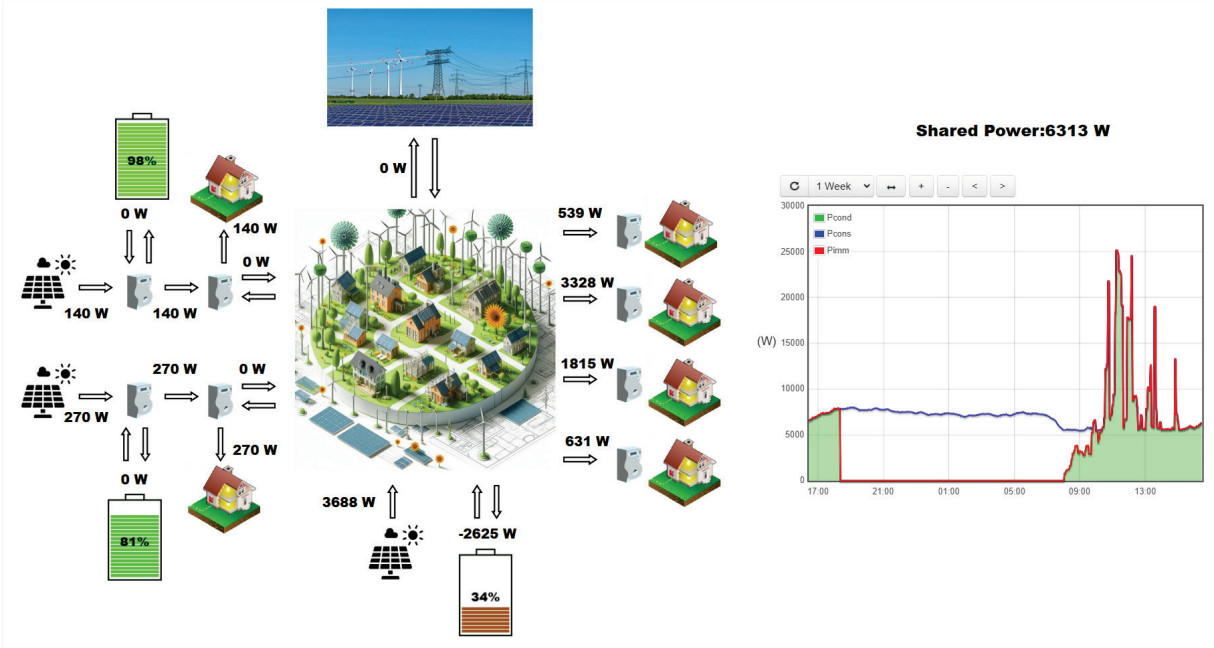

Figure 4.15 Dashboard for the energy community manager created in Emoncms.

C. Photovoltaic production forecast

The PV production forecast is a key point to determine the time at which a prosumer or a REC faces an excess of production and thus how to manage this excess, e.g. store it for later self-consumption or sell it to the energy provider. Typically, for planning purposes PV production forecasts based on historical data are used, one of the sources widely cited in literature is the Photovoltaic Geographical Information System also referred as PVGIS [130]. However, for the optimal operation purposes the randomness related to the daily weather conditions should be properly considered. Thus, real-time online tools such as satellite-enhanced weather forecasting services are employed. The use of real-time forecast integrated with historical data enhances the reliability of short-term PV production forecast thereby facilitating an effective decision-making process by the EMS to achieve the optimal operation.

Different online tools for weather and irradiation forecasting were tested, most of them offer some basic functionalities in the free version while for more advanced features a subscription is necessary. Among the solutions explored the final choice was the tool made available by ForecastSolar. Forecast solar integrates meteorological forecasts from different source as Dark Sky, Wunderground, and OpenWeatherMap with the historical database of PVGIS [147]. In the free version the weather forecast and solar production estimation are provided for the

next 48 hours with an hourly resolution. Without a subscription the max allowed number of API requests is limited to 12 per hour, however, for our purposes, this limit is sufficiently large as forecast update request is executed every 15 minutes.

The PV production estimation by Forecastsolar, for a precise area identified by latitude and longitude and for a specific PV installation characterized by rated power, azimuth and tilt angles is obtained by integrating in the API request the above listed installation characteristics. Figure 4.16 shows in dashed lines the forecast obtained by Forecastsolar. The shading transitions from light gray, representing the earliest forecast, to black, denoting recent forecasts. Initial forecasts, obtained the previous day, predict a cloudy day with low solar irradiation. However, as the time approaches the current day, forecast adjustments are obtained, predicting a higher solar irradiation. When compared with the measured PV production, shown in red, it becomes evident that the most recent forecasts are more reliable.

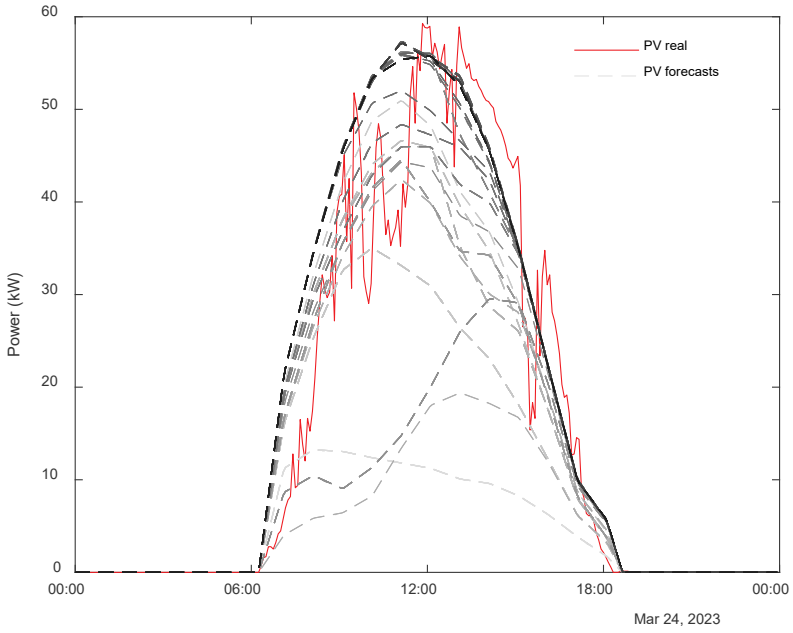

Figure 4.16 comparison between measured PV production and forecasts

D. Market price

To minimize the energy procurement cost the EMS should provide to the optimizer the energy prices for both the energy bought and sold. Price of the Italian day-ahead market is employed

for the case studies presented further. The day-ahead market price, i.e. the NSP, is applied to the energy fed into the grid by the prosumers, whereas for the energy purchased, a spread is added to the day-ahead market price.

The pricing profile to be applied to a specific customer depends on his supply contracts, the most common options are:

i. price defined ex-ante by the provider, which may either be constant throughout the day or vary by time slots, in this case the acquisition of the market price is not necessary as the price is already know;

ii. fixed price, calculated ex-post as the average values of market prices over the billing period;

iii. Time of Use (TOU) prices, calculated ex-post as the average values of market prices within the respective time slots over the billing period;

iv. Hourly varying price, where the hourly day-ahead market price is used.

The day-ahead market price fluctuation depends on the timespan of interest, in Figure 4.17 are reported the monthly average values from 2020 to present. In 2020 prices were notably low, it was the period of pandemic lockdown, during which many activities were either shut down or operating at reduced capacity. Prices faced a steep rise in 2022 concurrently to geopolitical instabilities. Looking at the market prices fluctuations on a shorter timespan, such as a day (see Figure 4.18), the hourly energy price rapidly changes within the same day. Thus, the knowledge of the price profile by the optimizer allows to manage the storage charge and discharge in an effective way. The same applies to the case of TOU tariff since the optimizer can favor the charge/discharge in one time slot over another. Thus, the prices of the following day are daily acquired from the file transfer protocol (FTP) server (see https://www.mercatoelettrico.org/it/tools/ftp.aspx) of the Italian energy market manager “Gestore dei Mercati Energetici” [148].

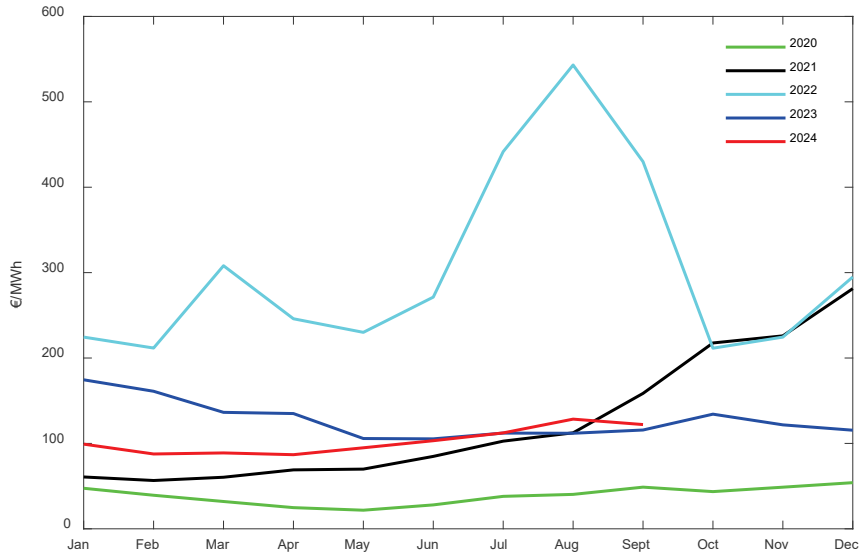

Figure 4.17 Monthly average price from 2020 to 2024

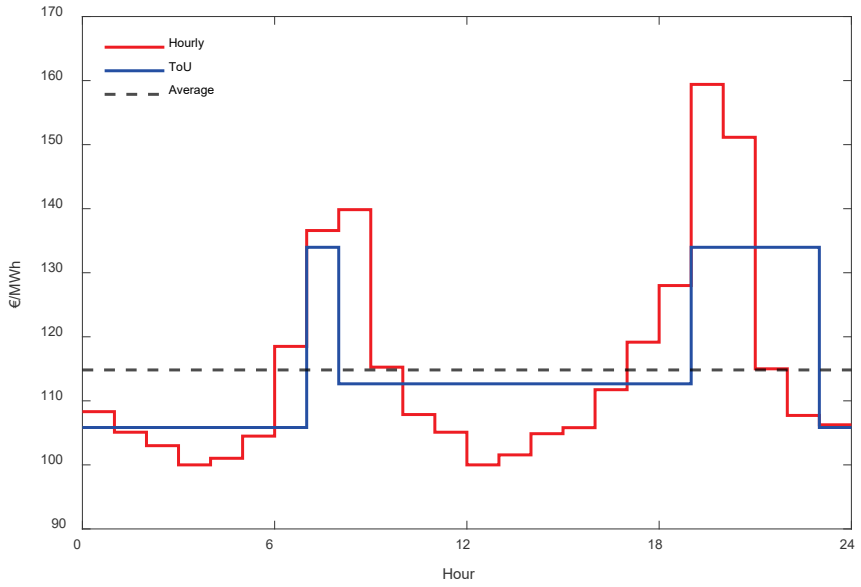

Figure 4.18 Hourly, ToU and average price on September the 18th 2024

4.3.3. Real-time simulator

The use of a real-time digital simulator facilitates the validation of newly developed algorithms employing closed-loop testing under safe and controlled conditions. This method combines both accuracy and flexibility, making it possible to recreate a wide range of scenarios to assess system responses under normal, emergency, or rare operating conditions. Real time

simulation can be performed as Software in the Loop (SIL) or Hardware in the Loop (HIL). SIL is a simulation-based method used to test and validate control algorithms without involving physical hardware, providing a cost-effective and flexible way to detect issues. HIL, on the other hand, involves real hardware interacting with a simulated environment in real time, allowing for more accurate and realistic testing of the hardware-software integration under operational conditions. The proposed EMS has been widely tested through SIL through the real-time simulator and also HIL test have been carried out as discussed in [149].

The SIL validation, carried out at the Power Systems Engineering Laboratory in the University of Bologna through an Opal-RT real-time simulator encompasses the whole EMS presented in section 4.3.1. To guarantee real-time operation in simulations, significant computational effort is required. As a result, ad-hoc parallel processing architectures have been adopted in the design of real-time digital simulators to meet these demands efficiently [150]. To be compliant with real-time timing the coding structure of the software to be implemented in the real-time simulator comprises three subsystems: the master, slave, and console subsystems. The master subsystem is essential for real-time implementation as it handles the fundamental computational tasks (the power system modeling in our case), thus it runs in the real-time simulator. Slave subsystems are used to distribute real-time processes across multiple cores running in parallel. The console subsystem, running on a PC (potentially the same PC as the EMS), allows the interaction with the system included in the real-time simulator and handles data acquisition and visualization asynchronously from the master subsystem [151]. In our case the console subsystem is employed to acquire measurements from SMs, PV and loads forecast, as well as BESs setpoints received by the optimizer. All this information is forwarded asynchronously to the master subsystem. The console subsystem, in turn, receives the results of the power system resolution, which are then plotted, sent to the database, or stored for later analysis.

In real-time simulations the occurrence of overruns should be properly monitored to ensure reliable results. Overruns happen when the computational time required to solve the master and slave subsystems is larger than the simulation time-step. Ideally, the number of overruns should be zero or negligible by the end of the simulation as the main objective of a real-time

simulation is to solve the system within the time-step in real-world timing [152]. In the simulation carried out a time-step of 250 µs is employed.

As formerly introduced the network model of the REC is developed in the master subsystem. The model is designed to be reconfigurable, allowing the simulation of a wide range of REC network configurations. Figure 4.19 illustrates a simple potential configuration with three active prosumers interconnected by three branches and linked to the distribution network, two additional prosumers are temporary disabled.

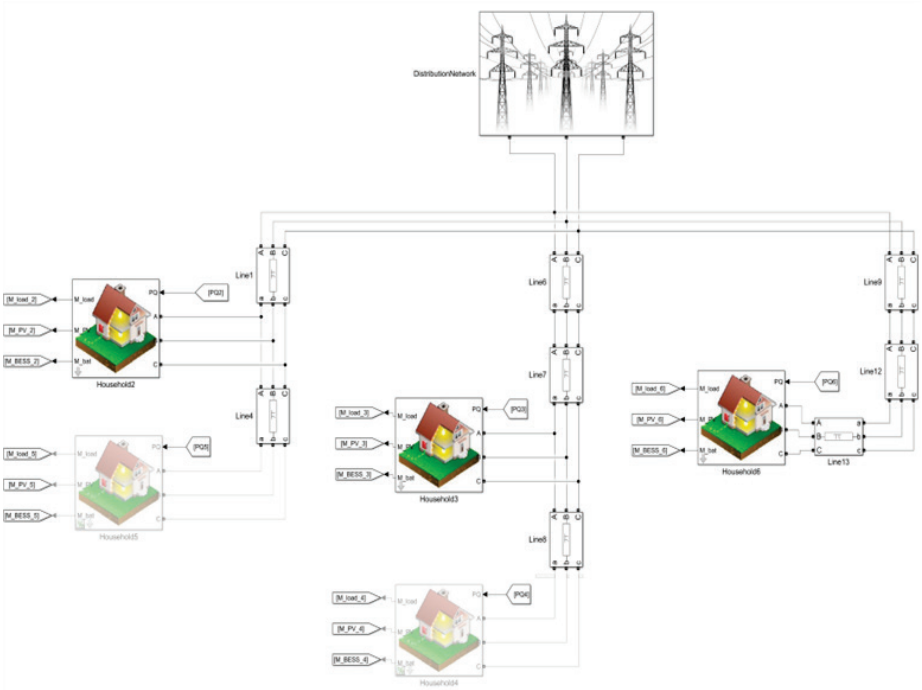

Figure 4.19 REC network model with three active prosumers

Figure 4.20 shows the generic prosumer model, which includes a PV source, a load, and a storage system, can also represent a simple consumer or producer by setting either the PV source or the load to zero, respectively. The measurements obtained from each prosumer element, such as active and reactive power, currents, voltages and SOC are sent to the database.

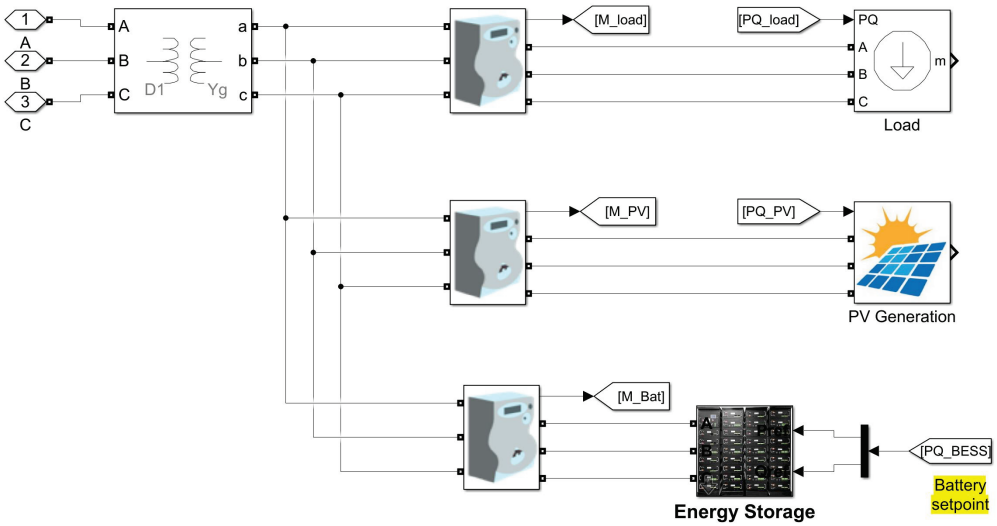

Figure 4.20 Prosumer Simulink model

The BES model, illustrated in Figure 4.21, comprise a charge limit block, shown in red, whose main function is to saturate the battery's output by enforcing critical limits: overcharge and undercharge limits, which prevents charging and discharging when the SOC reaches its maximum and minimum value, respectively. Moreover, the charge limit block ensures that the power capability of the BES is respected, ensuring that the nominal current is not exceeded.

Additionally, the stored energy calculation block, indicated in green, is tasked with determining the SOC at any given time. The SOC in each time-step is calculated basing on the SOC at previous time step, active and reactive power outputs of the BES according to equations (4.1)-(4.2). It is important to highlight that the BES's model employed in this context disregards the transient behavior of the BES and the inverter dynamics.

If charging $$SOC_{t+T_s} = SOC_t + \frac{\sqrt{P^2+Q^2}\cdot\eta\cdot T_s}{E_t^{BES}} \quad (4.1)$$

If discharging $$SOC_{t+T_s} = SOC_t + \frac{\sqrt{P^2+Q^2}\cdot T_s}{\eta\cdot E_t^{BES}} \quad (4.2)$$

where T_s is the real-time simulation time-step, P and Q are the BES active and reactive power, η is the battery efficiency, assumed equal during both charging and discharging and E_t^{BES} is the energy stored in the BES at time t.

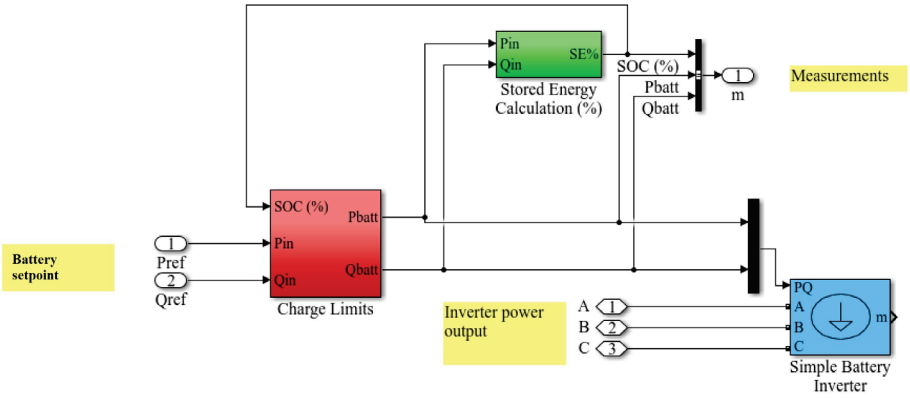

Figure 4.21 BES Simulink model

Chapter 5. Load Forecast for Energy Communities

Introduction

Data availability is fundamental for the effective development of RECs, both in the design and operational phases [125]. The most crucial element of this is the metering infrastructure, which enables the measure of energy consumption and production in real-time or quasi-real-time, facilitating the monitoring and optimization of REC operation [141]. The main purposes of this chapter are the identification of standard customer profiles to be used in the design phase of RECs, and the deployment of forecasting methods suitable for operational optimization.

The first section of the chapter focuses on the development of standard energy profiles for various building types, including schools, residential buildings, offices, and warehouses. These profiles are derived from measurement campaigns conducted as part of the GECO and Self-User projects. Additionally, data from primary and secondary substations are analyzed to explore potential energy communities in the Pilastro-Roveri district. By evaluating the district's feeder power flows, this section estimates the area's consumption patterns, the PV production already in place, and overall energy demand. Analysis of the data reveals that different energy consumption profiles are needed for different days of the week, as patterns on weekdays vary significantly from those on Saturdays and holidays.

The second section of the chapter introduces different load forecasting methods tailored for use in rolling horizon optimization procedures. These methods combine historical data stored in the database with real-time measurements provided by advanced metering infrastructure. By continuously updating forecasts with the latest available data, these methods offer more reliable predictions of load consumption, improving the overall accuracy of REC operations.

In summary, this chapter presents a comprehensive approach to create standard consumption profiles and deploying load forecasting techniques, both of which are fundamental to the efficient design and management of RECs.

5.1 Available Dataset and Standard Profiles

The measurement campaigns carried out during the GECO and Self-User projects lead to the creation of a considerable dataset of consumption measurements. This dataset comprises data from various types of consumers at different levels of aggregation, enabling the characterization of diverse consumption profiles. This aspect is fundamental in the planning stage of a REC as it allows to test different configurations of PV installations and BESs as well as different member compositions of the REC facilitating an effective estimation of the self-consumption and energy sharing ratios.

The load profiles described in this section encompass a range from residential to industrial consumers. Residential data were collected both at the individual user level and in aggregated form, utilizing NILM and DU meters concurrently. Non-residential loads monitored include office buildings, cold storage units in a fruit and vegetable warehouse, and an exhibition area. Additionally, data were gathered at the feeder level of primary substations, with information on the secondary substations supplied in the area.

The standard profiles are obtained following a systematic procedure:

i. Data cleaning: the raw data can contain not-a-number values, missing data or anomalous measurements due to connection issues or malfunctioning SMs. Anomalous data, such as values outside of realistic ranges or measurement “stuck”, i.e. the values are repeated in time. These data are removed from the dataset to prevent skewing the standard profile.

ii. Data filling: after the data cleaning step, if the dataset contains only short missing intervals, the gaps are filled using interpolation. However, if a significant time interval is missing, the entire day's data is discarded.

iii. Data fitting: collected data span from the 1 s timescale of NILM to the 15 minutes of DU. For standard profiles creation, a 15-minute timescale is adopted. Thus, the average value is considered for data collected on a lower timescale.

iv. Creation of day-type profile: for each month days are classified per day-type, i.e. weekday, Saturday and Holidays. The choice of differentiating weekend days on Saturday and Holidays is related to the possible different behavior linked to the customer monitored: some users may behave differently in these days, such as activities that are open on Saturday morning but not on Sunday. Holidays of the area in which the customer is located must be accounted, in the case of customers located in Bologna the festivity of San Petronio (4th October) is considered. For each, day-type profiles are generated by averaging the data for each respective day type.

v. Reconstruction of the yearly profile for a specific year: The day-type profiles are used to construct an annual profile, incorporating the specific holidays for that year. The final profile is normalized to a yearly consumption base, set at 1 MWh/year for our purposes.

5.1.1. Residential buildings

Electricity consumption within individual domestic households is highly dependent on occupancy levels and the corresponding use of electrical appliances. Daily activity patterns can vary significantly from household to household as they are influenced by habits and the working status of each family member [153]. Therefore, it is not feasible to define a single standard consumption profile at the individual customer level. Even synthetically generated profiles must align with user-specific patterns to reflect unique consumption behaviors. However, when aggregating residential customers, it becomes possible to define a standard profile applicable to the customer cluster.

The residential measurement campaign involves an apartment building located in the municipality of Scandiano (Italy). Data collection started in September 2020 and continued up until May 2023, leading to the creation of a consistent dataset. The SMs employed are of NILM type and were installed in the framework of Self-User project. A total of 56 NILM meters were installed, of which 13 monitored appliances serve common services and areas, such as lighting, elevators, heating, and ventilation systems. The collected data has a 1 s resolution.

Additionally, a second measurement campaign was carried out as part of the GECO project. This campaign involved eight residential customers located in the Pilastro district of Bologna, Italy. In this case DU meters were employed. The measurement campaign started in January 2022 and concluded in September 2023, the monitored customers, in contrast to Self-User project do not belong to the same building but are sparse in the Pilastro district.

Figure 5.1 illustrates the consumption power profile of a residential user belonging to the Scandiano apartment building. The profile is characterized by a base load around 300 W with periodic spikes typical of a fridge. During daylight hours some high-load spikes are present that indicates the presence of people in the apartment and the use of high-power appliances as dishwasher, washing machine, oven, iron or hairdryer. The use of NILM enables the detection of short-duration power peaks, which can be leveraged to disaggregate overall load consumption and identify the electrical footprint of individual household appliances [154]. However, this specific application falls outside the scope of our current analysis.

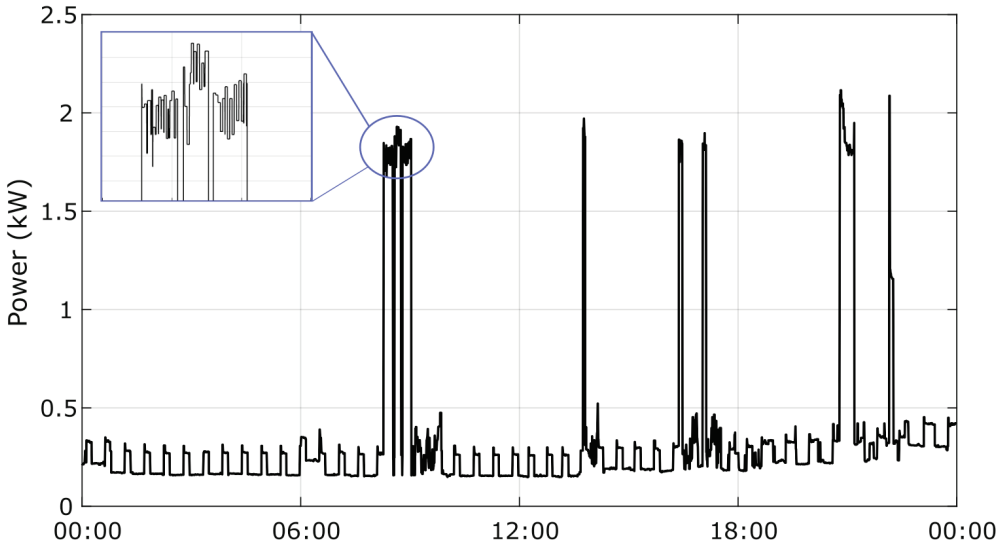

Figure 5.1 Load of residential consumer measured with NILM meter

Figure 5.2 illustrates the consumption power profile of a set of appliances serving the common areas. The load consumption is almost flat during the night, several spikes start to appear in the morning when people leave the building likely to go to work. Spikes are present also in the late afternoon and during the evening. According to the power value and spikes duration it is

reasonable to assume that they represent the stairs lighting. During the afternoon a reduced-power load is connected for a few hours resulting in a step in the base load.

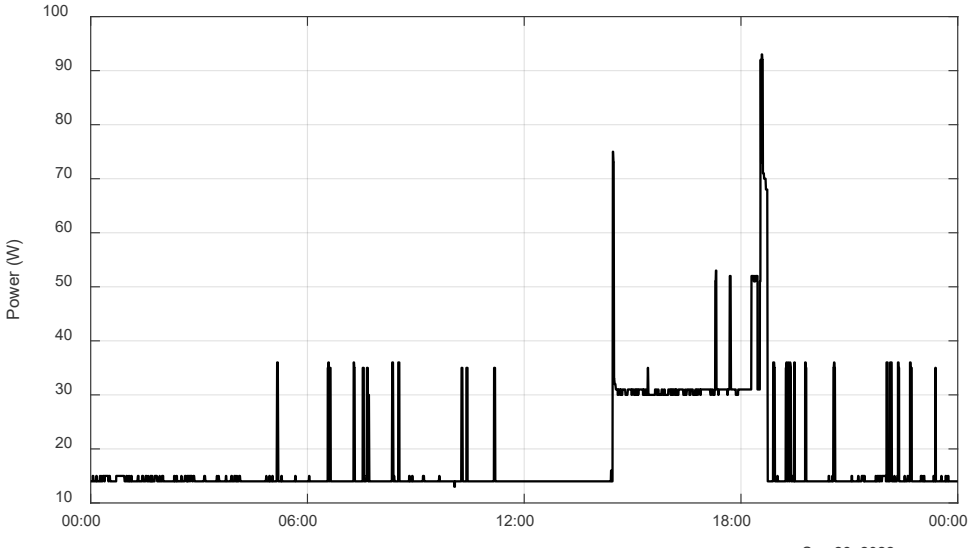

Figure 5.2 Apartment building common areas' consumption measured with NILM meter

Figure 5.3 shows the aggregated load profile, which is significantly different from that of an individual dwelling. The aggregate profile is obtained by summing the data received from both households and common areas meters. This profile is characterized by a valley, representing low consumption, during the night hours and a by a consumption peak during the evening. The evening peak is typical of residential profiles as it coincides with the time most residents return home from work. It is common to find residential profiles to exhibit two peaks, one in the late morning and another in the evening; however, this is not the case for the day represented here.

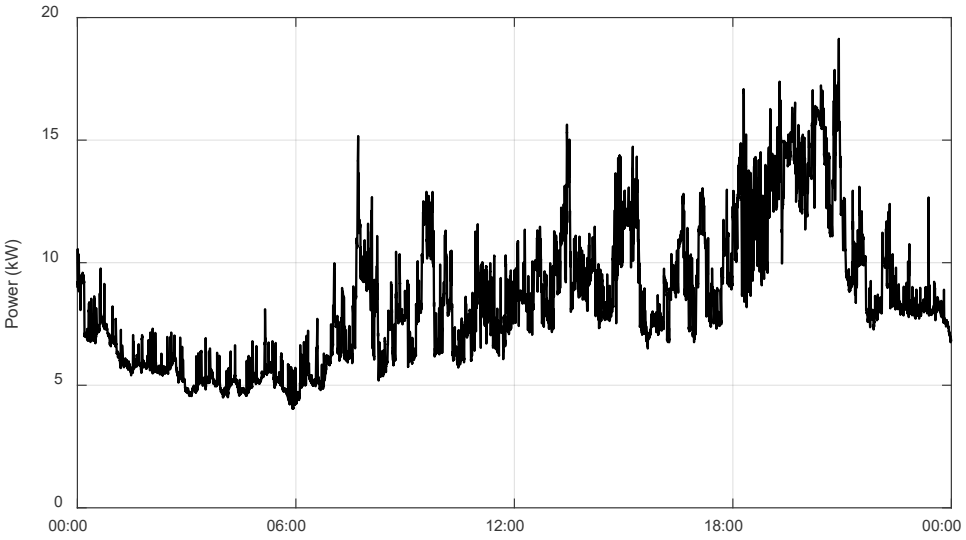

Figure 5.3 aggregate consumption of the apartment building

Starting from the aggregated profile and applying the standardization procedure described above, standard profiles are obtained for each month. The profiles vary month by month in both pattern and values. This variation is largely due to changes in the usage of electrical appliances influenced by different weather conditions. For example, the use of heat pumps or air conditioning is directly correlated with perceived temperature and its fluctuations [155]. Additionally, variations in daylight hours and the tendency to spend more time outdoors can alter consumption patterns.

Figure 5.4 illustrates the standard profiles obtained for two distinct months, April and July respectively. Two main differences need to be highlighted: first, the April holiday profile (blue line) exhibits two load peaks instead of the evening peak only. Second, the consumption in July, characterized by higher temperatures, is noticeably higher compared to April, which generally experiences more comfortable temperatures. Moreover, during weekdays, consumption tends to be lower than on weekends, as people spend more time at home.

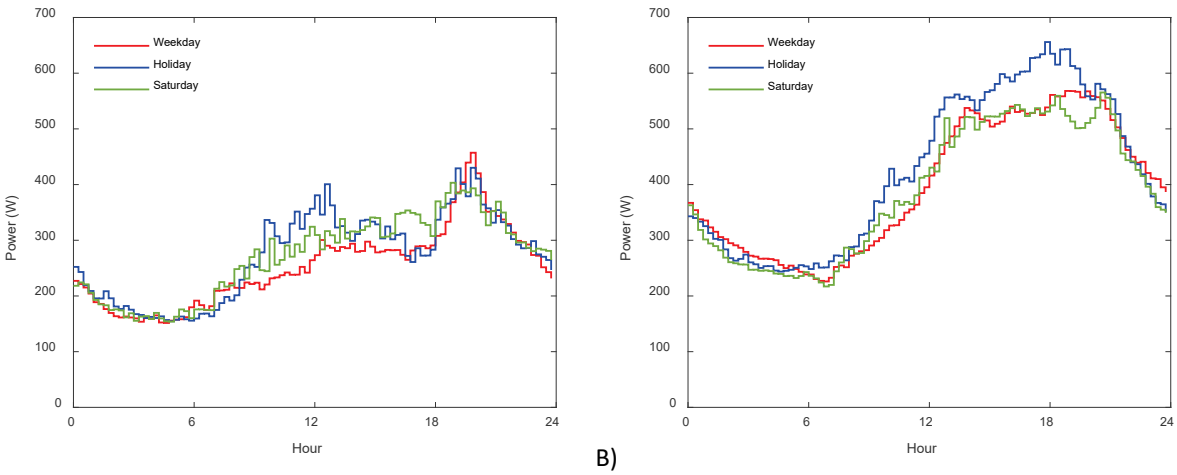

A) B)

Figure 5.4 Residential standard load profile. A) April. B) July.

If no measurements are available, an additional possibility to generate load profile to be used in REC sizing is to adopt profiles available in literature. As the developed project are located in Italy, profiles made available by the Italian energy service manager, i.e. Gestore dei Servizi Energetici – GSE, are employed. These profiles are yearly updated and are used by the GSE to reconstruct the consumption (or production) profile, to allocate economic incentives, if measurements from DSO's fiscal meter are not received. The first version of the document was published in 2022 [156], the information contained in the document is still in-force however, the profiles have been updated: profiles for the years 2023 and 2024 are available at [157], [158], respectively. Figure 5.5 shows the comparison between the hourly average of the measured aggregated profile and the estimated consumption obtained employing the curve provided by the GSE. The main difference is in the matching of the evening peak as the profile estimated from GSE curves is characterized by a lower peak shifted ahead in time.

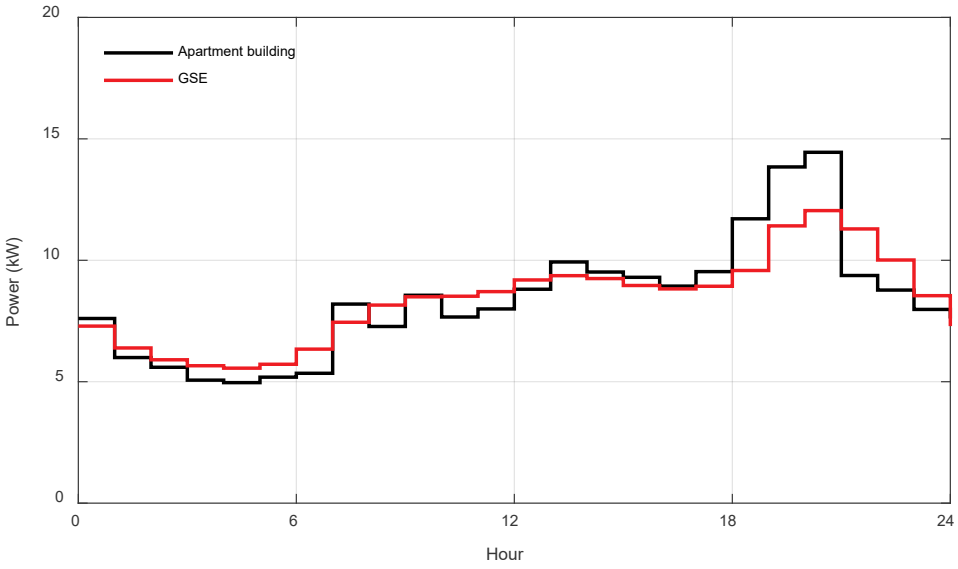

Figure 5.5 Measured load consumption (black) and estimated consumption from GSE curve (red)

5.1.2. Offices

The office profile is obtained from the measurement collected from NILM meters in the Self-User project framework. The monitored office is closed on Saturday, thus only two standard profiles for each month have been adopted: one for the working days and the other for the weekend days and holidays. Profiles for working days and weekends are shown in Figure 5.6-A and Figure 5.6-B, respectively. During weekends and holidays no activity is present in the office, this results in a flat consumption profile almost constant during the year. The profile of the working days has a bell shape with a valley at lunch time. During the night the consumption is flat as on non-working days, while it starts to rise around 8 a.m. when people start to work. After 9 p.m. the consumption profile returns flat. The peaks of the working days consumption vary throughout the year, the months characterized by a larger consumption are July and June.

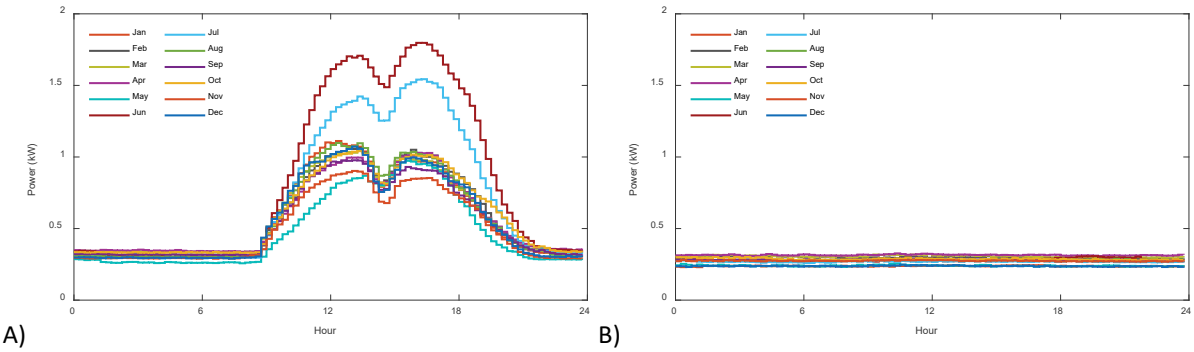

Figure 5.6 A) Office standard profiles A) working days, B) weekend days and holidays

5.1.3. Warehouse prosumer

The CAAB area, monitored within the GECO project framework, exhibits substantial energy consumption due to the presence of numerous cold-rooms and offices equipped with analysis tools used for food quality testing. The market operates predominantly at night when trucks deliver fruit and vegetables, and early in the morning when resellers arrive to purchase goods. Figure 5.7 illustrates the consumption profiles for both cold-rooms and the associated offices (negative values indicate consumption). The cold-rooms are characterized by large power spikes corresponding to the start-up of cooling systems. Unlike traditional office consumption patterns discussed earlier, the offices and laboratories at the market remain operational during the night, resulting in significant energy consumption both during nighttime hours and in the early morning.

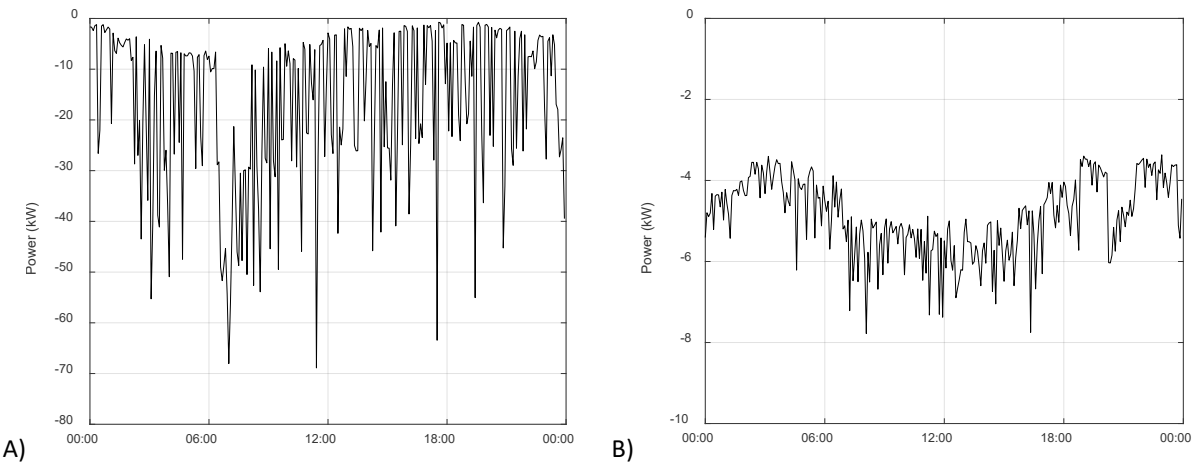

Figure 5.7 A) cold-room consumption profile; B) Office-laboratory consumption profile

As mentioned in section 4.1.1, the CAAB area is of particular interest due to the significant presence of PV installations. Many customers in the area are prosumers, allowing for the characterization of profiles having both consumption and injection. The standard profiles presented below are derived from data collected from three prosumers, two of which have PV systems with a rated power of 200 kWp each, while the third has a PV system with a rated power of 450 kWp.

Figure 5.8-A and Figure 5.8-B illustrate the obtained standard profiles for working days and weekend days, including holidays. While the overall trend is similar, the energy consumption during weekends is lower. Due to the considerable PV production, the energy withdrawn from the grid during daylight hours is negligible, except for months like January and February, which are characterized by weak solar radiation. However, even during these months, the energy consumption during daylight hours remains limited. These profiles are representative of users with PV system whose production consistently exceeds consumption.

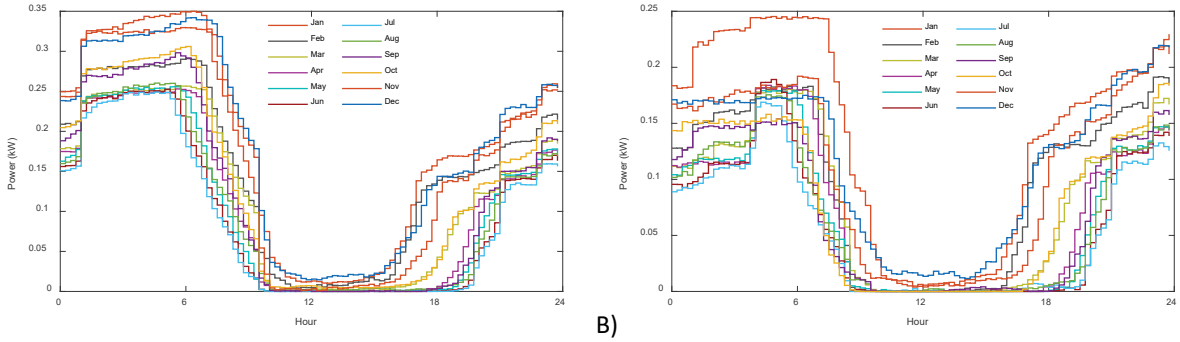

A) B)

Figure 5.8 CAAB prosumer standard profiles A) working days, B) weekend and holidays

The GSE proposes standard profiles for non-residential customers equipped with PV system in [157]. However, these profiles shown in Figure 5.9 differ from those derived from CAAB data, as they exhibit non-zero consumption during daylight hours, indicating that PV generation does not fully meet the prosumer's load. Additionally, the trend of these profiles differs significantly. For this reason, the knowledge of a customer's specific consumption habits is fundamental to selecting the appropriate profile to employ in the load estimation procedure.

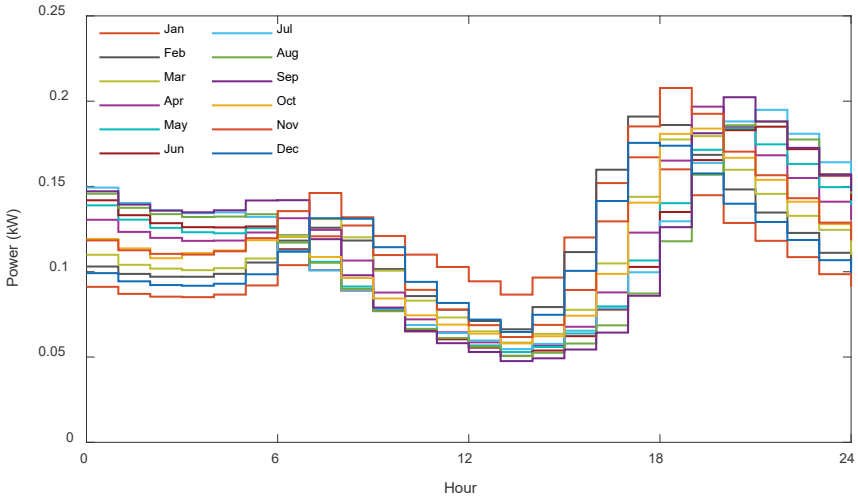

Figure 5.9 GSE standard profiles for non-residential prosumers equipped with PV system

5.1.4. School

The school profiles are obtained by joining profiles available in literature [159] and adapting them to the school calendar and vacation periods, which typically span more days than other working activities. The profiles for working days are illustrated in Figure 5.10-A, during the months in which the school activities are open the profiles exhibit a bell-shape with tail in the afternoon when the activity is reduced. During July, working day profiles resemble those of Saturdays, as school activities are limited. While in August the school is closed, thus, the profile aligns to holiday one, illustrated in Figure 5.10-C. The profile for Saturday, illustrated in Figure 5.10-B is characterized by lower peak respect to working days, also in this scenario the August Saturdays are equal to holidays.

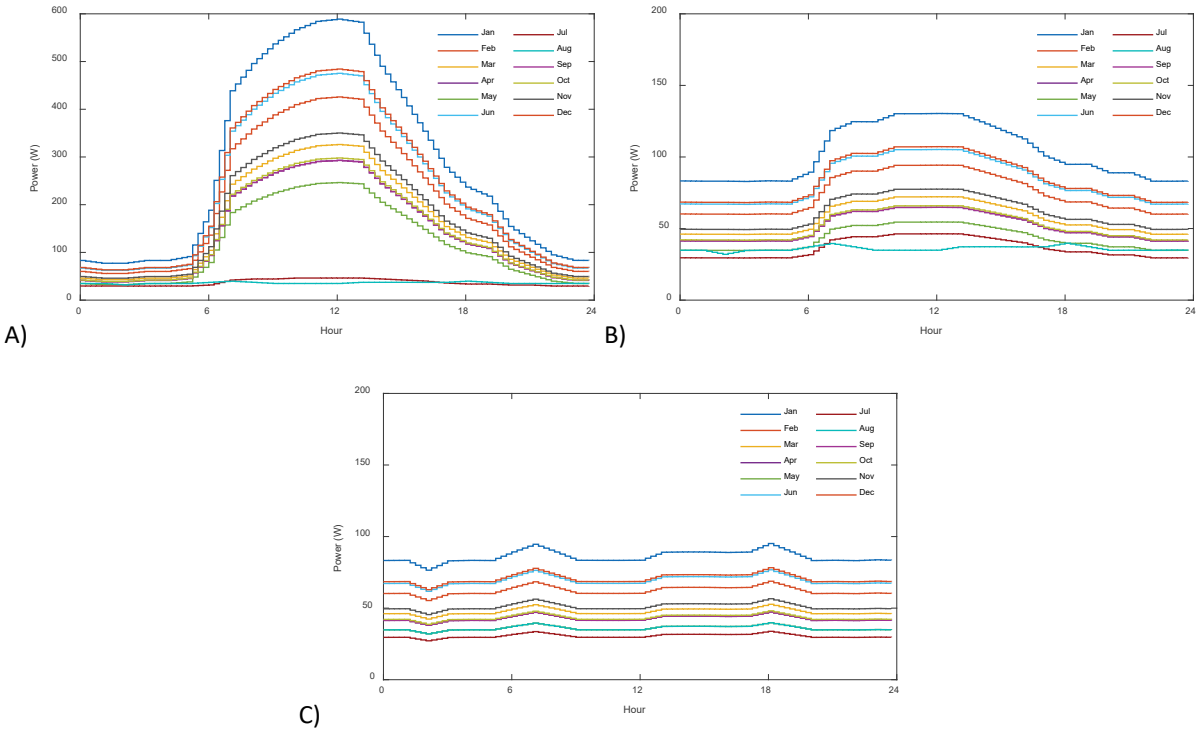

Figure 5.10 Schools standard profiles A) Working days, B) Saturdays, C) Sundays and school Holidays

5.1.5. Medium-Voltage feeders and primary substations

In the context of GECO project the consumption pattern at district level has been analyzed. The consumption data of the two primary substations feeding the Pilastro and Roveri districts are analyzed. The data collected from January 2020 to December 2021 have a time resolution of 10 minutes. The gathered data encompasses the power measured at the starting point of each MV feeder at primary substations, the overall power of the transformers in the primary substation, the information of the supplied secondary substations by each feeder and the information of the user connected to each secondary substation. For each secondary substation the following data are available:

- CP_Den: primary substation which fed the secondary substation
- Linea_Den: feeder which fed the secondary substation
- Address
- Nodo_Cod: identifier of the substation

- Latitude and longitude
- n_TR: number of transformers installed (0 means transformer owned by final customer and not by the DSO)
- Pot_tot: total power of the installed transformers
- Tot_cli: total number of customers connected to the substation
- CFT_Den: identifier of the technical area jurisdiction
- BT_n_UT_mon: n° of single-phase LV users
- BT_pot_UT_mon: total contractual consumption power of single-phase LV
- BT_n_UT_tri: n° of three-phase LV users
- BT_pot_UT_tri: total contractual consumption power of three-phase LV users
- BT_n_prod: n° of LV prosumers
- BT_pot_prod: total power that can be injected into the grid by LV prosumers
- MT_N_cli: n° of MV users
- MT_Pot_prel: total contractual consumption power of MV users
- MT_Pot_imm: total injectable power by MV prosumers
- MT_Pot_imm: aggregated nominal power of the MV prosumers generators

As the project started during the Italian temporary regulation on REC, i.e. the proximity limits for the members was the secondary substation, an interactive map has been realized to facilitate the identification of the candidates eligible to join the REC in a specific location. The map is illustrated in Figure 5.11, each pin placeholder represents a secondary substation; by clicking on the placeholder a pop-up appears and shows the information of the selected secondary substation. The area is covered by two different primary substations named *Quarto Inferiore* and *San Donato,* identified by circle placeholder. As mentioned in section 3.3.1, in

2021 the proximity constraint for REC member has been extended to the primary substation, thus placeholder supplied by the same primary substation are painted with the same color giving a preliminary and immediate idea of the area coverable with a unique energy community. The tool illustrated in the figure hereafter was developed before the publication of the conventional areas covered by primary substation on the GSE website (available at https://gse-sta.maps.arcgis.com/apps/webappviewer/index.html?id=ecd9746921164f03868b2c47a8d41235).

Figure 5.11 primary and secondary substations supplying the Pilastro and Roveri districts.

By aggregating the information of secondary substations at feeder level (see Table 5.1) it results that the distribution of total load power across feeders is not uniform. Feeders such as 'Alim 2' and 'Pilast' are devoted to supplying customers having an overall contractual power an order of magnitude higher than those of feeders like 'Cadran'. Similarly, the number of supplied customers varies: 'Pilast' and 'Fiesso' serve nearly two thousand LV users, whereas 'Alim 1' and 'Poligr' serve only a few dozen. Feeders 'Alim 1' and 'Alim 2', which supply the CAAB-FICO area, host the highest generation capacity, with over 10 MW of installed PV facilities, accounting for almost half of the district's total generation.

The data on the number of clients per connection type and their corresponding contractual power can provide insight into the type of customers connected to the substation. A high number of LV single-phase users typically indicates a residential area or one with small businesses. In contrast, a significant number of LV three-phase or MV users suggests the presence of industrial, commercial, or craft sectors characterized by a higher energy demand.

Table 5.1 contractual power, number of customers, generators rated power by connection type per feeder.

Primary Substation	Feeder	LV Single-phase power (kW)	n° of LV single-phase users	LV 3-phase power (kW)	n° of LV 3-phase users	LV Generation (kW)	n° of LV prosumer	MV power (kW)	n° of MT users	MV Generation (kW)	Tot. Power (kW)	Tot. Generation (kW)
QUARTO I.	ALIM1	18	5	2671	55	1256	13	5249	14	4168	7938	5277
QUARTO I.	ALIM2	193	57	3324	80	867	12	7114	18	4959	10630	5259
QUARTO I.	CADRAN	522	152	563	30	76	14	186	2	1000	1271	1076
QUARTO I.	ERRE	111	30	2410	59	489	11	1083	5	399	3604	889
QUARTO I.	FIESSO	5775	1769	3450	186	759	87	419	2	16	9643	775
QUARTO I.	FRULLO	473	151	827	29	6	1	1056	3	126	2356	132
QUARTO I.	INCENE	0	0	0	0	0	0	5609	3	144	5609	142
QUARTO I.	MONTI	2596	807	1979	141	86	24	3753	6	999	8328	1085
QUARTO I.	NOVA	1290	400	5191	200	385	24	2248	4	2734	8729	2565
QUARTO I.	POLIGR	39	8	815	14	90	1	4148	3	109	5002	189
QUARTO I.	TELECO	208	64	1659	58	122	4	7066	4	2833	8933	504
S. DONATO	CAB1	968	337	3040	63	194	3	4097	12	291	8105	486
S. DONATO	CAB2	176	56	1204	12	0	0	1496	4	0	2875	0
S. DONATO	CARLIN	132	41	2520	50	210	4	5755	7	140	8407	350
S. DONATO	COLAMA	396	117	2127	66	44	4	1640	5	0	4163	44
S. DONATO	DATI	0	0	0	0	0	0	2000	1	0	2000	0
S. DONATO	FOSOLO	645	191	1577	60	96	9	2009	5	177	4230	288
S. DONATO	LARGA	878	260	3600	125	132	13	5765	15	1622	10243	1506
S. DONATO	MACELO	3807	1259	1228	118	0	0	445	1	0	5480	0
S. DONATO	PEEP	2609	809	2923	115	150	25	2701	4	0	8233	150
S. DONATO	PIANET	123	40	1706	58	166	6	3294	6	164	5123	331
S. DONATO	PILAST	4547	1482	3021	181	35	8	4026	5	264	11594	299
S. DONATO	ROVERI	671	186	5451	179	689	41	2637	11	0	8758	689
QUARTO I.	**TOTALE**	**11224**	**3443**	**22888**	**852**	**4136**	**191**	**37931**	**64**	**17487**	**72042**	**17894**
S. DONATO	**TOTALE**	**14950**	**4778**	**28396**	**1027**	**1717**	**113**	**35865**	**76**	**2660**	**79211**	**4142**

The power values obtained by current and voltage measurements in feeders are significantly lower than the overall contractual power of customers due to usage and contemporaneity factors. In Figure 5.12 and Figure 5.13 are represented the power measurement of the first week of April for the year 2019 and 2020 in the feeders ‘Roveri’ and ‘Macelo’, respectively. To facilitate comparison, the 2019 profile has been time-shifted to align weekday and weekend days.

The ‘Roveri’ feeder serves the homonym industrial-artisanal area with 25 secondary substations; the number of customers supplied, divided in single-phase LV, three-phase LV and MV, is 186, 179 and 11 respectively. The total contracted power is 671 kW, 5.5 MW, and 2.6 MW, respectively. The power profile is typical of an artisanal area: looking at the 2019 profile, the black one, consumption is concentrated in the day-hours of working days, toward midday-1p.m. there is a dip in concurrence with launch time. On Saturday morning some activities are open, and a smaller peak is present. On Saturday afternoon and during Monday the consumption is reduced, a reversed bell shape valley is present that is compatible with the production of PV installations in the feeder for an overall rated power of 689 kWp. The 2020 power profile (blue) reflects the impact of the Covid-19 pandemic, as many businesses were closed or operating at reduced capacity. This resulted in a substantial decrease during working days’ consumption. Weekend consumption remained relatively consistent.

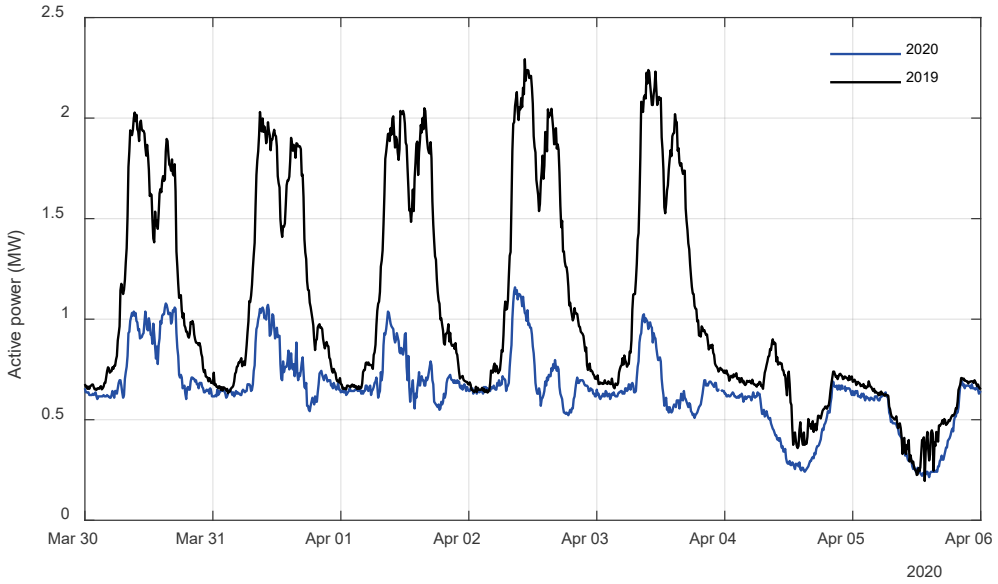

Figure 5.12 feeder ‘Roveri’ power profile, years 2019 and 2020

The ‘Macelo’ feeder supplies six secondary substations in a residential area with a consistent presence of apartment buildings. The number of single-phase LV customers is relevant: 1259 for an overall power of 3.8 MW; the three-phase LV users are 118 for a total power of 1.2 MW, which is less than the single-phase customers one. There is only 1 MV user that has a contractual power of 445 kW. In the feeder there is no generation, neither in LV nor in MV.

The power profile of the 'Macelo' feeder aligns with typical residential consumption patterns, exhibiting an evening peak. Additionally, due to the predominantly residential nature of the area, the consumption peaks are relatively consistent across weekdays. In contrast to the ‘Roveri’ feeder as during lock down period most people were at home the 2020 consumption profile results higher than 2019 one.

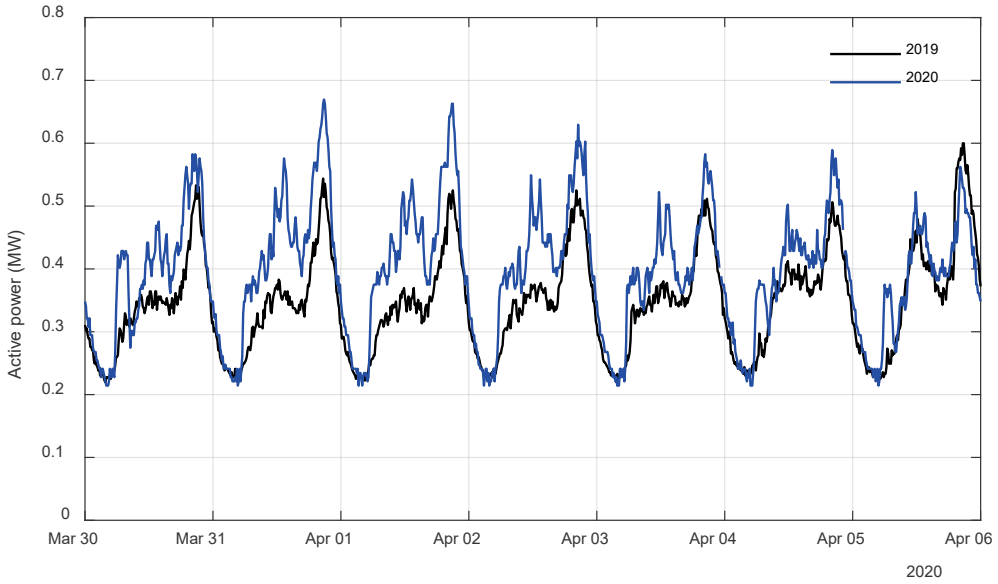

Figure 5.13 feeder 'Macelo' power profile, years 2019 and 2020

In feeders to which are connected generation systems whose aggregated rated power is significant with respect to the consumption it may happen to observe the power flow reversal in the feeder, i.e. the feeder is supplying energy to the primary substation busbar. This phenomenon can be observed in the two feeders supplying the CAAB area, i.e. 'Alim1' and 'Alim2'. Figure 5.14 shows the daily power profile (black curve) of feeder 'Alim1', during the morning a reduction in the power consumption up to zero can be observed. As production continues to increase the current measured at the starting point of the feeder change sign.

The knowledge of the nominal power of PV generators in the area and the measurement performed at the primary substation level facilitate the estimation of the real load unbundled from the local generation. The process is carried out employing the PVGIS [130] historical data of the corresponding year to estimate the PV generation, then adding the estimated generation to the measured power the gross load is estimated. The figure hereafter shows in blue the measured power, in red is represented the estimation of the local generation while in black the load consumption.

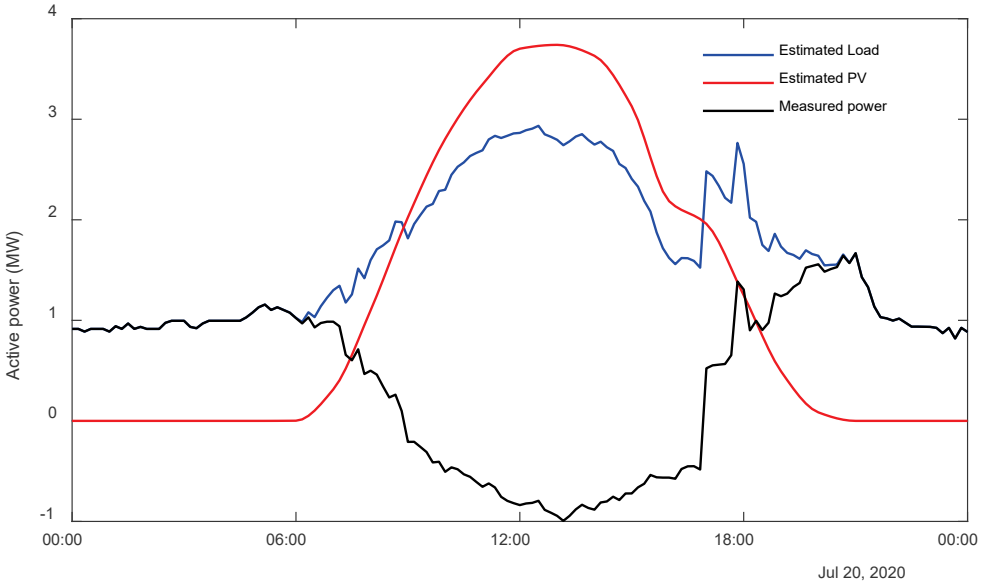

Figure 5.14 feeder 'Alim1' measured power, estimated PV production and estimated load

5.2 Load Forecast for Rolling-Horizon Optimization

Alongside PV production forecast also an accurate load prediction is fundamental for the optimal management of BESs within RECs, facilitating savings in energy procurement cost [160]. Although precise short-term load forecasting in RECs is more challenging compared to grid-scale systems due to the smaller capacity and higher randomness [137], [161]. In larger grids, the abundance of consumers allows for statistical smoothing and more stable predictions. However, at the REC scale, the unique behaviors of individual residents introduce greater variability, making load forecasting more susceptible to fluctuations. As a result, precise forecasting methods tailored to these community-specific factors are essential for optimizing energy management and achieving economic benefits for REC members.

Traditional forecasting methods primarily rely on historical load and meteorological data from the previous days to build models, often lacking real-time data updates. However, incorporating real-time information from the current day can significantly enhance prediction accuracy [162]. Therefore, a rolling update load forecast approach, which continuously updates the model's input data throughout the day using known real-time information by SMs, improving the precision of load forecasts, is employed. As the main purpose of the load forecast is to support the optimal management of BESs, a balance must be achieved between the advantages of a longer forecast horizon and the computational demands of the algorithm, as well as the forecast's accuracy. In the proposed method, a 48-hour time window is adopted. Following a common approach [138], [163], the days of the week have been clustered in weekdays, Saturday and holidays to better align with customers' consumption patterns.

Various load forecasting methods have been developed and tested. The approaches discussed in sections 5.2.1, 5.2.2 and 5.2.3 are based on a base forecast profile derived from the average measured profiles of previous days. At each iteration i, the load forecast $L^f_{t,i}$ is updated employing the base forecast profile L^f_t and a weighting factor k_i whose calculation is described in the following sections.

$$L^f_{t,i} = L^f_t \cdot k_i \qquad (5.1)$$

In addition to the methods based on the former day average, a short-term load forecast employing a Seasonal Autoregressive Integrated Moving Average (SARIMA) model has been developed (see section 5.2.4). The SARIMA model [164] is capable of tracking the characteristic periodicities of electrical load, i.e. daily, weekly, and seasonal patterns [165]. The SARIMA model is fitted using the historical data of the customers collected in the DB. The forecasts are continuously updated at each optimization step by incorporating the latest available load measurements.

5.2.1. Average

The first method (referred to as method *a*) assumes that the load consumption profile for a given day is equal to the average consumption profiles from a specific number of prior days belonging the same day type, weekday, Saturday or holidays. In the proposed procedure the three former days are used to calculate the average profile, however this number can vary. With this approach no adjustments are made by the EMS during intra-day optimization. Thus, the scaling factor for this method remains constant at 1. The use of a scaling factor will be clarified in the two subsequent methods (see sections 5.2.2 and 5.2.3).

$$L_t^f = \sum_{d=1}^{D} \frac{L_{t,d}}{D} \qquad \forall t \in T \qquad (5.2)$$

L_t^f is the load forecast at time step *t*.

$L_{t,d}$ is the load measured at time *t* in the former day *d* of the same type.

D is the number of former days to be used in the average

T is the forecast time-window

$$k_i = 1 \qquad (5.3)$$

5.2.2. Constant daily energy

This method (referred to as method *b*) introduces an intraday adjustment to method illustrated in section 5.2.1. It assumes that the total energy consumed by the end of the

current day is equal to the daily energy of the profile obtained with the previous forecasting method. This is the case of a customer having regular daily energy consumption with activities performed at different times. Therefore, method *b,* in case of lower consumption in the first part of the day will forecast an increase in power absorption in the remaining part of the day as show in Figure 4.15.

At each load forecast iteration *i*, the load forecast profile is scaled by a factor calculated according to the following equation:

$$k_i = \frac{E^{f,tot} - E_i^{cum}}{E^{f,tot} - E_i^{f,cum}} \qquad (5.4)$$

where:

$E^{f,tot}$ is the daily energy forecast to be consumed in the current day

E_i^{cum} is the amount of energy effectively consumed by the beginning of the day to current time step.

$E_i^{f,cum}$ is the cumulated energy forecast expected to be consumed from the beginning of the day to the current time step.

To avoid large deviations from the forecast profile elaborated in the former iteration, i.e. *i-1*, the scaling factor *k* is limited between 0.8 and 1.2. Thus, the profile can be reshaped within ±20% of the original forecast profile.

5.2.3. Proportional consumption

This method (referred to as method *c*) considers that energy consumption in the rest of the ongoing day follows the trend observed by the beginning of the day up to the current time. The forecast profile is then reshaped by applying a scaling factor which is calculated as follows:

$$k_i = \frac{E_i^{f,cum}}{E_i^{cum}} \qquad (5.5)$$

the variables present in equation (5.5) are the same introduced in equation (5.4). As in the former case the scaling factor *k* is limited between 0.8 and 1.2.

The three methods and their effects on reshaping the load power profile are schematically illustrated in Figure 5.15. In the proposed example, the energy consumed by midday is lower than the forecasted amount. Method (*a*) is represented in solid black line, no adjustments are made to the forecast, so the profile remains unchanged. In method (*b*) the yellow area on the left represents the difference between the forecast and actual consumption up to the current time step, denoted as $E_i^{f,cum} - E_i^{cum}$. In this method, is assumed that this difference will be consumed by the end of the day (yellow area on the right) corresponding to $\left(k_i - 1\right) \cdot \left(E_i^{f,tot} - E_i^{f,cum}\right)$. Method (*c*) assumes that the reduced consumption measured so far will continue for the rest of the day, adjusting the forecast downward to reflect this trend.

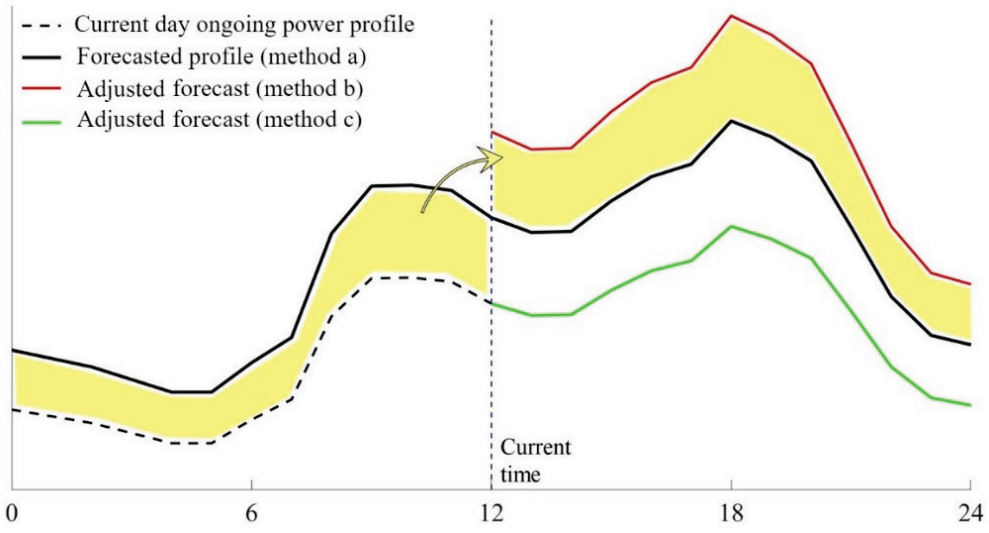

Figure 5.15 Measured load consumption and forecast profiles by methods *a*, *b* and *c*

5.2.4. SARIMA

The SARIMA model is a widely used time series forecasting technique that extends the ARIMA framework to account for seasonality in data. By incorporating seasonal differencing and seasonal autoregressive and moving average components, SARIMA provides a robust approach for modeling and predicting complex seasonal patterns [165], making it suitable for load forecasting in power systems. Load demand, which often exhibits daily, weekly, or yearly seasonality, can be effectively predicted using SARIMA by capturing both the underlying trend

and cyclic fluctuations [166]. For the EMS implementation purposes the focus is on short-term load forecast, particularly a forecast of 48 hours ahead.

The SARIMA model combines the concept of seasonality with autoregressive, integrated and moving average components. The seasonal component identifies the repeating patterns at regular intervals, like daily or weekly trends. The autoregressive part captures how current data points relate to their past values. The integrated component applies differencing to make non-stationary data stationary, i.e. the value of time series is not dependent on time [167]. Lastly, the moving average component models the relationship between the current data point and past errors, helping to account for short-term variations and noise in the data. The compact representation of a SARIMA model is commonly expressed as $SARIMA(p, d, q)(P, D, Q, s)$ [168] where:

p and *P* are the order of the autoregressive and seasonal autoregressive components, respectively

d and *D* are the order of the integrated and seasonal integrated components, respectively

q and *Q* are the order of the moving average and seasonal moving average components, respectively

s is the seasonal period

The mathematical formulation of the SARIMA model is reported in equation (5.6).

$$\left(1-L-\ldots-\phi_p B^p\right)\left(1-\sum_{h=1}^{P}\phi_{h\cdot s}L^{h\cdot s}\right)\cdot\left(1-L\right)^d\cdot y_t=\left(1+\theta_1 B+\ldots+\theta_q B^q\right)\cdot\left(1+\sum_{h=1}^{Q}\Theta_{h\cdot s}L^{h\cdot s}\right)\cdot\varepsilon_t \quad (5.6)$$

where *L* is the one-lag time delay operator.

An example of the 48-hour ahead SARIMA forecast, for two different profiles, compared with the real measurements collected afterwards is shown in Figure 5.16. The SARIMA model is trained by employing historical data gathered from SMs. Prior to model training, the data must

be filtered and cleaned, employing a similar process as done for creating standard profiles. If there is a significant change in the customer's consumption pattern, the model may require retraining to maintain accuracy.

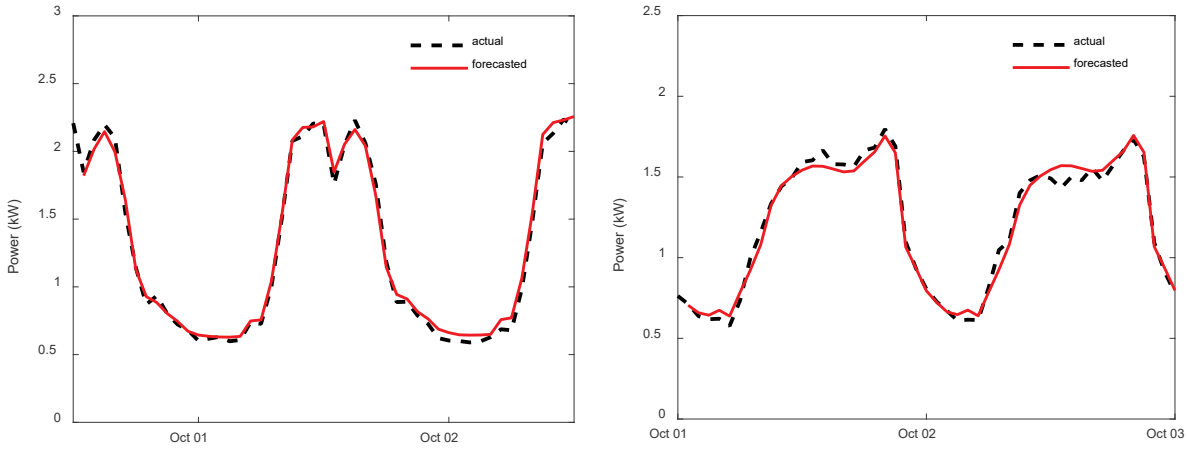

Figure 5.16 SARIMA load forecast compared to measured values

Chapter 6. Optimization Models for Renewable Energy Community's Energy Management System

Introduction

This chapter deals with the optimization models employable in the EMS to achieve the optimal operation of RECs. The proposed models are designed to be solved periodically, enabling them to incorporate updated PV and load forecasts, thereby enhancing the accuracy of the optimal power output for BESs. By regularly updating the input data, the models ensure a more accurate energy management maximizing the benefits for REC participants [169].

The chapter is divided into five sections. Section 6.1 introduces the prosumer models used in the optimization framework. These models reflect the regulatory-compliant metering schemes and are designed to represent the types of meters typically installed in real-world settings. Additionally, this section outlines the constraints related to BESs power and energy capacities, providing the foundation for the optimization formulation. Accurate modeling of prosumers and their energy storage systems is crucial for ensuring the realistic and feasible operation of the optimization algorithms.

Section 6.2 discusses two non-optimized algorithms, which serve as benchmarks for evaluating the performance of the proposed optimization models. The first benchmark algorithm implements a control strategy commonly integrated into commercial BMS, focusing on maximizing behind-the-meter self-consumption. The second benchmark model is designed to maximize the community self-consumption instead of the behind the meter one. By comparing the optimized models against these benchmarks, the chapter aims to demonstrate the improvements in efficiency and cost-effectiveness achieved through optimization.

Sections 6.3 and 6.4 present the optimized models developed for REC operation. The first model, introduced in section 6.3, seeks to minimize energy procurement cost for RECs in cases

where economic incentives are applied to shared energy, such as in the Italian regulatory framework. This model involves a non-linear formulation, and a linearization procedure is introduced to simplify the computational process. Section 6.4 expands on this by proposing a second linear optimization model, denoted as the 4-price model. This model is designed to minimize energy procurement cost in scenarios where a direct price agreement between consumers and producers is allowed. The model is also capable of approximating the performance of the incentivized energy-sharing model. Several case studies are presented to compare the performance of the optimized models with each other and with benchmark algorithms, providing a comprehensive evaluation of their effectiveness in real-world scenarios.

The last section of the chapter introduces a stochastic formulation to address the uncertainties inherent in load demand and PV generation forecasts. This formulation generates stochastic events, which are then handled using scenario-tree reduction techniques to manage the computational complexity of solving a large number of scenarios. Overall, this chapter provides a detailed examination of the proposed optimization models for the optimal operation of RECs, showcasing both deterministic and stochastic approaches.

6.1 Prosumer and BES models

The prosumer is modeled according to the scheme illustrated in Figure 6.1-A, the key elements are the load, PV system and storage system. In the proposed formulation the metering infrastructure employing two meters is adopted. However, a metering infrastructure employing three meters can also be employed (see Figure 6.1-B). In both configurations the exchange meter, denoted as M1, is bidirectional and measures the energy exchanged by the prosumer with the public grid. In the two-meter configuration the production meter, denoted as M2, encompasses both the PV system and BES. Thus, it must be bidirectional as the storage can be charged by withdrawing energy from the grid instead of from the PV system thereby this amount of energy cannot be considered from renewable sources. The possibility of charging the storage from the grid can be exploited to take advantage of favorable energy tariff during some hours or time slots of the day. In the three-meter configuration the production meter M2 covers only the PV system thus, it can be only mono-directional. In this scenario an additional bidirectional meter M3 is dedicated to the BES.

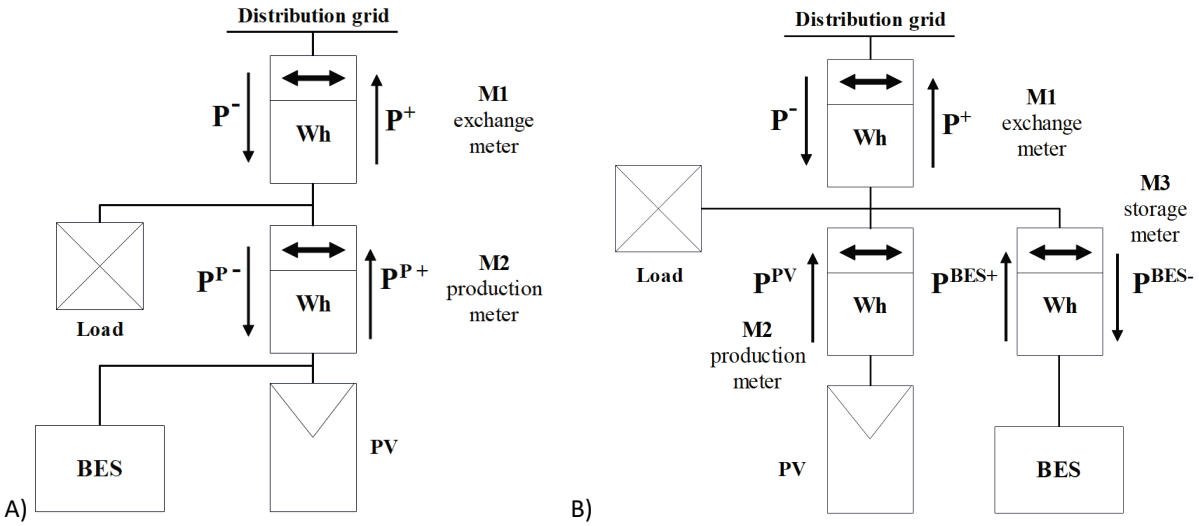

Figure 6.1 A) prosumer metering scheme employing two meters. B) prosumer metering scheme employing three meters. Adapted from [170]

The power balance for the exchange meter M1 and production meter M2 is represented by equations (6.1) and (6.2) respectively.

$$P_{t,j}^{+} - P_{t,j}^{-} = P_{t,j}^{P+} - P_{t,j}^{P-} - L_{t,j}^{S} \qquad (6.1)$$

$$P_{t,j}^{P+} - P_{t,j}^{P-} = P_{t,j}^{PV} + P_{t,j}^{BES+} - P_{t,j}^{BES-} \qquad (6.2)$$

where:

j and *t* are the prosumers and time indexes.

$P_{t,j}^{+}$ and $P_{t,j}^{-}$ are the measured power injected into and withdrawn from the public grid by prosumer *j* at time *t*, respectively

$P_{t,j}^{P+}$ and $P_{t,j}^{P-}$ are the measured power injected and withdrawn by the production meter of prosumer *j* at time *t*, respectively

$L_{t,j}^{S}$ is the load power forecast of prosumer *j* at time *t*

$P_{t,j}^{PV}$ is the PV power forecast of prosumer *j* at time *t*

$P_{t,j}^{BES+}$ and $P_{t,j}^{BES-}$ are the discharging and charging BES power prosumer *j* at time

All the aforementioned variables are non-negative. Additionally, variables belonging the same couple, i.e. $P_{t,j}^{+}$ - $P_{t,j}^{-}$, $P_{t,j}^{P+}$ - $P_{t,j}^{P-}$ and $P_{t,j}^{BES+}$ - $P_{t,j}^{BES-}$, cannot both be non-zero in the same interval *t* by the introduction of binary variables. This ensures the non-contemporaneity of injection and withdrawal or charging and discharging.

The BES power during both charging and discharging must be at maximum equal to the rated power $P_{j}^{BES,max}$ thus, constraints (6.3) and (6.4) are implemented. Moreover, equation (6.5) ensures that BES energy is comprised between minimum and maximum limits, i.e. $E_{j}^{BES,min}$ and $E_{j}^{BES,max}$, respectively.

$$0 \le P_{t,j}^{BES-} \le P_{j}^{BES,max} \qquad (6.3)$$

$$0 \le P_{t,j}^{BES+} \le P_{j}^{BES,max} \qquad (6.4)$$

$$E_{j}^{BES,min} \le E_{t,j}^{BES} \le E_{j}^{BES,max} \qquad (6.5)$$

The energy stored in the BES of prosumer *j* at each time step *t* is computed according to equation (6.6). Where Δt is the time interval occurring between two consequent time step and η_j is the efficiency of prosumer *j* BES. Efficiency is assumed to be equal in charging and discharging. $E_j^{BES,0}$ represents the initial energy stored in the BES. In the proposed approach the minimum allowed energy level for the BES corresponds to 10% of the capacity.

$$E_{t,j}^{BES} = E_j^{BES,0} + \left(\sum_{h=1}^{t} P_{h,j}^{BES-} \eta_j - \sum_{h=1}^{t} P_{h,j}^{BES+} \Big/ \eta_j \right) \Delta t \quad (6.6)$$

In the proposed formulation the initial SOC is treated as an input parameter enforced through a constraint. The choice of the final SOC is a critical aspect of rolling-horizon-based procedures, as it affects the BES power profile determined resulting by the optimization algorithm. In day-ahead approaches the final SOC, i.e. the SOC at the end of the day, is often set to a specific value (e.g. 50%). However, in rolling-horizon approaches (where rolling time-step is shorter than a day) setting a fixed final SOC may cause feasibility issues. In [171] it is proposed to constrain the final SOC to be equal to the initial one. However, if the current SOC is low with respect to the target one the necessary charge would limit the use of the BES for local load. Conversely, if the current SOC is high with respect to the target one an unnecessary discharge will be produced resulting in uneconomical operation [172]. The optimization models proposed in sections 6.3 and 6.4, employed in a rolling horizon fashion, do not contain a constraint on the final SOC because it is assumed that there is no economic convenience to reserve energy stored in the BES at the end of the time horizon as in case of possible islanded operation. The energy stored at the end of the time horizon $E_{T,j}^{BES}$, according to the proposed model, will result equal to $E_j^{BES,min}$ because the energy stored $E_{T,j}^{BES}$ does not represent a revenue. The solution is as if a constraint $E_{T,j}^{BES}$ equal to $E_j^{BES,min}$ were present. To deal with the uncertainty intrinsic of load consumption and PV production, the surplus energy discharge is scheduled, price being equal, towards the end of the time horizon. This strategy allows for postponing discharges as much as possible, enabling adjustments in subsequent rolling steps before the discharge actually occurs. This phenomenon is emphasized when 48-hour optimization time window is used: the potential energy surplus discharge is expected to occur on the second day. However, as the time horizon continuously rolls forward, the discharge is indefinitely postponed, ensuring that system performance remains unaffected. This approach

leaves margin to the optimizer to deal with unusual initial SOC or unexpected variations in solar irradiation and load consumption.

6.2 Non-optimized

In this section, two algorithms for BESs management are illustrated. The proposed algorithms do not make use of optimization procedures but instead rely solely on real-time measurements received from local measurements or SMs. These algorithms are used as benchmarks for the proposed optimization procedures discussed in the following sections.

The first proposed non-optimized algorithm (denoted as non-opt-1) employs a widely used control strategy of BES: when the prosumer's production exceeds its consumption the BES absorbs the surplus. Conversely when consumption exceeds production the BES delivers the power necessary to cover the shortfall. BES charge/discharge takes place only if the SOC is within the allowed limits and for power values not greater than the system's rated power. This approach leads to maximum behind the meter self-consumption. The control strategy relies on local measurement of PV and load or grid power exchange, this information due to their local origin is typically available through the direct connection of CTs to the BMS.

The second non-optimized approach (denoted as non-opt-2) aims to maximize the community self-consumption by coordinating the BESs of multiple prosumers as if they were a single centralized storage. The virtually aggregated BES absorbs the surplus power during production excess and covers deficits during production shortfalls. Each BES operates within its own rated power and SOC limits. Despite this method enables the minimization of energy import from the external grid from an economic point of view, in most of the regulations, the BES charge from another customer is not costless due to the difference between the selling and buying prices. Moreover, it is reasonable that the customer who invests in a BES and shares its capacity to provide benefits to other REC members or to the community expects in return a financial compensation.

6.3 Cost Minimization Incentive-based

6.3.1. Mathematical formulation

The EMS optimization function, defined in equation (6.7), aims to minimize the energy procurement cost for prosumers, considering the economic incentive recognized to the community for the shared energy. This objective function is suitable to be used in RECs optimization where an economic incentive for the shared energy is granted, this is the case of the Italian scenario.

$$OF = \sum_{\substack{t\in T \\ j\in J}} (\pi^{-}_{t,j} P^{-}_{t,j} - \pi^{+}_{t,j} P^{+}_{t,j}) \Delta t - \sum_{t\in T} I_E E^S_t \qquad (6.7)$$

where:

$\pi^{-}_{t,j}$ and $\pi^{+}_{t,j}$ are the prices agreed with the energy suppliers for the energy bought and sold, respectively. Suppliers for the energy sold can be different from the one for the energy bought.

E^S_t is the shared energy, defined by equations (6.8) and (6.9), in compliance with the Italian regulation.

I_E is the unitary economic incentive granted for shared energy.

As introduced in section 3.3.1 the shared energy is expressed as the minimum, in each hour, between the overall energy absorbed by the REC's members and the energy of renewable source produced by the REC's prosumers. Prosumers' own load is not taken into account in the calculation of the shared energy, because it already constitutes a saving on the bill and therefore receives no incentive, hence the shared energy is computed from the measurements of the exchange meters, i.e., M1 in Figure 6.1-A [99]. In the proposed formulation the incentive is taken constant and equal to 110 €/MWh.

The shared energy within the community is defined through constraints (6.8) and (6.9), that are more restrictive than the definition in [99] since the constraints are evaluated for each forecast period *t* instead of on a hourly basis.

$$E_t^S \leq \sum_{j \in J} P_{t,j}^{+} (1 - R_j) \Delta t \qquad (6.8)$$

$$E_t^S \leq \sum_{j \in J} P_{t,j}^{-} \Delta t \qquad (6.9)$$

where R_j is a correction factor that ensures the incentive for the shared energy is granted only for the energy provided by the renewable source. In the Italian regulation [99], [173], energy discharged from BES not generated by the local renewable source, it can still be injected into the grid but does not qualify for incentives, even if provided to another member of the REC. A monthly correction factor is computed to determine the ratio between energy supplied by the renewable source and energy stored from external sources, ensuring that renewable energy is incentivized only once. This is also the case of a customer recharging its BES using renewable energy from another REC member, the charging faces as a load, contributing to energy sharing. However, when this energy is later discharged, it is not counted towards energy sharing valorization, as it was already recognized during the charge phase. In the developed procedure, see equations (6.10) and (6.11), the correction factor is calculated over a 48-hour time horizon to reflect this regulation in the optimization process.

$$R_j \sum_{t \in T} P_{t,j}^{P+} = \sum_{t \in T} P_{t,j}^{P-} \qquad (6.10)$$

$$0 \leq R_j \leq R_j^{lim} \leq 1 \qquad (6.11)$$

The upper limit R_j^{lim} can be restricted to values lower than 1 to limit the BES grid-recharge rate.

It is worth noting that the proposed formulation includes bilinear constraints (6.8) and (6.10), thus the problem formulation is not linear. The non-linear formulation is solved in Matlab,

adopting the *Gurobi* 10.0 solver (see https://www.gurobi.com/). This solution is then compared to the results obtained through a linearized approach, which is proposed hereafter.

McCormick envelopes [174] have been used to obtain a linear approximation of the bilinear constraints. Thus, each bilinear constraint is replaced by a set of four inequalities. Additionally, to improve accuracy the domain of linearized variables is split into several subdomains, resulting in piecewise envelopes [175]. The choice of subdomains numbers is a tradeoff between desired accuracy and computational effort.

Equation (6.10) is replaced by the set of constraints (6.12)-(6.15), *m* is a binary variable which identify the "active" subdomain of the piecewise linearization; constraint (6.16) ensures that there is a unique "active" sub-domain.

$$Z_{j,n} \geq G_{j,n}^{L} K_{j,n} + G_{j,n} K_{j}^{L} - m_{j,n} G_{j,n}^{L} K_{j}^{L} \qquad (6.12)$$

$$Z_{j,n} \geq G_{j,n}^{U} K_{j,n} + G_{j,n} K_{j}^{U} - m_{j,n} G_{j,n}^{U} K_{j}^{U} \qquad (6.13)$$

$$Z_{j,n} \leq G_{j,n}^{U} K_{j,n} + G_{j,n} K_{j}^{L} - m_{j,n} G_{j,n}^{U} K_{j}^{L} \qquad (6.14)$$

$$Z_{j,n} \leq K_{j}^{U} G_{j,n} + K_{j,n} G_{j,n}^{L} - m_{j,n} G_{j,n}^{L} K_{j}^{U} \qquad (6.15)$$

$$\sum_{n} m_{j,n} = 1 \qquad (6.16)$$

where $G_{j,n}^{U}$ and $G_{j,n}^{L}$ are the upper and lower bounds for the *n*-th sub-interval of customer *j*. The bounds are obtained by dividing the interval 0- R_{j}^{lim} in *N* equally spaced sub-intervals. Lower and upper bounds of variable $K_{j,n}$ to are represented by equations (6.17) and (6.18), respectively, where $n°(T)$ is the number of considered time steps. Production meter injection is defined non-negative thus lower bound is 0 while the maximum value is given by the sum of BES and PV nominal power multiplied by the number of time periods contained in *T*.

$$K_{j}^{L} = 0 \qquad (6.17)$$

$$K_j^U = (P_j^{PV,max} + P_j^{BES,max}) \cdot n°(T) \qquad (6.18)$$

Constraints (6.19) and (6.20) force to be zero the variables belonging the non-active n intervals.

$$m_{j,n} G_{j,n}^L \le G_{j,n} \le m_{j,n} G_{j,n}^U \qquad (6.19)$$

$$0 \le K_{j,n} \le m_{j,n} K_j^U \qquad (6.20)$$

Equations (6.21) and (6.22) bind the variables used for the piecewise linearization to the production meter, i.e. M2, absorption and injection, respectively. The same applies to equation (6.23) which relates the McCormick envelopes to the penalization variable $\left(1 - R_j\right)$

$$\sum_n Z_{j,n} = \sum_t P_{t,j}^{P-} \qquad (6.21)$$

$$\sum_n K_{j,n} = \sum_t P_{t,j}^{P+} \qquad (6.22)$$

$$\sum_n G_{j,n} = 1 - \sum_n Y_{j,n} \qquad (6.23)$$

The same procedure applies to the second bilinear constraint (6.8) which is substituted by the set of equations (6.24)-(6.27).

$$W_{t,j,n} \ge Y_{j,n}^L X_{t,j,n} + Y_{j,n} X_j^L - m_{j,n} Y_{j,n}^L X_j^L \qquad (6.24)$$

$$W_{t,j,n} \ge Y_{j,n}^U X_{t,j,n} + Y_{j,n} X_j^U - m_{j,n} Y_{j,n}^U X_j^U \qquad (6.25)$$

$$W_{t,j,n} \le Y_{j,n}^U X_{t,j,n} + Y_{j,n} X_j^L - m_{j,n} Y_{j,n}^U X_j^L \qquad (6.26)$$

$$W_{t,j,n} \le X_j^U Y_{j,n} + X_{t,j,n} Y_{j,n}^L - m_{j,n} Y_{j,n}^L X_j^U \qquad (6.27)$$

The shared energy is therefore defined as:

$$E_t^S \leq \sum_{\substack{j\in J \\ n\in N}} W_{t,j,n}\Delta t \qquad (6.28)$$

Similarly to (6.17)-(6.18), equations (6.29)-(6.30) represent the lower and upper bounds of the exchange meter M1 measured injection, respectively.

$$X_j^L = 0 \qquad (6.29)$$

$$X_j^U = P_j^{PV,max} + P_j^{BES,max} \qquad (6.30)$$

Constraint (6.31) assures that variable $Y_{j,n}$ is non-zero only in the "active" *n* sub-domain and in that subdomain is constrained between the lower and upper bounds. Lower and upper bounds are defined for each one of the *N* sub-intervals. Each sub-interval is obtained by equally spacing the interval R_j^{lim}-0. Constraint (6.32) forces $X_{j,n}$ to be zero in non-active sub-intervals.

$$m_{j,n}Y_{j,n}^L \leq Y_{j,n} \leq m_{j,n}Y_{j,n}^U \qquad (6.31)$$

$$0 \leq X_{j,n} \leq m_{j,n}X_j^U \qquad (6.32)$$

Equation (6.33) together with (6.34) bound the linearization variables to the value of R_j. The relation between the piecewise variable $X_{t,j,n}$ and the injection of the exchange meter is represented by equation (6.34).

$$\sum_n Y_{j,n} = (1 - R_j) \qquad (6.33)$$

$$\sum_n X_{t,j,n} = P_{t,j}^+ \qquad (6.34)$$

The problem formulation resulting from the implementation of McCormick envelopes results in a Mixed-Integer Linear Programming (MILP) problem.

6.3.2. Test cases

Two case studies are proposed. The first one considers real-world REC, i.e. with measurement received in real-time, which includes five customers connected to the LV distribution grid. One of them, that is the only prosumer of the REC, is equipped with a 94 kW PV system and a 30 kW/60 kWh BES.

The developed platform allows for the simulation of RECs different from the real-world one by generating synthetic SM measurements. This is the case of the second considered case, i.e., a REC which involves customers, connected to MV distribution grid, characterized by a larger energy demand with respect to the LV scenario. In this case study two prosumers have been included in the REC, both equipped with PV and BES. Prosumer 1 is equipped with a 300 kW PV system and a 100 kW/500 kWh BES, while Prosumer 2 has a 250 kW PV and a 100 kW/350 kWh BES.

As mentioned in section 4.3.2.D the energy purchase price is equal to the NSP plus a spread, defined by the energy provider. The selling price is instead assumed equal to the NSP. The optimization problem considers the updated values of the NSP for the following day as soon as they become available. The same price profile of the current day is considered, otherwise.

The real-time simulation is carried out for two consecutive days, March 23rd and 24th, comparing the Load Forecast (LF) methods presented in sections 5.2.1, 5.2.2 and 5.2.3, for both considered RECs. Scenarios resulting by methods illustrated in sections 5.2.1, 5.2.2 and 5.2.3 are denoted as '*a*', '*b*' and '*c*', respectively.

In both considered case studies, the BESs have an initial SOC of 40%, a minimum admissible SOC of 10% and an efficiency equal to 95% in both charging and discharging. In this study, the following price scenarios have been considered:

i. NSP of 23-25 March 2023, spread equal to 15 c€/kWh;

ii. NSP of 23-25 March 2023, spread equal to 22 c€/kWh;

iii. NSP of 5-7 December 2022, spread equal to 15 c€/kWh, applied to loads and PVs of 23-25 March 2023.

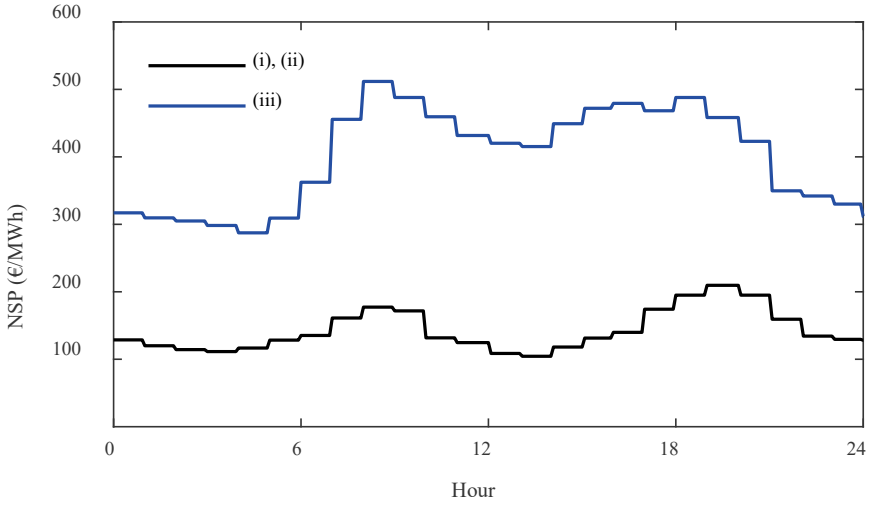

Figure 6.2 Hourly NSP considered in the proposed scenarios

A. LV REC

Loads of passive consumers belonging to the REC have been aggregated and represented as "*REC load*" while the load of the prosumer is indicated as "*Load*"; both the figures refer to the results obtained with LF method *a* (see section 5.2.1). In the following figures, positive/negative BES power values for discharging/charging have been adopted.

Figure 6.3 presents the BES profile forecast resulting from the optimization step performed on March 23rd at midnight, as well as the loads and PV forecasts used by the optimizer. In Figure 6.3, for the sake of clarity, only the first 24 hours are shown although the optimizer uses 48-hour time window. As shown by the BES plot the optimizer forecasts to sell energy when the NSP is higher, such as from around 5 to 9 p.m. Similarly, forecasts to charge the BES either when the PV generation exceeds the REC load or when the hourly NSP is lower, i.e., around and after noon. Prices of scenario (*i*) have been considered in this case.

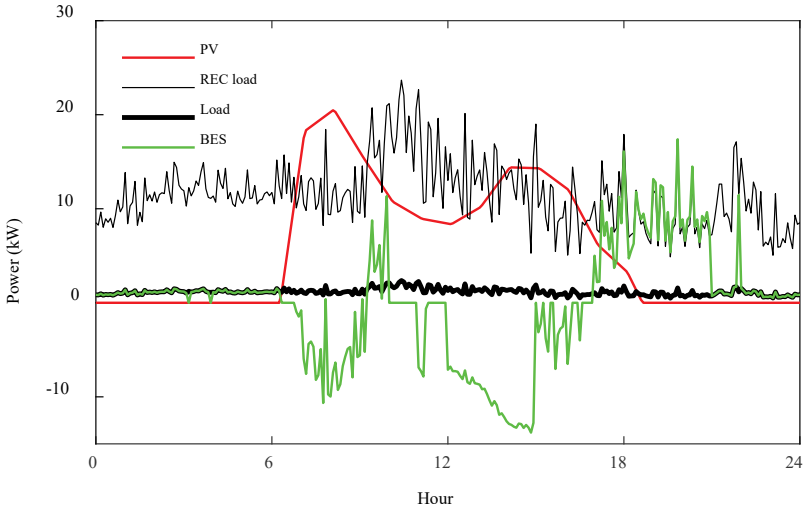

Figure 6.3 24 hours day-ahead results with PV and load forecasts of March 23rd at midnight with LF method *a*

Figure 6.4 shows the BES power profile resulting by rolling-horizon optimizations, along with the real measured PV production and load consumption. The different BES behavior depicted in Figure 6.4, compared to the forecast in Figure 6.3, arises from the continuous updating of forecasts facilitated by the rolling approach.

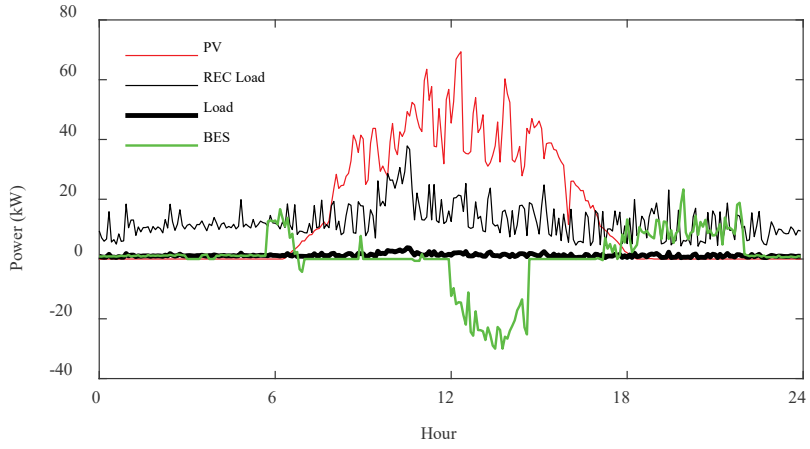

.

Figure 6.4 PV, Load and BES prosumer's power profiles and aggregated REC load after the first day of the simulation with LF method *a*

Table 6.1 shows the main energy and economic results of the non-optimized methods which maximize the behind the meter self-consumption and rolling optimization algorithms after the two considered days of simulation. Total revenues are calculated as the difference between incomes from energy sold and costs for energy bought by prosumers, to which the incentive for the shared energy is added. The cost of the energy bought by the passive consumers of

the REC has not been included in the table since it cannot be optimized by the algorithm and remains the same among the scenarios.

In this setup, the benefits of using a rolling optimization approach to manage the BES with respect to a non-optimized approach are linked with a better exploitation of its storage to share energy with REC's members. This happens because the only prosumer of the REC has a small load, and the BES is sufficient to cover the self-consumption requirements. In the non-optimized approach, the BES reaches a final SOC of 90%. The remaining energy is abundant respect the load requirement until the next day's PV production. Whereas, in the optimized approach, the surplus energy is shared with the community, resulting in final SOCs of 20.6%, 22.9%, and 21.3% in scenarios a, b, and c, respectively.

Table 6.1 LV REC energy and economic results

	Energy (kWh)				**Cost/Revenue (€)**			
	Non-Opt.	**Rolling**			**Non-Opt.**	**Rolling**		
		a	***b***	***c***		***a***	***b***	***c***
Buy	0	3.68	2.80	2.60	0	1.00	0.76	0.73
Sell	659.38	698.90	696.50	697.40	79.20	93.44	92.70	93.19
E_s	253.25	345.10	345.40	344.00	27.86	37.96	37.99	37.84
Revenue – Cost					107.06	**130.40**	129.93	130.30

B. MV REC

The second considered REC involves two prosumers and customers with larger energy requirements, PV generation and BES capacity. Figure 6.5 shows prosumer-1 measured PV and load during the first 24-hour along with the aggregated REC load.

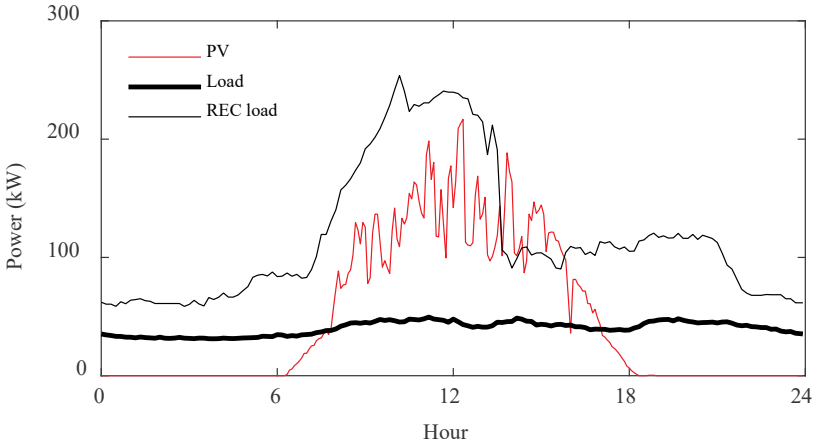

Figure 6.5 Prosumer-1 PV and Load along with REC load measured in the first day of simulation

Figure 6.6 and Figure 6.7 show prosumer-1 BES power profiles and SOCs, respectively, resulting from the rolling approach performed on March 23rd for the three price scenarios considered. Each price scenario leads to a different management of the BES. In scenario (*ii*), which exhibits a higher spread compared to scenario (*i*), the priority is given to prosumer self-consumption over energy sharing after 7 p.m. In scenario (*iii*), which incorporates a different NSP profile, the BES is charged from the grid approximately from 4 a.m. to 6 a.m., taking advantage of lower energy prices and performing energy arbitrage.

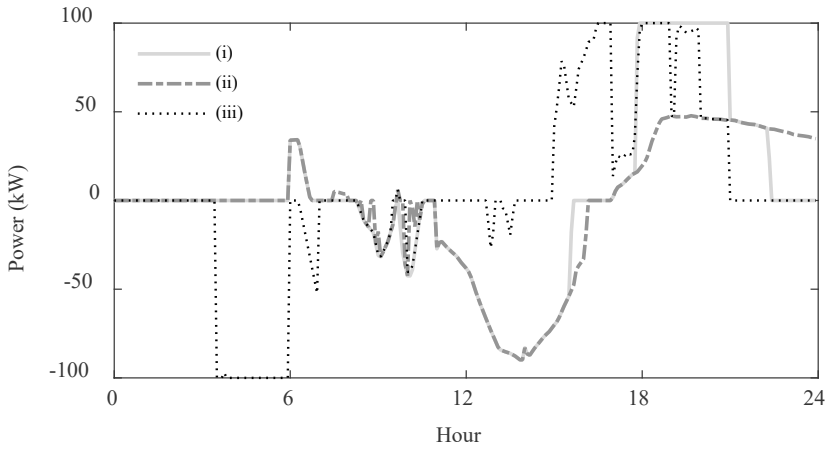

Figure 6.6 Prosumer-1 BES power, in the first day of simulation with LF method a, for the three price scenarios

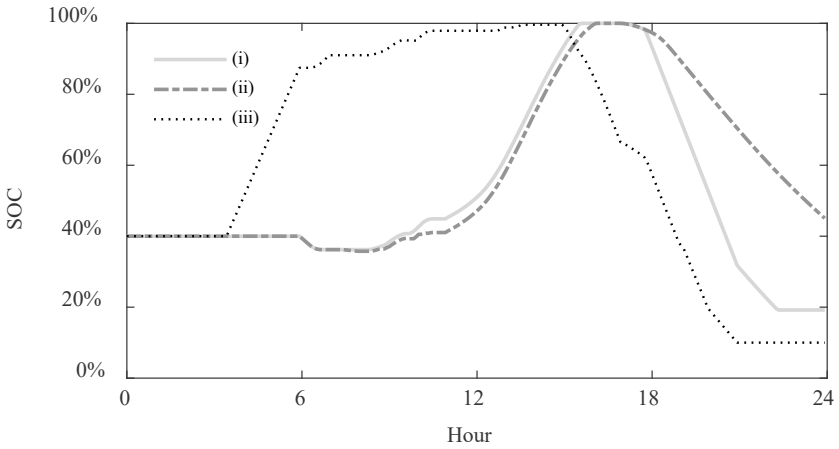

Figure 6.7 Prosumer-1 SOC, in the first day of simulation with LF method a, for the three price scenarios

Table 6.2 and Table 6.3 show the results for price scenarios (*i*) and (*ii*), respectively after the two-day simulation. In scenario (*i*) the optimal solution is obtained by sharing more energy within the REC with respect to scenario (*ii*).

Table 6.2 MV REC energy and economic results in price scenario (*i*)

		Energy (kWh)				Cost/Revenue (€)			
		Non-opt.	Rolling			Non-opt.	Rolling		
			a	*b*	*c*		*a*	*b*	*c*
Pros. 1	**Buy**	158	520	533	551	44.57	142.53	145.91	151.16
	Sell	478	892	879	925	55.80	131.15	127.70	136.74
Pros. 2	**Buy**	20	277	274	288	5.64	75.87	75.17	79.03
	Sell	791	1171	1181	1168	87.38	173.13	174.51	172.70
	E_s	1098	2035	2043	2065	120.74	223.85	224.73	227.18
Revenue – Cost						213.71	309.73	305.87	306.43

In price scenario (*ii*) the spread between energy sold and bought is greater than in scenario (*i*), thus the optimization algorithm preserves the energy stored in the BES to favor prosumer self-consumption and reducing the amounts of energy bought, sold and shared within the REC. The rolling approach leads to a reduction of the costs for the REC with respect to the non-optimized approach.

Table 6.3 MV REC energy and economic results in price scenario (*ii*)

		Energy (kWh)				Cost/Revenue (€)			
		Non-opt.	Rolling			Non-opt.	Rolling		
			a	*b*	*c*		*a*	*b*	*c*
Pros. 1	**Buy**	158	349	369	375	55.66	120.13	126.37	129.43
	Sell	478	673	715	691	55.80	88.09	94.64	91.05
Pros. 2	**Buy**	20	123	129	132	7.02	42.89	45.04	45.75
	Sell	791	963	993	954	87.58	134.22	138.92	131.28
	E_s	1098	1636	1708	1644	120.74	179.93	187.90	180.80
Revenue – Cost						201.25	239.22	250.06	227.95

In the two presented price scenarios, coefficient *R*, which curtails the incentive on shared energy, is always equal to 0 for both prosumers. Table 6.4 reports the results of price scenario (*iii*); within this scenario the algorithm performs energy arbitrage resulting in *R* equal to 0.2, for prosumer-1 in the *a, b, c* load forecasting scenarios, while for prosumer-2 *R* is equal to 0.2, 0.21, and 0.21 in the *a, b, c* load forecasting scenarios, respectively.

Table 6.4 MV REC energy and economic results in price scenario (*iii*)

		Energy (kWh)				Cost/Revenue (€)			
		Non-opt.	Rolling			Non-opt.	Rolling		
			a	*b*	*c*		*a*	*b*	*c*
Pros. 1	**Buy**	158	1306	1265	1319	77.51	603.93	583.32	610.70
	Sell	478	1793	1750	1816	200.88	787.06	768.20	793.44
Pros. 2	**Buy**	20	860	840	865	10.14	393.76	383.28	395.98
	Sell	791	1814	1790	1822	318.59	786.19	773.20	788.70
	E_s	1098	2690	2645	2700	120.74	295.97	290.96	297.04
Revenue – Cost						552.57	871.52	866.29	**872.50**

6.4 Four-prices Model

The proposed algorithm aims to minimize the energy procurement costs for a REC in which P2P non-competitive internal energy transactions are allowed.

The prices of the energy exchanged within the REC, i.e. the price agreed between the local prosumers and local consumers, are established ex-ante and are comprised between the energy selling and buying prices with the energy retailers not belonging to the REC.

The energy sold to the retailer typically is remunerated at a lower price with respect to the energy bought from the retailer. Consistent with the retailer pricing scheme, prices for energy exchanged directly between community members (P2P) fall between these two extremes, to be more profitable for both producers and consumers, provided that the internal selling price should be lower or equal to the internal buying one. This results in a four-prices model. The four-prices model, at community level, is capable to represent national regulations in which the price of the energy shared within the community is agreed by the parties, this is the case of Germany, France and Spain. Moreover, by properly setting the internal prices spread, the four-prices model is also capable of well-approximate the regulation schemes employing an economic incentive to reward the shared energy, as the Italian one.

6.4.1. Mathematical formulation

The power exchanged by the REC with the external grid, i.e. the power measured at REC's PCC (either physical or virtual) is defined as:

$$P_t^{PCC} = \sum_j P_{t,j}^- - P_{t,j}^+ \qquad (6.35)$$

The power flow is assumed to be positive when the REC is importing energy at the PCC and negative otherwise. The objective function to be minimized is:

$$OF = \sum_{\substack{t\in T \\ j\in J}} (\pi_t^{REC-} P_{t,j}^- - \pi_t^{REC+} P_{t,j}^+) \Delta t + \sum_t C_t^{PCC} \qquad (6.36)$$

where C_t^{PCC}, defined by constraints (6.37) and (6.38), represents the additional cost incurred during each time interval t for the energy imported from or exported to the external grid (i.e., the energy exchanged with external suppliers). This cost is additional respect to the cost that would be incurred if the energy were exchanged within the REC. Difference between the external price and internal one for the energy bought and sold is defined in equations (6.39) and (6.40) respectively; the first one is positive while the latter one is negative.

$$C_t^{PCC} \geq \Delta\pi_t^- P_t^{PCC} \Delta t \qquad (6.37)$$

$$C_t^{PCC} \geq \Delta\pi_t^+ P_t^{PCC} \Delta t \qquad (6.38)$$

$$\Delta\pi_t^- = \pi_t^- - \pi^{REC-} \qquad (6.39)$$

$$\Delta\pi_t^+ = \pi_t^+ - \pi^{REC+} \qquad (6.40)$$

The problem is formulated as a MILP problem.

The economic incentives I_E, discussed in section 6.3, to valorize the energy sharing can be reconducted as shadow-price in the price differences $\Delta\pi_t^-$ and $\Delta\pi_t^+$ proposed in this section. To ensure consistency between the two formulation equation (6.41) must hold. The incentive I_E is shared among REC's prosumers and consumers according to an ex-ante agreement, similarly this effect can be replicated on the prices difference: considering a certain value of I_E favoring $\Delta\pi_t^-$ leads to allocate more saving to the consumers vice versa increasing the absolute value of $\Delta\pi_t^+$ prioritize the producer remuneration.

$$I_E = \Delta\pi_t^- - \Delta\pi_t^+ \qquad (6.41)$$

6.4.2. Test cases

Two configurations of RECs are considered, the former is a small one containing three users: a pure consumer, a prosumer with PV and a prosumer with PV and BES, the latter is a larger community with several users. The small REC is simulated with deterministic forecasts of

production and consumption, i.e. the forecast is considered not affected by uncertainty, the larger REC is used by assuming forecast errors, in order to face more realistic case studies. The outcomes obtained for the smaller REC, i.e. REC-1, results by considering the BES power profile obtained at the first iteration of the optimization procedure without implementing the subsequent rolling optimization steps and the respective adjustments. Therefore, the effect of continuously postponing the BES energy surplus discharge introduced by the rolling approach, discussed in section 6.1, does not occur: the SOC at the end of time horizon is at the minimum level. This is done as the main focus of the REC-1 scenario is to demonstrate the capability of the four-price model to approximate the incentive-based one and their behavior respect the non-optimized ones. The effect of the rolling approach is then introduced in the REC-2 case study.

The consumption data are inferred by using the measurements of the power flows in MV feeders provided by the DSO of an urban district in Bologna, with a time resolution of 5-minute, in the GECO project framework. The LFs are generated adopting SARIMA models as discussed in section 5.2.4.

The data relevant to the reduced REC are reported in Table 6.5. The prosumer equipped with the BES is the only one that can provide flexibility within the REC, thus the self-consumption rate of the community depends on this user only.

Table 6.5 PV rating, BES rating and daily energy load of REC-1

User	PV (kWp)	BES_{Power} (kW)	BES_{Energy} (kWh)	Load (kWh)
1	300	0	0	1464
2	100	100	350	451
3	0	0	0	682

In the second REC, the community is represented through six users all equipped with PV and BES units except for user-5 only equipped by PV system and user-6 which is an equivalent consumer aggregating all the passive members of the REC. Storages at t=0 are assumed to be partially charged (SOC equal to 40%). Table 6.6 reports the nominal data of PV and BES units.

Table 6.6 PV rating, BES rating and load energy (over the simulated period) of REC-2

User	1	2	3	4	5	6
PV (kWp)	300	400	30	200	150	0
BES_{Power} (kW)	125	150	75	100	0	0
BES_{Energy} (kWh)	500	500	100	400	0	0
Load (kWh)	3460	4252	1705	1888	2037	11319

In the following sections 6.4.2.*A* and 6.4.2.*B*, respectively, the results by considering a reduced REC and implementing flat and ToU tariffs are presented. For the reduced REC case a deterministic scenario is considered, i.e. the forecasts of PV and load correspond to real values. The storage at *t*=0 is at the minimum allowed SOC. The optimization algorithm employing four prices is compared with the ones adopting the economic incentive (both non-linear and linearized), and with the two non-optimized approaches that disregard the energy prices and consider only the power deficit/surplus. In section 6.4.2.*C* the comparison between the results obtained from the implementation of the rolling optimization procedure, applied to the second REC, for five subsequent days and the outcomes of the non-optimized approaches is reported.

To ensure consistency in the models comparison the spread between the internal purchasing and selling prices has been set to 55 €/MWh, thus according to (6.39)-(6.40) $\Delta\pi_t^- = -\Delta\pi_t^+ = 55\,€/MWh$. The value has been assumed considering the Italian incentive equal to 110 €/MWh halved between producers and consumers according to (6.41).

A. REC-1, Flat price

In Figure 6.8 customer-2 load, PV and BES power profiles, resulting from the internal price optimization algorithm, are shown. The BES power is positive during discharging phase and negative otherwise; the profile is obtained from the optimization procedure described in section 6.4.1. The profile of customer-1 and customer-3, which are not optimizable since not equipped with BESs, have been aggregated and represent as 'REC' adopting the load convention. The optimization starts to charge the BES when production exceeds the community-load, therefore approximately from 7 a.m. to 8 a.m. customer-2 is selling its surplus to the REC's members. Around 1 p.m. the charging power increases, overcoming the

self-production surplus, thus customer-2 is buying energy; the recharge power exactly balances the community-production surplus, as shown in Figure 6.9, contributing to the shared energy. Therefore, the energy is bought by customer-2 at the internal price (lower than external retailer one), simultaneously customer-1 is selling at the internal price (higher than external retailer one). As the PV production decreases the BES compensates for the shortfall to cover the self-load; finally, moving toward the end of the time horizon the energy exceeding the behind-the-meter self-consumption is shared within the REC, not injecting energy outside the REC thus obtaining greater revenue.

The choice of postponing energy sharing, both in charge and discharge, is related to the uncertainty of PV production and self-load which increase with time: typically, the behind-the-meter self-consumption is economically convenient with respect to energy sharing, therefore the energy is preserved in case of forecasts updates implemented in the rolling approach. The conditioning of BES charge/discharge is obtained by applying small weighting factors to π_t^- and π_t^+.

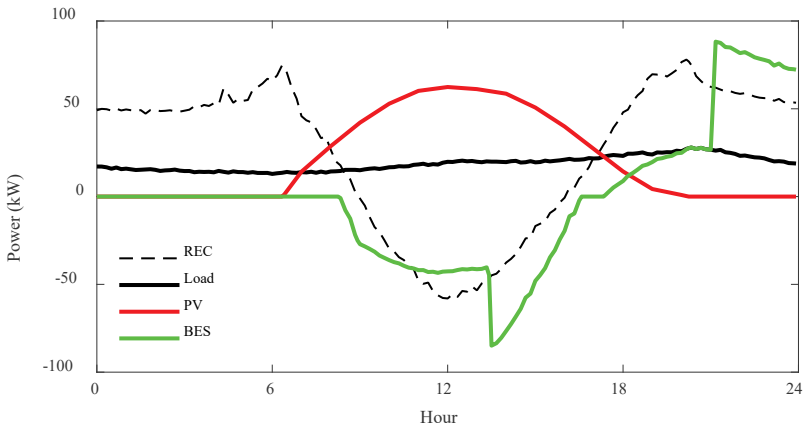

Figure 6.8 Daily power profile of REC and customer-2's load, PV and BES

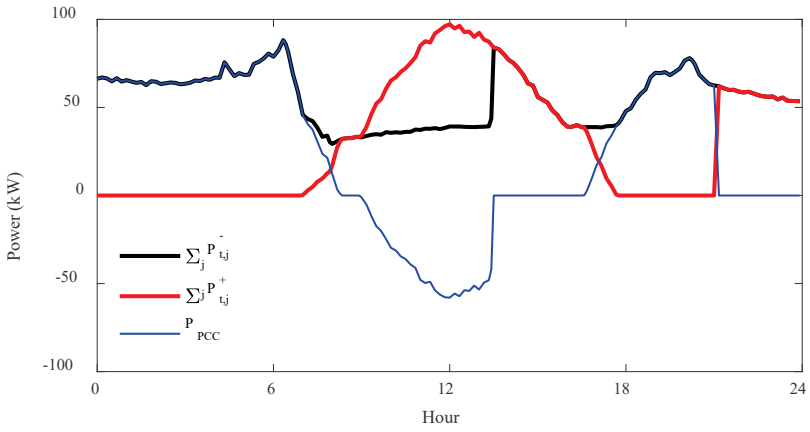

Figure 6.9 Daily power profile of total power withdrawn and fed by REC's members and power at the REC PCC

Figure 6.10 and Figure 6.11 shows the BES power and SOC profiles, respectively, in the three optimized approaches. The profiles are the same except for the hours when customer-2 charges the BES and simultaneously buys energy. As in the linear model with internal prices the BES recharge/discharge from the grid is postponed as late as possible, compatibly with the community self-consumption maximization.

The non-linear optimization, implementing the Italian regulation, introduced in section 6.3, introduces penalty on the shared energy if the storage is recharged from the grid. According to equations (6.2) and (6.10) the computation of factor *R* considers that PV production is firstly allocated to the BES charge and then to the load. Therefore, the non-linear formulation bought the energy to satisfy the load while the PV production coincides with the BES charging power, thus the absorption measured by meter M2, namely $P_{t,j}^{P-}$, remains equal to 0 as well as the penalization factor *R*. The energy shared within the community corresponds to 572.7 kWh.

The model implementing the McCormick linear approximation employs the same strategy of the non-linear approach. However, the power profile shows some differences due to the linearization process. The linearized *R* value calculated by the EMS during the optimization (equal to 0.017) differs from the actual *R* value calculated ex-post (equal to 0.020), using equation (6.10), due to the linearization process. In a similar way the linearization introduces an error on the shared energy computation, the linearized estimation, and the real value ex-

post calculated corresponds to 568.9 kWh and 572.7 kWh, respectively. The use of a higher number of McCormick intervals can reduce the error, in contrast, the computation time rise.

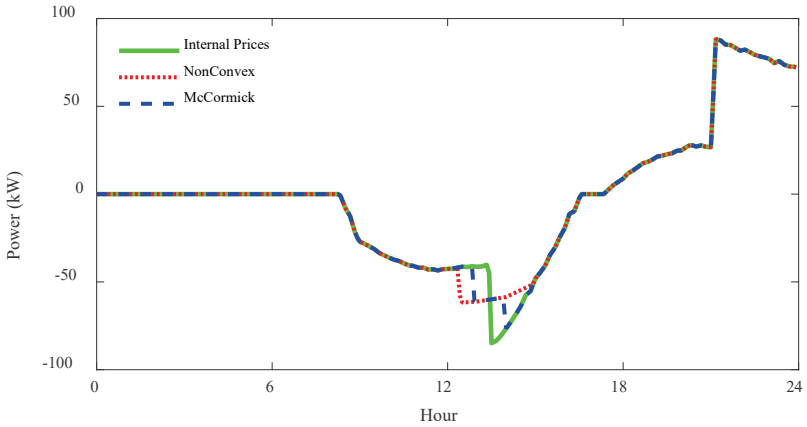

Figure 6.10 BES power profiles, optimized approaches, flat prices

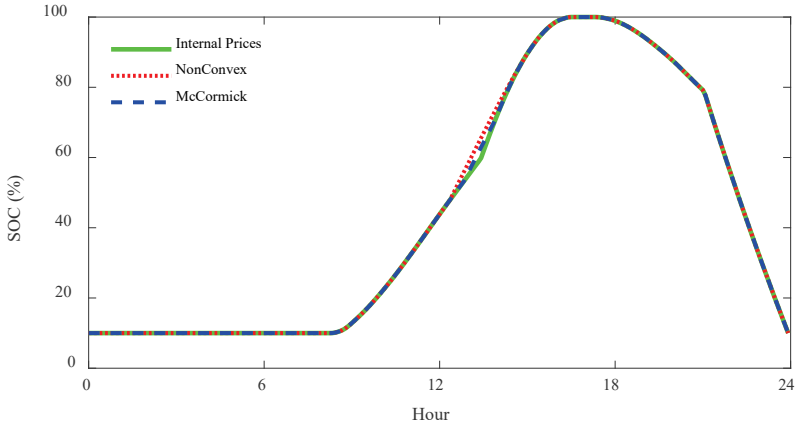

Figure 6.11 BES SOC profiles, optimized approaches, flat prices

Figure 6.12 and Figure 6.13 show the power profiles resulting from the non-optimized approaches formerly introduced. The time at which the BES starts to recharge is the same in the non-opt-2 and in the optimized approaches. In contrast the non-opt-1 approach starts the BES recharge as soon as the self-production overcomes the self-load.

The discharging process differs in non-opt-1, non-opt-2 and optimized approaches. Non-opt-1 starts the discharge as soon the PV production is not sufficient to cover the self-load; non-opt-2 starts the discharge as soon the overall PV production is not sufficient to cover the

overall community load, thus customer-2 BES cover also the load of other REC members for a certain time but around 9 p.m. the energy stored ends and its self-load remain uncovered. Optimized approaches, in contrast, prioritize covering of customer-2 load and improving self-consumption within the REC whenever possible. The SOC profiles resulting from the two non-optimized approaches are illustrated in Figure 6.14.

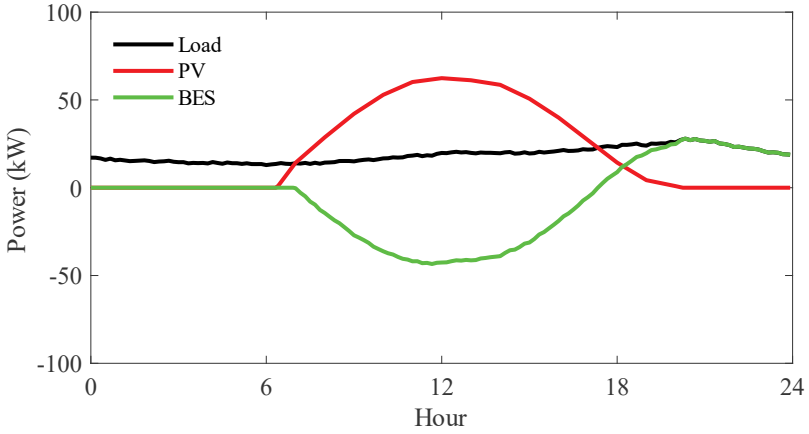

Figure 6.12 Daily power profile of customer-2's load, PV and BES, non-opt-1

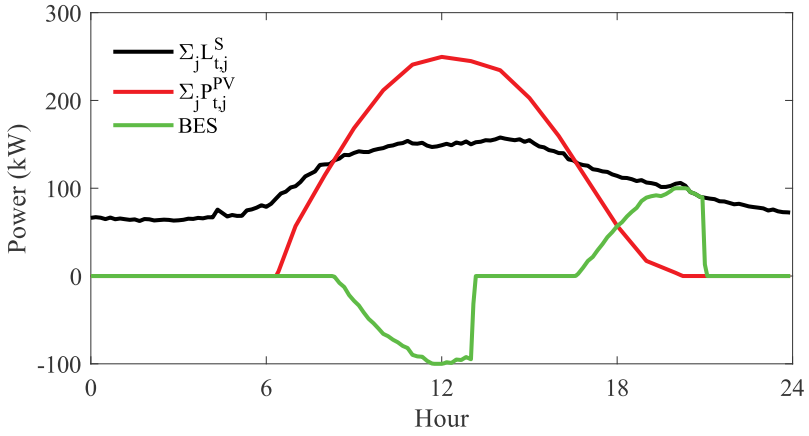

Figure 6.13 Daily power profile of REC's load, PV and BES, non-opt-2

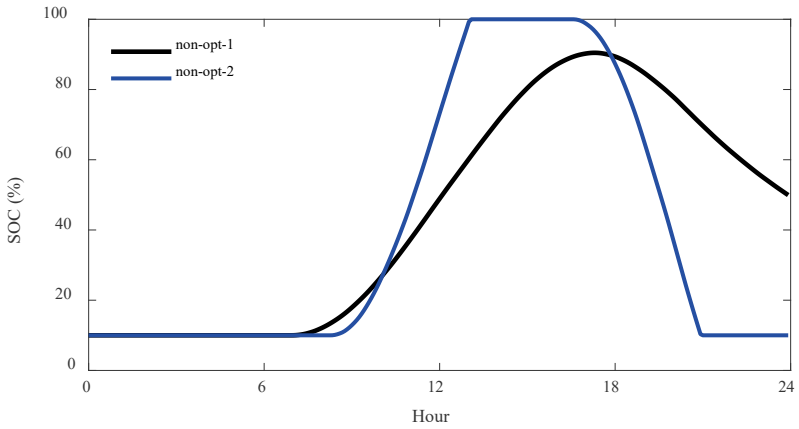

Figure 6.14 SOC profile of prosumer-2

Table 6.7 summarizes the energy results obtained from the different approaches; as introduced, only the results related to customer-2 and to the REC are reported since they are the only ones affected by the different BES control strategies.

Table 6.7 Energy imported, exported and self-consumed

		Non-Lin.	Lin. McCormick	Int. Prices	Non-opt-1	Non-opt-2
E_{imp} (kWh)	Pros	159.9	159.9	159.9	98.3	327.5
	REC	753.3	753.3	753.3	944.3	753.3
E_{exp} (kWh)	Pros	191.0	191.0	191.0	0.0	358.6
	REC	182.7	182.7	182.7	244.3	182.7
Energy Self-Cons. (kWh)	Pros	291.3	292.3	293.4	352.9	132.8
	REC	1843.5	1843.5	1843.5	1652.5	1843.5
Energy Self-Cons. (%)	Pros	56.6	56.8	57.0	68.6	25.3
	REC	89.6	89.6	89.6	80.3	89.6

The optimized methods yield identical imported and exported energy values for both prosumer-2 and the REC, as well as the same amount of community self-consumption. The community self-consumption resulting from optimized approaches is equivalent to the one obtained from the non-opt-2 method, which represents the maximum achievable self-consumption. Despite the non-opt-2 method reaches the best community self-consumption

it yields to a reduced customer self-consumption due to the greater energy exchanges derived from BES sharing with the REC.

From the customer-2 viewpoint the best behind the meter self-consumption could be achieved implementing the non-opt-1, however it disregards the REC viewpoint leading to a lower community self-consumption.

The energy self-consumption values are calculated as the sum of the instantaneous self-consumption (6.42)-(6.43) for customer and the REC, respectively. Typically, the instantaneous single-user self-consumption is evaluated as the minimum between the load and the production, i.e. $P_{t,j}^{P+}$, to account for the BES. However, the proposed optimized algorithms, as well as non-opt-2 approach are capable to recharge the BES from the grid, this energy should not be accounted as self-consumption as it not comes from the PV system, thus a second term is added in (6.42). The energy drawn from the grid and stored in the BES, measured by $P_{t,j}^{P-}$, for later exploitation, must be subject to both charging and discharging efficiency, assumed to be equal.

$$E_j^{SC} = \sum_t min\left(L_{t,j}^S, P_{t,j}^{P+} \right) \Delta t - \sum_t P_{t,j}^{P-} \eta_j^2 \Delta t \quad (6.42)$$

$$E^{SC,REC} = \sum_t min\left(\sum_j L_{t,j}^S, \sum_j L_{t,j}^S - P_t^{PCC} \right) \Delta t \quad (6.43)$$

B. REC-1, ToU tariffs

A comparison among different methods, similarly to the previous sub-section, is now performed by implementing variable prices. Typically, variable price can adopt ToU tariffs or hourly prices, as shown in Figure 6.15. This analysis focuses on the first case, which is more common for customers not directly involved in the electricity market. The ToU tariffs for the energy sold outside the REC and imported by the REC, namely π_t^+ and π_t^- are represent as solid lines in Figure 6.15.

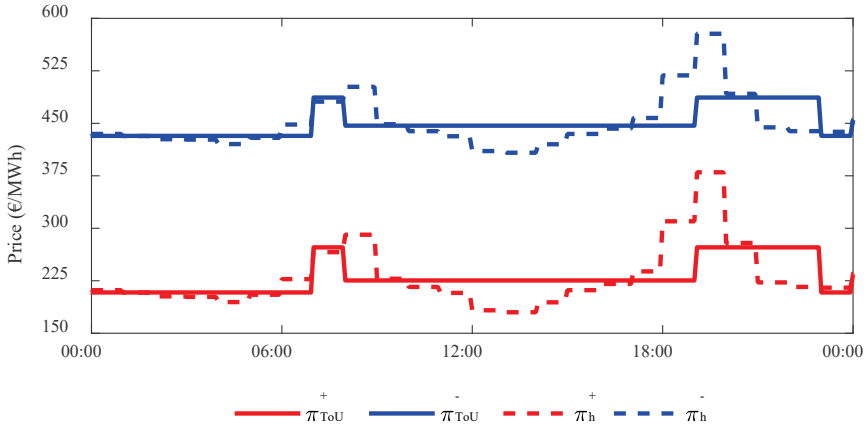

Figure 6.15 ToU and hourly retailer prices

In Figure 6.15 and Figure 6.17 the resulting BES power and SOC profiles from the optimization algorithms are shown. The non-optimized algorithms do not depend on the electricity prices, thus the results shown in Figure 6.12 and Figure 6.13 the respective values reported in Table 6.7 remain unchanged.

Concerning the optimized approaches, similarly to the former scenario, the BES' SOC is at the minimum allowed value at the initial time, thus the first part of the day remains identical; the difference is in the discharging phase, where the algorithm tends to sell the energy surplus during high price hour, while preserving enough energy to cover the customer load up to the end of the time horizon. From the energy viewpoint the results are the same of Table 6.7 since there is only a time-shift of the energy sharing phase.

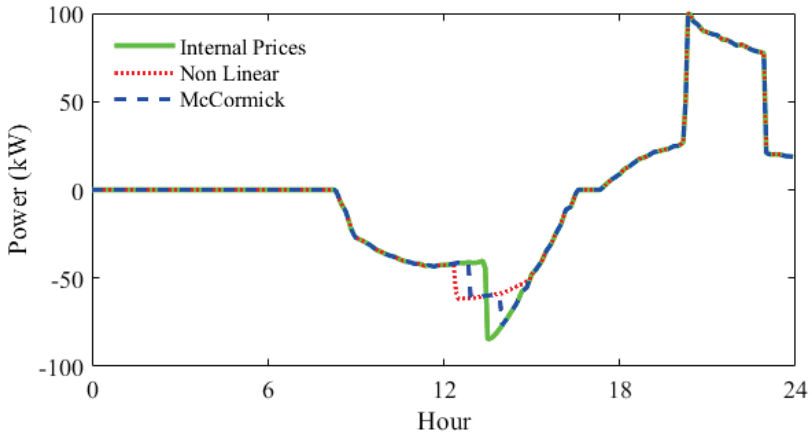

Figure 6.16 BES profiles, optimized approaches, ToU prices

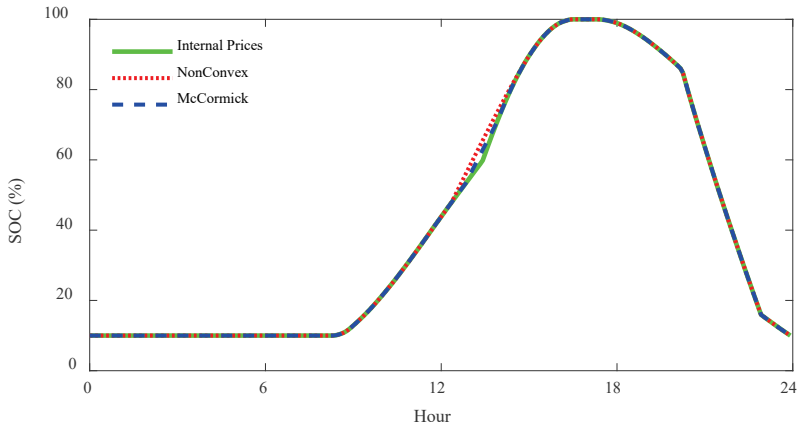

Figure 6.17 BES SOC profiles, optimized approaches, ToU prices

Even though the three proposed optimization algorithms have different objective functions, based on economic value (€), all of them lead to the same energy results in both price scenarios. Thus, the model adopting four energy prices can be considered energetically equivalent to the one employing the incentive.

C. REC-2

This section presents the economic and energy results from implementing the rolling procedure to both the internal-prices and Italian models. The rolling procedure has been conducted over a five-day period. The proposed approach is tested for both variable pricing methods, i.e. ToU tariff and hourly prices, and the results are compared with the non-optimized algorithms. In all scenarios presented in this section, the initial SOC is the same for all BESs and is equal to 40%. In this section real load and PV production are not equal to forecasts obtained from SARIMA model and meteorological service, respectively, to consider a realistic scenario with uncertainties.

Figure 6.18 and Figure 6.19 show the *customer-1* results, for a 24-hour time-window, of the rolling procedure when implementing the ToU and hourly tariffs, shown in Figure 6.15, respectively. The measured PV production and load consumption are represented in red and blue, respectively, while the green line indicates the storage power calculated by the optimizer using the PV and load forecasts. The black line represents the power at the customer's PCC, while the dotted light-blue line represents the BES SOC.

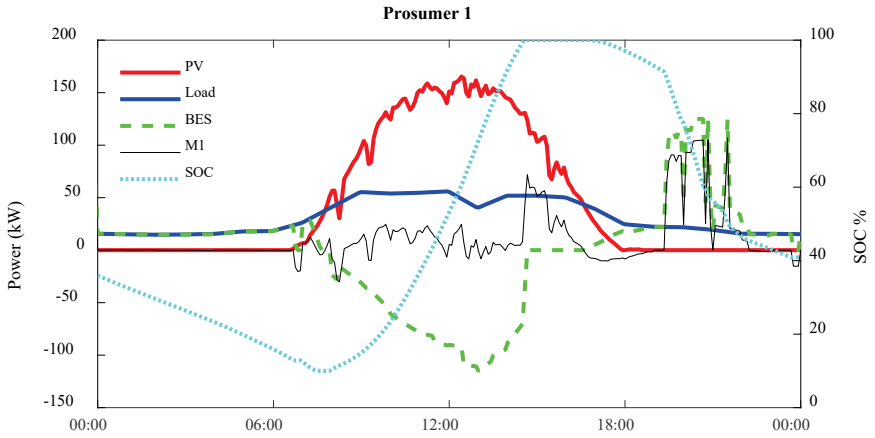

Figure 6.18 24-hour power profiles for PV generation, load, BES, and M1 meter, along with the SOC profile derived from optimization using ToU tariffs

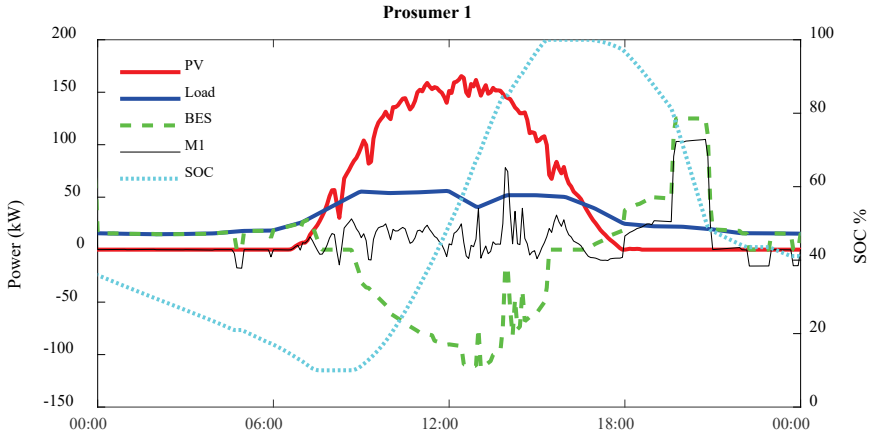

Figure 6.19 24-hour power profiles for PV generation, load, BES, and M1 meter, along with the SOC profile derived from optimization using hourly tariffs

The two price scenarios lead to similar behavior in part of the day, such as from midnight to 7.40 a.m., during this period, the storage is discharged to cover the load, contributing to behind-the-meter self-consumption. The time at which the BES recharge process begins is different: in the ToU tariffs scenario the recharge starts at 8 a.m. while in the hourly price one it waits approximately 9 a.m. when the price peak of the energy sold passes. When production is in deficit with respect to the load, after 4 p.m., the BES starts to discharge to cover the lack. If the battery stores enough energy to cover the forecasted load until the next morning, the exceeding energy can be shared with the REC's members. In the ToU tariffs scenario this takes place after 7 p.m. when the price for the energy sold is larger while in the hourly case the energy surplus sharing takes place at 6 p.m. and continues up to 9 p.m., i.e. the three evening hours with the highest price.

In Table 6.8 the energy values, for each prosumer, resulting from the two non-optimized algorithms and from both price scenarios of the optimized ones are presented. *Customer-5* and *customer-6* are not equipped with the BES, thus their energy bought, sold, and self-consumed are the same across all approaches.

The non-opt-1 as introduced in section 6.2 aims to maximize the behind-the-meter self-consumption, thus the energy bought by each prosumer is the lowest.

The non-opt-2 approach provides the maximum value of shared energy (reported in Table 6.9) as opposite to the non-optimized method 1; despite that the non-opt-2 approach leads to the lowest self-consumption rate and to the highest amount of energy bought. The optimized approaches, from the single-customer perspective, provide results biased toward the non-opt-1 method performances. It is worth noting that the model implementing internal prices for P2P transactions and the model including the economic incentive for the shared energy provide values of energy bought and sold almost equal, while the self-consumption rates are equal excepts for *customer-3* in the hourly price scenario.

Table 6.8 Prosumers energy performance

	Prosumer	1	2	3	4	5	6	Tot.
E_{buy} (kWh)	Non-opt-1	0	319	1137	0	1099	11319	13874
	Non-opt-2	722	1266	1376	524	1099	11319	16306
	ToU - int. prices	227	567	1186	172	1099	11319	14570
	ToU - incentive	232	576	1187	175	1099	11319	14586
	Hourly - int. prices	226	464	1201	163	1099	11319	14473
	Hourly - incentive	234	466	1223	153	1099	11319	14494
E_{sell} (kWh)	Non-opt-1	1589	3053	0	1455	1760	0	7857
	Non-opt-2	2569	4125	192	2162	1760	0	10808
	ToU - int. prices	1964	3239	4	1733	1760	0	8699
	ToU - incentive	1974	3248	4	1735	1760	0	8720
	Hourly - int. prices	1933	3137	3	1675	1760	0	8508
	Hourly - incentive	1974	3139	3	1723	1760	0	8599
Self Cons.	Non-opt-1	63%	54%	100%	51%	35%	-	
	Non-opt-2	50%	41%	63%	37%	35%	-	
	ToU - int. prices	58%	50%	99%	46%	35%	-	
	ToU - incentive	58%	50%	99%	46%	35%	-	
	Hourly - int. prices	58%	52%	95%	47%	35%	-	
	Hourly - incentive	58%	52%	91%	47%	35%	-	

Table 6.9 reports the energy exported outside the REC and imported from the REC, i.e. the energy measured at the REC PCC, either virtual or physical, according to (6.35). The non-opt-2 approach minimizes the energy import, i.e. maximize the community self-consumption rate computed according to (6.43), as opposite to the non-opt-1 which leads to the lowest rate. From a community perspective the results of the optimized algorithm provide an intermediate self-consumption rate biased toward the non-opt-2 result.

The results provided in Table 6.8 and Table 6.9 show that the optimization algorithm is capable to manage the prosumers' BESs in an efficient way to obtain a good trade-off between the energy performance at single-customer level and the performance at community level.

Table 6.9 REC energy performance

	Eimp (kWh)	Eexp (kWh)	Self-Cons.	BES Resid. (kWh)	Eshared (kWh)
Non-opt-1	10102	4084	48%	735	3772
Non-opt-2	6507	1009	66%	24	9727
ToU - int. prices	8021	2150	59%	386	-
ToU - incentive	7948	2082	59%	380	6630
Hourly - int. prices	7528	1563	61%	486	-
Hourly - incentive	7450	1554	62%	423	7040

The energy results of the non-optimized algorithms presented in the previous tables are unaffected by the energy prices since the BESs control strategy disregards the economic value of the energy. When focusing on the economic performance to assess the behavior of the optimized algorithm with respect to the non-optimized ones it is necessary to distinguish the economic results also for the latter ones in the two price scenarios considered. Moreover, to properly compare the economic performance, the amount of exploitable energy remaining in the BESs, i.e. the one exceeding the minimum SOC, when the five-day time windows observation ends is valorized. The valorization is computed in the worst-case scenario, thus applying the lowest energy bought price foreseen in the next day.

Table 6.10 reports the results obtained from ToU price scenario. As introduced, the non-opt-1 and non-opt-2 algorithms lead to the lowest and highest values of energy bought/sold respectively; therefore, they lead to the lowest and highest cost/revenues, respectively. At the end of the observation period the non-opt-1 has a significant amount of energy stored to be valorized in the BESs as opposite to non-opt-2 approach.

The knowledge of the energy prices implemented in the rolling optimized procedure leads to a community profit maximization; the profit is computed considering as positive the revenues from energy sold, incentives for energy shared (if applicable) and BESs residual energy, while the costs for the energy bought are considered negative.

Both optimized approaches lead to a higher community profit with respect to the two non-optimized approaches used as benchmark. Compared to each other the internal prices and incentives algorithms lead to almost the same result (difference is less than 1%).

Assuming to equally share the economic incentives between producers and consumers thus reducing the energy bought cost of half of the incentive and increasing the revenues for energy sold of the same amount. As a result, the costs and revenues from energy transactions for the incentive model and the P2P transaction model would be nearly equal.

Table 6.10 Economic performance ToU

(€)	Ebuy	Esell	Incentive	BES resid.	Profit
Non-opt-1 - int. prices	6265	2146	0	334	-3785
Non-opt-1 - incentive	6472	1939	415	334	-3784
Non-opt-2 - int. prices	7040	3283	0	11	-3746
Non-opt-2 - incentive	7579	2745	1070	11	-3753
ToU - int. prices	6404	2579	0	176	-3649
ToU - incentive	6774	2236	729	173	-3625

In Table 6.11 the results of the hourly pricing scenario are shown, the behavior of the algorithms is similar to the ToU price scenario nevertheless the optimized algorithm can better exploit the price fluctuations among hours to gather more profit or saving. Consistent with the findings from the TOU scenario, the hourly-price scenario reveals equivalent performance between the P2P transaction model and the model with economic incentives.

Table 6.11 Economic performance NSP

(€)	E_{buy}	E_{sell}	Incentive	BES resid.	Profit
Non-opt-1 - int. prices	6270	1851	0	323	-4096
Non-opt-1 - incentive	6477	1643	415	323	-4096
Non-opt-2 - int. prices	7012	3219	0	11	-3782
Non-opt-2 - incentive	7551	2680	1070	11	-3790
Hourly - int. prices	6328	2583	0	213	-3532
Hourly - incentive	6724	2231	774	183	-3536

A comparison of algorithms, for both price mechanisms, in the same days considered before, has been conducted in a scenario in which energy prices are lower and spread between energy bought and sold is reduced with respect to the economic incentive. Under these price conditions the optimization algorithm tends to behave as the non-opt-2 approach, thus the profit gap between the two approaches is reduced. In contrast, the profit gap between the non-opt-1 algorithm and the optimized one increases. Therefore, the proposed optimization algorithm is capable to fade its logic toward the behind-the-meter self-consumption or toward the community self-consumption depending on the prices, loads and PV production forecast.

6.5 Stochastic Approach

Since forecasts for both renewable energy production and load consumption involve a degree of unpredictability, primarily due to short-term meteorological events for the former and human activities for the latter, stochastic optimization approaches are often proposed to account for these uncertainties [176]–[178] to reduce power systems costs [179].

In the context of the proposed EMS for RECs optimal operation, the stochastic component is implemented in the optimization procedure to address the inherent uncertainties in load demand and PV generation forecasts. To account for these uncertainties, multiple stochastic events are generated for both load and PV production. This events generation process captures a range of possible outcomes, reflecting the variability and unpredictability of these elements.

Typically, a large number of scenarios are generated to cover a wide range of possible events. Solving the optimization problem for each of these events would require huge computational resources. Therefore, a scenario reduction process is applied to manage the computational complexity of handling a large number of scenarios. The considered events consist of forecasts along the time a multiperiod stochastic formulation is employed [180]. Thus, the reduction technique uses the k-means clustering algorithm [181] to create a scenarios tree model. The k-means clustering algorithm groups forecast profiles into clusters by minimizing the sum of distances between each profile and its corresponding cluster center, i.e. the centroid. Typically, the Euclidean distance is used to determine proximity. Profiles closest to a centroid are assigned to the same cluster.

Once the reduced scenario set is obtained to each scenario is then assigned a probability. The probability is weighted according to the number of events belonging to the scenario, and these weights are incorporated into the objective function.

As the scenario tree branches out ahead in time, for the common path of the tree branches it must be ensured that the optimization solution is unique among scenarios belonging to the same path. The whole process is performed according to the following process:

- Generation of a base-forecast profile from which the stochastic events are generated. For PV production the base-forecast coincides with the PV production forecast obtained from meteorological services illustrated in section 4.3.2.C. While for the load base-forecast the SARIMA forecasting techniques described in section 5.2.4 is employed.

- Generation of N_E stochastic events for each PV and load. The events are generated employing Probability Distribution Functions (PDFs) obtained by comparing the past recorded forecasts with the corresponding measured real data. Forecast stochastic events are generated according to a non-parametric distribution, in particular the normal smoothed kernel distribution. To preserve time correlation between forecasts belonging the same event a Markov-process as proposed in [133] is implemented. The base-forecast profile is normalized (denoted as y_t),then for each scenario the normalized forecast (denoted as $z_{\omega,t}$)is obtained as:

$$z_{\omega,t} = y_t + x_{\omega,t} \qquad (6.44)$$

$$x_{\omega,t} = x_{\omega,t-1} \cdot \phi + \varepsilon_{\omega,t} \qquad (6.45)$$

where the one-lag auto-correlation parameter ϕ is assumed equal to 0.99 while ε is the random component generated according to the modeled PDF.

Figure 6.20 shows an example of the generated load forecast events and in bold red the original SARIMA forecast from which the events are generated. In the proposed figure N_E has been assumed to be 300 as a larger number would affect the figure clarity.

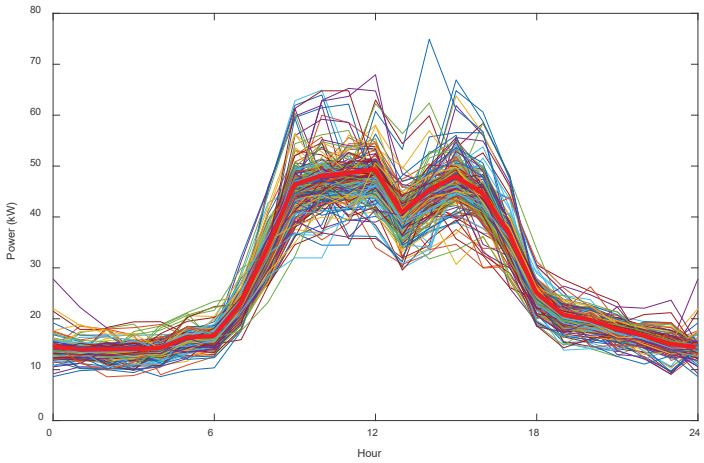

Figure 6.20 Base profile and the generated stochastic events

- Normalization: the stochastic events are normalized before the clustering process. The PV production profiles are normalized with respect to the rated power. While the load consumption profiles are normalized considering the maximum consumption peak.

- Clustering process and scenarios tree generation. Given J the number of prosumers considered to be optimized, for each prosumer two stochastic variables are considered, i.e. PV and load. Thus, the initial number of stochastic profiles is $2 \cdot J \cdot N_E$. The number of tree's final scenarios N_{SC}, is determined by the number of tree nodes, i.e. N_D, and by the branches for each node, i.e. N_B, (we assume that the number of branches is equal in each node).

$$N_{SC} = N_B^{N_D - 1} \qquad (6.46)$$

The clustering procedure is repeated for each branch of the tree, for the first branch all the events are considered, while for the successive branches only the events belonging to the parent branch are considered. The procedure starts with the selection of N_B initial centroids randomly selected among the events. For each event ω belonging the parent branch, the distance from the k-th centroid is calculated according to (6.47)

$$d_{\omega,k} = \sqrt{\sum_{t,j} \left(e_{t,j,\omega} - c_{t,k} \right)^2} \qquad (6.47)$$

The ω-th event is assigned to the k-th centroid having the lowest distance. After events assignment the centroid is updated as the average of the events belonging to it. The procedure is iterated until the difference between the centroids and their respective cluster in two subsequent iterations is lower than a threshold or until the maximum iteration limit is reached.

After the clustering procedure the tree branches are represented by resulting centroids. The probability of each scenario w_i is assumed to be the ratio between the events allocated to that scenario and the total number of events N_{SC}.

- An anti-normalization procedure is applied to the scenario tree reduction's output to restore real-world power values. An example of the resulting scenario trees for PV and load, respectively, is illustrated in Figure 6.21. In the figure N_D and N_B are to be assumed 6 and 4, respectively.

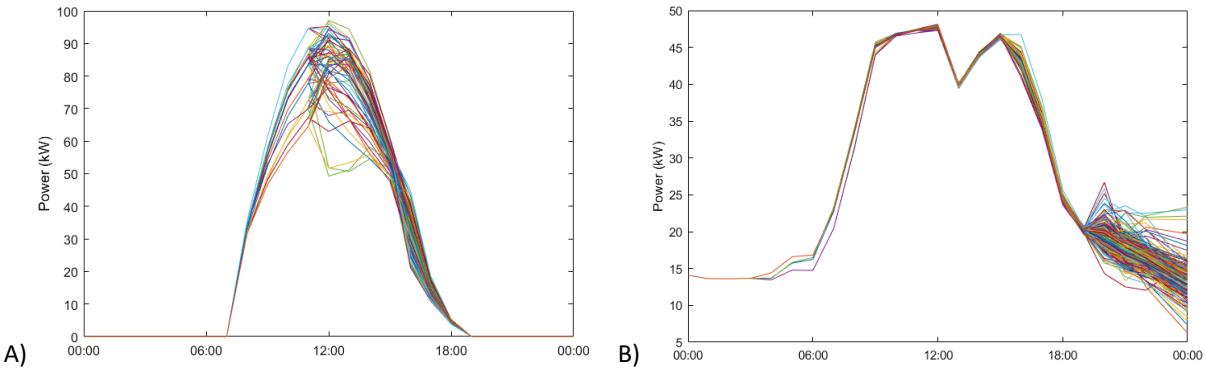

Figure 6.21 Scenarios tree of A) PV and B) Load

- The overall objective function of the stochastic optimization to be minimized is given by the weighted sum of the objective functions calculated per each of the N_{SC} tree final scenarios. The objective function to be used in the formulation can be chosen from the ones formerly illustrated in this chapter.

$$OF = \sum_{i=1}^{N_{SC}} w_i \cdot OF_i \qquad (6.48)$$

As the scenario tree branches out ahead in time, for the common path of the tree branches it must be ensured that the optimization solution is unique among scenarios belonging to the same path. Therefore, non-anticipativity constraints are added to formulation constraints to ensure that the tree-common paths have the same optimization results among different scenarios.

6.5.1. Test case

The proposed test case considers a REC of five prosumers equipped with PV and BES, except for user-5 only equipped by PV system. Additionally, a pure consumer is considered, this consumer represents the aggregate of all the REC's consumers. Storages at *t*=0 are assumed to be partially charged with a SOC of 40%. Table 6.12 illustrates the REC members characteristics in terms of PV and BES rated power and energy consumption.

The simulation encompasses five consecutive days, with LFs generated using SARIMA models as the basis for stochastic events generation. The simulation aims to analyze a realistic scenario by considering deviation between the forecast and the data from PVs and loads. PV and LF data for the optimization phase are provided at a 5-minute time resolution. The number of stochastic events generated from the base-forecast is equal to 50 thousand. In the proposed case the scenario tree is formed by 4 nodes and 3 branches per node. The stochastic approach is tested using the mathematical formulation employing four-prices described in section 6.4. The assumed price scenario is the one with hourly varying tariffs and the price spreads $\Delta\pi_t^-$ and $\Delta\pi_t^+$ are equal to 30 €/MWh and 80 €/MWh, respectively.

Table 6.12 PV rating, BES rating and load energy (over the simulated period) of REC

User	1	2	3	4	5	6
PV (kWp)	300	400	30	200	150	0
BES_{Power} (kW)	125	150	75	100	0	0
BES_{Energy} (kWh)	500	500	100	400	0	0
Load (kWh)	3774	4179	1614	1885	1879	11674

The energy performance, for each single prosumer and for the overall REC, resulting from the two non-optimized algorithms and from the optimized one employing the stochastic process are illustrated in Table 6.13 and Table 6.14, respectively. The stochastic approach preserves the capability of the 4-prices formulation of trading between the single-prosumer maximization of the behind the meter self-consumption and the community self-consumption.

Table 6.13 Prosumers energy performance

	Prosumer	**1**	**2**	**3**	**4**	**5**	**6**	**Tot.**
E_{buy} (kWh)	**Non-opt-1**	0	221	964	0	994	11674	13853
	Non-opt-2	597	1042	1218	403	994	11674	15928
	Stochastic opt.	152	285	1025	125	994	11674	14225
E_{sell} (kWh)	**Non-opt-1**	2145	4121	0	2036	2234	0	10536
	Non-opt-2	2970	5088	209	2604	2234	0	13105
	Stochastic opt.	2405	4173	18	2248	2234	0	11077
Self Cons.	**Non-opt-1**	56%	46%	98%	41%	28%	-	
	Non-opt-2	49%	37%	64%	34%	28%	-	
	Stochastic opt.	55%	45%	94%	40%	28%	-	

Table 6.14 REC energy performance

	E_{imp} (kWh)	**E_{exp} (kWh)**	**Self-Cons.**	**BES Resid. (kWh)**
Non-opt-1	9134	5817	63%	732
Non-opt-2	5320	2497	79%	0
Stochastic opt.	6291	3113	75%	383

Table 6.15 reports the economic results of the stochastic optimized approach compared with the two non-optimized benchmark models. For the REC the use of the stochastic approach leads to a reduction in the overall energy procurement cost.

Table 6.15 Economic performance

(€)	E_{buy}	E_{sell}	BES resid.	Profit
Non-opt-1	3621	1486	189	-1946
Non-opt-2	3984	2419	0	-1565
Stochastic opt.	3606	2014	99	-1493

Chapter 7. Conclusions

The increase of the use of Renewable Energy Sources (RES) for electrical energy production is considered one of the major means for achieving climate-altering emission reduction targets, along with the progressive electrification of loads. In countries where the exploitation of RES is in an advanced state, as in Europe, the further exploitation of RES is hampered by the challenges these sources pose to the control systems governing the proper operation of power systems. Among these difficulties, the reduction of the overall system's inertia due to disuse of rotating generators in favor of Converter-Interfaced Sources (CISs) is considered one of the major challenges. Other obstacles to the further exploitation of RES arise from their intermittent and random nature, which makes them poorly controllable/dispatchable, unless suitable de-loading techniques are implemented. In order to improve the capability of hosting RES by distribution systems, where the most widely used renewable source is solar photovoltaics, a number of legislative acts have recently been adopted at the European and member country levels that aim to create an environment conducive to the development of energy markets, in which even small producers, or rather prosumers, can gain access. Within this framework, the Renewable Energy Communities (RECs) were recently introduced in European Union (EU) member states by means of legislative and regulatory acts that, as a result of their recent introduction, have been subject to several amendments and updates.

Regarding the impact of RES on the power system's overall inertia, the thesis addresses the real-time estimation of the inertia of a power system. Such an estimation is considered a critical issue for the correct set-up of the microgrid control as well as for the safe and secure operation of the microgrid.

The thesis addresses also the optimal sizing and management of RECs by proposing tools to maximize the profitability, or to minimize their energy procurement costs, acting on the controllable resources of RECs, and in particular the Battery Energy Storage (BES).

The proposed Energy Management System (EMS) of the controllable resources of RECs accounts for the different legislative and regulatory acts of the main EU Member States.

Concerning the proposed procedure to perform online inertia estimation, it consists of two stages: an optimization-based Primary Frequency Control (PFC) parameters identification and a regression-based inertia estimation. The use of inertia estimation based on the Dynamic Regression Extension and Mixing method (DREM) depends on the knowledge of PFC's dynamic parameters, which are typically unknown. To overcome this limitation, the integration of a parameter identification stage is proposed. The PCF's parameters identification stage minimizes the difference between the measured frequency response during a disturbance and the frequency response derived from the analytical formulation. This analytical approach results in a highly efficient and fast optimization process to determine the optimal set of parameters that accurately describe the PFC dynamics.

A sensitivity analysis is performed to evaluate the impact of two factors on the algorithm performance: the time delay of the operator (t_d) and the learning rate of the gradient algorithm (λ). When the PFC parameters are updated, the estimated inertia does not depend significantly on these two factors. However, when the PFC parameters are not updated, e.g., when a set of generators is disconnected, the estimated inertia is different for different values of t_d or λ. This property is used as criterion to decide when the PFC parameters need to be updated.

The performance of the proposed approach has been tested using the IEEE 39-bus benchmark network model, under normal load variations, under large disturbances, and in the presence of CISs controlled in both grid-following and grid-forming modes. The change in the effective inertia when CISs are connected to the power system can be successfully identified. Additionally, the results of the real-time simulations confirm the applicability of the algorithm, which is characterized by low computational times.

Concerning the legal framework of energy communities in the EU, it is analyzed emphasizing how different countries have transposed the EU directives into national regulations. Key

differences between national regulations include proximity constraints, the maximum allowed rated power of RES installations, the type of grid (private or public) used for energy sharing, and the methods of valuing locally produced energy, either through economic incentives or price agreements between producers and consumers.

The proposed optimal management of RECs considers the impact of Photovoltaic (PV) systems and BESs systems on both energy production and economic outcomes. The proposed EMS for REC, providing the optimal BESs power set points, encompasses an advanced metering infrastructure capable of gathering energy and power data from prosumers assets. Data are stored and secured in a database which makes them available for further elaboration. Moreover, the database features a graphic user interface enhancing user awareness of their consumption. The EMS implements a rolling horizon procedure aimed at minimizing the energy procurement cost for the REC by controlling the BES units of the prosumers. The rolling optimization algorithm is designed to make use of both historical and online smart-meter measurements and of continuously updated forecasts for both load and PV generation and energy prices. Simplified forecasting methods, such as autoregressive and averaging techniques, are proposed for use in the proposed EMS. The EMS is further interfaced with a real-time simulator to validate the communication infrastructure and real-time operation of the proposed optimization procedure.

The measurement campaigns developed in the framework of GECO and Self-User projects lead to the creation of a consistent dataset used for load forecasting by the EMS and the creation of standard consumption profiles for different customer and day types, which are employed in the REC sizing process when no smart-meter data is available.

The final part of the thesis presents an incentive-based model and a four-prices market model to be implemented in an EMS for the optimal operation of RECs. The proposed incentive-based model is compliant with the national regulations transposing the European Renewable Energy Directive II (RED II) which grant an economic incentive to shared energy. While the four-prices model is compliant with national regulations which employ a price agreement between the local producers and local consumers. The four-prices model, adopting the proper

internal prices, is also capable of well-representing national regulations that employ incentives on the energy shared within the REC. The optimization is tested with both hourly pricing and time-of-use tariffs: in both price scenarios the optimized approach leads to a reduction of the energy procurement cost for the REC with respect to non-optimized approaches used for benchmarking. The findings show that the proposed optimization approach is capable of balancing trade-offs between community and single-customer welfare. Additionally, a stochastic formulation is proposed, to deal with the intrinsic unpredictability and uncertainty of load and PV forecast followed by a K-means clustering technique to reduce the number of stochastic scenarios to limit the computational efforts.

An in-progress development of this work is related to the integration of ancillary services into the optimal management of the REC. The RED II grants the REC the right to participate in energy markets, including the ancillary service ones. Moreover, in recent time grid operators lowered the minimum power required to participate in ancillary services auctions enabling the participation of REC as an aggregation entity. The provision of ancillary services by RECs may lead to additional benefits for both the REC members and grid operators as the latter may benefit of power modulation not only provided by few large systems but from several distributed ones, potentially reducing the risk of service unavailability due to network congestion.

Appendix A. ILT and DREM

Introduction

This appendix presents the mathematical formulation used to derive the time-domain model of PFC dynamics. Additionally, the steps of the DREM procedure are described, detailing its three stages: regression, extension, and mixing.

Inverse Laplace Transform of PFC Dynamics

A rearrangement of the expression for Γ(*s*) in equation (2.9) yields:

$$\Gamma(s) = -R \cdot \frac{1 + a_1 s + a_2 s^2}{1 + b_1 s + b_2 s^2 + b_3 s^3} \qquad \text{(A.1)}$$

where

$$a_1 = \tau + \tau_p \qquad a_2 = \tau \tau_z$$
$$b_1 = 2HR + \tau_z \qquad b_2 = 2HRa_1 \qquad b_3 = 2HRa_2 \qquad \text{(A.2)}$$

The term (-*R*) is omitted for simplicity and will be reintroduced later. The transfer function Γ'(*s*) can be rewritten as

$$\Gamma'(s) = -R \cdot \frac{1 + a_1 s + a_2 s^2}{(s + r_1)(s + r_2)(s + r_3)} \qquad \text{(A.3)}$$

The roots of (A.3) are

$$
\begin{aligned}
r_1 &= -\frac{h_3}{3\sqrt[3]{2}b_3} + \frac{\sqrt[3]{2}h_2}{3b_3h_3} + \frac{b_2}{3b_3} \\
r_2 &= \frac{\left(1-i\sqrt{3}\right)h_3}{6\sqrt[3]{2}b_3} - \frac{\left(1+i\sqrt{3}\right)h_2}{3\sqrt[3]{4}b_3h_3} + \frac{b_2}{3b_3} \\
r_3 &= \frac{\left(1+i\sqrt{3}\right)h_3}{6\sqrt[3]{2}b_3} - \frac{\left(1-i\sqrt{3}\right)h_2}{3\sqrt[3]{4}b_3h_3} + \frac{b_2}{3b_3}
\end{aligned}
\qquad \text{(A.4)}
$$

in which the following auxiliary variables have been defined as

$$
\begin{aligned}
h_1 &= 9b_1b_2b_3 - 2b_2{}^3 - 27b_3{}^2 \\
h_2 &= 3b_1b_3 - b_2{}^2 \\
h_3 &= \sqrt[3]{\sqrt{h_1{}^2 + 4h_2{}^3} + h_1}
\end{aligned}
\qquad \text{(A.5)}
$$

To find the inverse Laplace transform (ILT) of Γ'(*s*), it is rearranged as

$$
\begin{aligned}
\Gamma'(s) = {} & \frac{1}{(s+r_1)(s+r_2)(s+r_3)} + a_1\frac{s}{(s+r_1)(s+r_2)(s+r_3)} \\
& + a_2\frac{s^2}{(s+r_1)(s+r_2)(s+r_3)}
\end{aligned}
\qquad \text{(A.6)}
$$

The ILT of the first term is [182]:

$$
\begin{aligned}
\mathcal{L}^{-1}\left\{\frac{1}{(s+r_1)(s+r_2)(s+r_3)}\right\} = {} & \frac{e^{-r_1t}}{(r_1-r_2)(r_1-r_3)} \\
& + \frac{e^{-r_2t}}{(r_1-r_2)(r_3-r_2)} + \frac{e^{-r_3t}}{(r_1-r_3)(r_2-r_3)}
\end{aligned}
\qquad \text{(A.7)}
$$

Considering also the second and third terms (time derivatives of the first term), and reintroducing the term (-*R*), we obtain the ILT of Γ(*s*):

$$
\begin{aligned}
\gamma(t) = -R\Bigg[& \frac{1-r_1a_1+r_1{}^2a_2}{(r_1-r_2)(r_1-r_3)}e^{-r_1t} + \frac{1-r_2a_1+r_2{}^2a_2}{(r_1-r_2)(r_3-r_2)}e^{-r_2t} \\
& + \frac{1-r_3a_1+r_3{}^2a_2}{(r_1-r_3)(r_2-r_3)}e^{-r_3t}\Bigg]
\end{aligned}
\qquad \text{(A.8)}
$$

The final form can be generalized as

$$\gamma(t) = -R \cdot \left(k_1 e^{-r_1 t} + k_2 e^{-r_2 t} + k_3 e^{-r_3 t} \right) \qquad \text{(A.9)}$$

Dynamic Regression Extension and Mixing

The DREM method constructs a linear regression based on equation (2.3). Assuming that p_{PFC} is known, the unknown parameters are H and p^*. Equation (2.3) is repeated here in a rearranged form for convenience:

$$\dot{f} = \frac{1}{H}\left(\frac{1}{2} \frac{p_{PFC} - p_e}{f} \right) + \frac{p^*}{H}\left(\frac{1}{2f} \right) \qquad \text{(A.10)}$$

The regression equation is constructed by applying a filter $\mathcal{F} = \alpha / (s + \alpha)$ to (2.3), where α>0 is a parameter of the filter. This filtering technique is employed to avoid a direct derivative action applied to f [183]. Defining the unknown parameters and the three filtered coefficients as

$$x_1 = \frac{1}{H}; \qquad x_2 = \frac{p^*}{H} \qquad \text{(A.11)}$$

$$\begin{aligned} \xi_1 &= \mathcal{F}\left[\frac{1}{2} \frac{p_{PFC} - p_e}{f} \right] = \frac{\alpha}{s+\alpha}\left(\frac{1}{2} \frac{p_{PFC} - p_e}{f} \right) \\ \xi_2 &= \mathcal{F}\left[\frac{1}{2f} \right] = \frac{\alpha}{s+\alpha}\left(\frac{1}{2f} \right) \\ \xi_3 &= \mathcal{F}\left[\dot{f} \right] = \frac{\alpha s}{s+\alpha} f \end{aligned} \qquad \text{(A.12)}$$

the regression takes the form

$$\xi_3 = x_1 \cdot \xi_1 + x_2 \cdot \xi_2 \qquad \text{(A.13)}$$

As there are two unknown parameters but one equation, the regressor is extended by applying a dynamic operator $\mathcal{H}$ to (A.13). The delay operator is used because of its recognized efficiency in engineering applications [54]. It has the form:

$$\left[\mathcal{H}(\cdot)\right](t) = (\cdot)(t - t_d) \qquad \text{(A.14)}$$

where t_d is the time delay. By combining the original regression and its extension, the matrix form is obtained:

$$\underbrace{\begin{bmatrix} \xi_3 \\ \xi_3' \end{bmatrix}}_{\mathbf{A}} = \underbrace{\begin{bmatrix} \xi_1 & \xi_2 \\ \xi_1' & \xi_2' \end{bmatrix}}_{\mathbf{B}} \underbrace{\begin{bmatrix} x_1 \\ x_2 \end{bmatrix}}_{\mathbf{x}} \qquad \text{(A.15)}$$

where $\xi_{1,2,3}'$ are the coefficients modified by $\mathcal{H}$.

To decouple the regression, the mixing procedure consists of multiplying (A.15) by the adjoint (*adj*) of matrix **B**. Since $adj(\mathbf{B}) \cdot \mathbf{B} = \partial \cdot \mathbf{I}$, where ∂ is the determinant of **B** and **I** is the identity matrix, the regression takes its decoupled final form:

$$\mathbf{Z} = \partial \cdot \mathbf{x}\,, \qquad \text{(A.16)}$$

where **Z** is defined as

$$\mathbf{Z} = adj(\mathbf{B}) \cdot \mathbf{A}\,. \qquad \text{(A.17)}$$

For a complete mathematical description of the DREM, the reader is referred to [54], [184].

Appendix B. API for Data Exchange

Introduction

This appendix is devoted to the description of API employed in data exchange among the various components of the EMS. The API facilitates communication between the SMs, DB and the load forecasts generator enabling real-time data transfer among and seamless integration of elements coming from different manufacturers.

The SMs, supplied by various manufacturers and installed during the project development, enable the collection of measurements via API HTTP requests. However, the structure of the HTTP requests differs for each manufacturer and may be also non-homogeneous with the format used by the database. To address this issue, scripts have been developed to perform the HTTP request to the meter, rearrange the data structure if necessary, and subsequently send another HTTP request to the database to log the measurements.

Non-Intrusive Load Monitoring

APIs provided by Regalgrid allow to acquire power and energy data both in quasi-real-time and past data. The API HTTP request for real-time data can be executed not more frequently than 5 seconds. In Table B.1 are reported the API string to be used to perform a *GET* request the real-time data. In the string reported in the table the grid identifier and API key, i.e. the code which identifies the cluster of SMs and the password to access the data, have been replaced by '*y*' and '*x*' characters for both privacy and safety.

Table B.2 reports the structure of the JSON format obtained as response to the HTTP GET request.

Table B.1 HTTP API request for real-time data

Energy
https://regalgrid.net/UserApi/RealTime/GetGridEnergyTotal/xxxx-xxxx-xxxx-xxxx-xxxx/yyyy-yyyy-yyyy-yyyy-yyyy
Power
https://regalgrid.net/UserApi/RealTime/GetGridLiveData/xxxx-xxxx-xxxx-xxxx-xxxx/yyyy-yyyy-yyyy-yyyy-yyyy

Table B.2 HTTP API response for real-time data

Name	**Description**	**Data format**
	Energy HTTP response format	
Device ID	SNOCU unique ID	Integer
Last Update UTC	Date/time (in UTC format) of last data read from SNOCU.	Date
Status	SNOCU current status (Online/NoData/Offline).	String
PV Energy Total	Lifetime Photovoltaic energy (Wh), if available from inverter.	Integer
Load Energy Total	Lifetime Loads (Wh).	Integer
Battery Energy IN Total	Lifetime Battery Energy In (Wh), if available from inverter.	Integer
Battery Energy OUT Total	Lifetime Battery Energy Out (Wh), if available from inverter.	Integer
Exported Energy Total	Lifetime energy exported to grid (Wh).	Integer
Imported Energy Total	Lifetime energy imported from grid (Wh).	Integer
Inverter Energy OUT total	Lifetime energy produced by inverter (Wh), if available from inverter.	Integer
Inverter Energy IN total	Lifetime energy imported by inverter (Wh), if available from inverter.	Integer
	Power HTTP response format	
Device ID	SNOCU unique ID	Integer
Active Command	Inverter's current active command issued by SNOCU (SelfMode/BatteryCharge/BatteryDischarge/BatteryStop/SleepMode).	String
Last Update UTC	Date/time (in UTC format) of last data read from SNOCU.	Date
Status	SNOCU current status (Online/NoData/Offline).	String
Power PV	Photovoltaic real time power in Watts.	Integer
Power Load	Loads real time power in Watts.	Integer
Power Battery	Real time battery power in Watts (positive means charging, negative means discharging).	Integer
Power Grid	Realtime grid exchange in Watts (positive means export, negative means import).	Integer
Battery SOC	Battery State of Charge (%).	Integer

Table B.3 reports the structure to execute a HTTP POST request to acquire the historical data from the Regalgrid database. Both energy and power measurements can be requested according to the request structure. The maximum time-resolution for historical data is 5 minutes instead of the 5 seconds achievable with the real-time requests. In Table B.4 the structure of the JSON format response is provided.

Table B.3 HTTP API request for historical data

Energy		
https://regalgrid.net/UserApi/ HistoricalData/GetPowerDataPerInterval/JSONstructure		
Power		
https://regalgrid.net/UserApi/ HistoricalData/GetEnergyDataPerInterval/JSONstructure		
JSON Structure		
Name	**Description**	**Type**
API Key	Your unique user API_KEY provided by Regalgrid	String
From Date	Start Date and Time.	Date
To Date	End Date and Time.	Date
Time Offset	Time offset is an amount of time (hours) subtracted from or added to Coordinated Universal Time (UTC) time to get the current civil time.	Integer
Interval	data grouped by Interval (minutes)	Integer
Device ID	SNOCU unique ID	Integer

Table B.4 HTTP API ressponse for historical data

Name	Description	Type
	Energy	
Date	Date	Date
PV Energy	Photovoltaic energy (Wh), if available from inverter	Integer
Load Energy	Loads (Wh)	Integer
Battery Energy IN	Battery Energy In (Wh), if available from inverter	Integer
Battery Energy OUT	Battery Energy Out (Wh), if available from inverter	Integer
Exported Energy	Energy exported to grid (Wh)	Integer
Imported Energy	Energy imported from grid (Wh)	Integer
Inverter Energy OUT	Energy produced by inverter (Wh), if available from inverter	Integer
Inverter Energy IN	Energy imported by inverter (Wh), if available from inverter	Integer
	Power	
Date	Date	Date
Power PV	Photovoltaic power in Watts	Integer
Power Load	Loads power in Watts	Integer
Power Battery	Battery power in Watts (positive means charging, negative means discharging)	Integer
Power Grid	Grid exchange in Watts (positive means export, negative means import)	Integer
Battery SOC	Battery State of Charge (%)	Integer

User Device

Data coming from Urmet UDs installed within the GECO project are primarily stored in a DB owned by ENEA as it is the devices owner. The data acquisition is performed via API and employing a double request. All http API requests use the method POST. The first API request is devoted to obtaining a token to access the DB, the token has a limited validity in time, thus if it is expired the first API requested should be the one to obtain a valid token. Once the valid token is obtained the asynchronous power data and/or the 15 minutes average power can be collected employing the HTTP requests indicated in Table B.5. The table reports in bold uppercase the values that have to be compiled.

Table B.5 HTTP API request for UDs data

Token
curl -s -X POST "https://winter.bologna.enea.it/rdsIDP/user/login?password=**PASSWORD**&username=**USERNAME**" -H "accept: */*" -d ""
Power
curl -s -X POST "https://winter.bologna.enea.it/rdsIDP/data/getData" -H "accept: */*" -H "Authorization: **TOKEN**" -H "Content-Language: it_IT" -H "Content-Type: application/json" -d "{\"queryid\": 32, \"startDate\": \"**INITIALDATE**\", \"endDate\": \"**FINALDATE**\", \"deviceid\":\"**DEVICEID**\"}"
Energy
curl -s -X POST "https://winter.bologna.enea.it/rdsIDP/data/getData" -H "accept: */*" -H "Authorization: **TOKEN**" -H "Content-Language: it_IT" -H "Content-Type: application/json" -d "{\"queryid\": 33, \"startDate\": \"**INITIALDATE**\", \"endDate\": \"**FINALDATE**\", \"deviceid\":\"**DEVICEID**\"}"

Database

The Emoncms database offers a variety of APIs that allow for reading and writing data to both inputs and feeds, retrieving lists of nodes, inputs, and feeds, as well as deleting inputs or feeds, among other functionalities. These APIs support both GET and POST HTTP methods. The key elements to provide in the API request are:

- Database address: http://192.168.145.5/;
- Node identifier;
- Inputs names and values;
- Time in string or UNIX format (useful to assign a timestamp different from the current time);
- API key: unique identifier to authenticate a user.

As shown in Table B.6, data can be accessed or submitted in CSV or JSON formats depending on the HTTP method. Additionally, data can be written to a single node or to multiple nodes, the latter case allows the bulk data to reduce the communication efforts. In the provided examples for single node logging, the values 100, 200, and 300 are assigned to the inputs

power1, power2, and power3, respectively, for the node "nodeid". In case of bulk input each array should contain the following ordered elements: the first number represents the time offset; the second element indicates the node id while the other elements represent the data, one per input, to log.

Table B.6 APIs to log INPUT data

Description	HTTP Method	Example
Single Node		
JSON format	GET	http://192.168.145.5/input/post?node=nodeid&fulljson={"power1":100,"power2":200,"power3":300}
JSON format - with time	GET	http://192.168.145.5/input/post?node=nodeid&fulljson={"power1":100,"power2":200,"power3":300,"time":"2022-12-02T16%3A45%3A08%2B01%3A00"}
JSON like format	GET	http://192.168.145.5/input/post?node=nodeid&json={power1:100,power2:200,power3:300}
CSV format	GET	http://192.168.145.5/input/post?node=nodeid&csv=100,200,300
Set the input entry time manually	GET	http://192.168.145.5/input/post?time=1669995908&node=nodeid&csv=100,200,300
Node name as sub-action	GET	http://192.168.145.5/input/post/nodeid?fulljson={"power1":100,"power2":200,"power3":300}
To post data from a remote device you will need to include in the request URL your write apikey.	GET	http://192.168.145.5/input/post?node=nodeid&fulljson={"power1":100,"power2":200,"power3":300}&apikey=XYZ1234
JSON format	POST	curl --data "node=nodeid&data={power1:100,power2:200,power3:300}&apikey=XYZ1234" "http://192.168.145.5/input/post"
CSV format	POST	curl --data "node=nodeid&data=100,200,300&apikey=XYZ1234" "http://192.168.145.5/input/post"
Multiple nodes (bulk input)		
JSON format	GET	http://192.168.145.5/input/bulk?data=[[0,16,1137],[0,17,1437,3164],[0,19,1412,3077]]&time=1670001912&apikey=XYZ1234
JSON format	POST	curl --data data=[[0,16,1137],[2,17,1437,3164],[4,19,1412,3077]]&apikey=XYZ1234" "http://192.168.145.5/input/bulk"

The nodes and inputs name can be retrieved both from the DB's GUI or through API request. The APIs to get the list of nodes and inputs and the corresponding values are reported in Table B.7. Option to retrieve data from a specific node or input are available.

Table B.7 APIs for input retrieval

Description	HTTP Method	Example
List all nodes and associated inputs	GET	http://192.168.145.5/input/get
List inputs for specific node	GET	http://192.168.145.5/input/get/nodeid
Fetch specific input from node	GET	http://192.168.145.5/input/get/nodeid/power1

The APIs described in Table B.6 can be used to log data in the inputs, however this solution allows to write only one point related to a single time-stamp. In contrast the APIs related to feeds allows to log multiple pairs of data-timestamp as well as to fetch them from the DB. The time to be used is the UNIX format. Table B.8 provides an overview of the APIs available for logging or fetching data from feeds. These APIs offer various options, such as specifying the interval between data retrieval, choosing whether to fetch the nearest or average values, determining whether to skip missing values, and selecting between retrieving incremental values or absolute ones.

Table B.8 APIs for feeds logging and retrieval

Description	HTTP Method	Example
Insert multiple data points	GET	http://192.168.145.5/feed/insert.json?id=feedid&data=[[1670005600,100],[1670005610,150],[1670005620,200],[1670005630,250]]
Fetch a value at a given time	GET	http://192.168.145.5/feed/value.json?id=feedid&time=1670005600
Fetch data from a feed:	GET	http://192.168.145.5/feed/data.json?id=feedid&start=1670002002&end=1670005602&interval=60&average=0&timeformat=unix&skipmissing=0&limitinterval=0&delta=0

Bibliography

[1] International Energy Agency, “Greenhouse Gas Emissions from Energy Data Explorer,” 2023. [Online]. Available: https://www.iea.org/data-and-statistics/data-tools/greenhouse-gas-emissions-from-energy-data-explorer

[2] A. Stips, D. Macias, C. Coughlan, E. Garcia-Gorriz, and & X. S. Liang, “On the causal structure between CO 2 and global temperature OPEN,” *Nature Publishing Group*, 2016, doi: 10.1038/srep21691.

[3] United Nation Framework Convention on Climate Change, “The Paris Agreement,” in *Paris Climate Change Conference*, Paris, France, 2015.

[4] European Commission: Directorate-General for Energy, *Clean energy for all Europeans*. Publications Office, 2019. doi: 10.2833/9937.

[5] European Council, “European Council conclusions, 15-16 October 2020,” 2020. [Online]. Available: https://www.consilium.europa.eu/en/meetings/european-council/2020/10/15-16/

[6] European Union, “New electricity market design: a fair deal for consumers.”

[7] European Commission Directorate-General for Communication, “Smart cities - Cities using technological solutions to improve the management and efficiency of the urban environment.” [Online]. Available: https://commission.europa.eu/eu-regional-and-urban-development/topics/cities-and-urban-development/city-initiatives/smart-cities_en

[8] C. A. Nucci, “Neutralità climatica e transizione energetica: il ruolo delle città intelligenti e delle comunità energetiche,” *Annales. Proceedings of the Academy of Sciences of Bologna. Class of Physical Sciences*, Dec. 2023, doi: 10.30682/ANNALESPS2301L.

[9] European Commission Directorate General for Research and Innovation, “Proposed Mission: 100 Climate-neutral Cities by 2030-by and for the Citizens.” doi: 10.2777/347806.

[10] European Commission, “Commission announces 100 cities participating in EU Mission for climate-neutral and smart cities by 2030.” [Online]. Available: https://ec.europa.eu/commission/presscorner/detail/en/ip_22_2591

[11] International Energy Agency, “World Energy Outlook 2023,” Paris, 2023. [Online]. Available: https://www.iea.org/reports/world-energy-outlook-2023

[12] International Energy Agency, “World Energy Outlook 2023 Executive Summary,” 2023. [Online]. Available: https://www.iea.org/reports/world-energy-outlook-2023/executive-summary

[13] Q. Wu and Y. Sun, *Modeling and Modern Control of Wind Power*. John Wiley & Sons, Inc., 2018.

[14] IEEE Power & Energy Society, “Impact of Inverter Based Generation on Bulk Power System Dynamics and Short-Circuit Performance,” 2018. doi: 10.17023/gka4-3v54.

[15] T. Taner, A. Tiwari, and T. S. Ustun, *Renewable Energy*. Rijeka: IntechOpen, 2021. doi: 10.5772/intechopen.84929.

[16] A. Fernández-Guillamón, E. Gómez-Lázaro, E. Muljadi, and Á. Molina-García, “Power systems with high renewable energy sources: A review of inertia and frequency control strategies over time,” *Renewable and Sustainable Energy Reviews*, vol. 115, p. 109369, Nov. 2019, doi: 10.1016/J.RSER.2019.109369.

[17] North American Electric Reliability Corporation, “Integrating Inverter-Based Resources into Low Short Circuit Strength Systems,” 2017.

[18] Conseil international des grands réseaux électriques. Comité d’études B4, *Connection of wind farms to weak AC networks*. 2016.

[19] S. Weitemeyer, D. Kleinhans, T. Vogt, and C. Agert, “Integration of Renewable Energy Sources in future power systems: The role of storage,” *Renewable Energy*, vol. 75, pp. 14–20, Mar. 2015, doi: 10.1016/j.renene.2014.09.028.

[20] International Energy Agency, “World Energy Outlook Special Report Batteries and Secure Energy Transitions,” 2024. [Online]. Available: https://www.iea.org/reports/batteries-and-secure-energy-transitions

[21] G. Fitzgerald, J. Mandel, and J. Morris, “The Economics of Battery Energy Storage: How Multi-use, Customer-sited Batteries Deliver the Most Services and Value to Customers and the Grid (Technical Appendix),” 2015.

[22] L. Maeyaert, L. Vandevelde, and T. Döring, “Battery Storage for Ancillary Services in Smart Distribution Grids,” *Journal of Energy Storage*, vol. 30, Aug. 2020, doi: 10.1016/j.est.2020.101524.

[23] D. Metz and J. T. Saraiva, “Use of battery storage systems for price arbitrage operations in the 15- and 60-min German intraday markets,” *Electric Power Systems Research*, vol. 160, pp. 27–36, Jul. 2018, doi: 10.1016/J.EPSR.2018.01.020.

[24] J. M. Zepter, A. Lüth, P. Crespo del Granado, and R. Egging, “Prosumer integration in wholesale electricity markets: Synergies of peer-to-peer trade and residential

storage," *Energy and Buildings*, vol. 184, pp. 163–176, Feb. 2019, doi: 10.1016/J.ENBUILD.2018.12.003.

[25] European Union, *UE Directive 2018/2001 on the promotion of the use of energy from renewable sources*. 2018. [Online]. Available: https://eurlex.europa.eu/legalcontent/EN/TXT/PDF/?uri=CELEX:32018L2001&from=EN

[26] European Union, "Directive (EU) 2019/944 of the European parliament and of the council of 5 June 2019 on common rules for the internal market for electricity," 2019.

[27] J. Stute and M. Klobasa, "How do dynamic electricity tariffs and different grid charge designs interact? - Implications for residential consumers and grid reinforcement requirements," *Energy Policy*, vol. 189, p. 114062, 2024, doi: 10.1016/j.enpol.2024.114062.

[28] D. Frieden, J. Roberts, and A. F. Gubina, "Overview of emerging regulatory frameworks on collective self-consumption and energy communities in Europe," *International Conference on the European Energy Market, EEM*, vol. 2019-September, Sep. 2019, doi: 10.1109/EEM.2019.8916222.

[29] J. A. P. Lopes, C. L. Moreira, and A. G. Madureira, "Defining control strategies for microgrids islanded operation," *IEEE Transactions on Power Systems*, vol. 21, no. 2, pp. 916–924, May 2006, doi: 10.1109/TPWRS.2006.873018.

[30] U. Tamrakar, D. Shrestha, M. Maharjan, B. Bhattarai, T. Hansen, and R. Tonkoski, "Virtual Inertia: Current Trends and Future Directions," *Applied Sciences*, 2017, doi: 10.3390/app7070654.

[31] R. Ofir, U. Markovic, P. Aristidou, and G. Hug, "Droop vs. virtual inertia: Comparison from the perspective of converter operation mode," in *IEEE International Energy Conference (ENERGYCON)*, 2018. doi: 10.1109/ENERGYCON.2018.8398752.

[32] Q. Li, B. Ren, W. Tang, D. Wang, C. Wang, and Z. Lv, "Analyzing the inertia of power grid systems comprising diverse conventional and renewable energy sources," *Energy Reports*, vol. 8, pp. 15095–15105, Nov. 2022, doi: 10.1016/J.EGYR.2022.11.022.

[33] D. Pattabiraman, R. H. Lasseter, and T. M. Jahns, "Comparison of Grid Following and Grid Forming Control for a High Inverter Penetration Power System," *IEEE Power and Energy Society General Meeting*, vol. 2018-August, Dec. 2018, doi: 10.1109/PESGM.2018.8586162.

[34] B. K. Poolla, S. Bolognani, N. Li, and F. Dörfler, "A Market Mechanism for Virtual Inertia," *IEEE Transactions on Smart Grid*, vol. 11, no. 4, pp. 3570–3579, Jul. 2020, doi: 10.1109/TSG.2020.2969518.

[35] A. García, Á. Ortega, L. Rouco, and L. Sigrist, “A review of methods for the estimation of inertia and its distribution,” 2021, *Institute for Research in Technology, Comillas Pontifical University, Madrid*.

[36] S. C. Dimoulias, E. O. Kontis, and G. K. Papagiannis, “Inertia Estimation of Synchronous Devices: Review of Available Techniques and Comparative Assessment of Conventional Measurement-Based Approaches,” *Energies*, vol. 15, no. 20, 2022, doi: 10.3390/en15207767.

[37] E. Heylen, F. Teng, and G. Strbac, “Challenges and opportunities of inertia estimation and forecasting in low-inertia power systems,” *Renewable and Sustainable Energy Reviews*, vol. 147, p. 111176, Sep. 2021, doi: 10.1016/J.RSER.2021.111176.

[38] B. Tan, J. Zhao, M. Netto, V. Krishnan, V. Terzija, and Y. Zhang, “Power system inertia estimation: Review of methods and the impacts of converter-interfaced generations,” *International Journal of Electrical Power & Energy Systems*, vol. 134, p. 107362, Jan. 2022, doi: 10.1016/J.IJEPES.2021.107362.

[39] K. Prabhakar, S. K. Jain, and P. K. Padhy, “Inertia estimation in modern power system: A comprehensive review,” *Electric Power Systems Research*, vol. 211, p. 108222, Oct. 2022, doi: 10.1016/J.EPSR.2022.108222.

[40] E. Ørum *et al.*, “Future system inertia,” 2018, *ENTSO-e, Bruxelles, Belgium*. [Online]. Available: https://docs.entsoe.eu/dataset/nordic-report-future-system-inertia

[41] P. Du and J. Matevosyan, “Forecast System Inertia Condition and Its Impact to Integrate More Renewables,” *IEEE Transactions on Smart Grid*, vol. 9, no. 2, pp. 1531–1533, 2018, doi: 10.1109/TSG.2017.2662318.

[42] D. Zografos, M. Ghandhari, and R. Eriksson, “Power system inertia estimation: Utilization of frequency and voltage response after a disturbance,” *Electric Power Systems Research*, vol. 161, pp. 52–60, Aug. 2018, doi: 10.1016/J.EPSR.2018.04.008.

[43] P. K. Dhara and Z. H. Rather, “Non-synchronous Inertia Estimation in a Renewable Energy Integrated Power System with Reduced Number of Monitoring Nodes,” *IEEE Transactions on Sustainable Energy*, vol. 14, no. 2, pp. 864–875, Apr. 2023, doi: 10.1109/TSTE.2022.3227603.

[44] G. Cai, B. Wang, D. Yang, Z. Sun, and L. Wang, “Inertia Estimation Based on Observed Electromechanical Oscillation Response for Power Systems,” *IEEE Transactions on Power Systems*, vol. 34, no. 6, pp. 4291–4299, 2019, doi: 10.1109/TPWRS.2019.2914356.

[45] B. Tan and J. Zhao, “Data-Driven Time-Varying Inertia Estimation of Inverter-Based Resources,” *IEEE Transactions on Power Systems*, vol. 38, no. 2, pp. 1795–1798, 2023, doi: 10.1109/TPWRS.2022.3229869.

[46] R. K. Panda, A. Mohapatra, and S. C. Srivastava, “Online Estimation of System Inertia in a Power Network Utilizing Synchrophasor Measurements,” *IEEE Transactions on Power Systems*, vol. 35, no. 4, pp. 3122–3132, 2020, doi: 10.1109/TPWRS.2019.2958603.

[47] M. Liu, J. Chen, and F. Milano, “On-Line Inertia Estimation for Synchronous and Non-Synchronous Devices,” *IEEE Transactions on Power Systems*, vol. 36, no. 3, pp. 2693–2701, 2021, doi: 10.1109/TPWRS.2020.3037265.

[48] B. Tan, J. Zhao, V. Terzija, and Y. Zhang, “Decentralized data-driven estimation of generator rotor speed and inertia constant based on adaptive unscented Kalman filter,” *International Journal of Electrical Power & Energy Systems*, vol. 137, p. 107853, 2022, doi: https://doi.org/10.1016/j.ijepes.2021.107853.

[49] J. Guo, X. Wang, and B.-T. Ooi, “Estimation of Inertia for Synchronous and Non-Synchronous Generators Based on Ambient Measurements,” *IEEE Transactions on Power Systems*, vol. 37, no. 5, pp. 3747–3757, 2022, doi: 10.1109/TPWRS.2021.3134818.

[50] M. Mazidi, T. McKelvey, and P. Chen, “A Pure Data-Driven Method for Online Inertia Estimation in Power Systems Using Local Rational Model Approach,” *IEEE Transactions on Industry Applications*, vol. 59, no. 5, pp. 5506–5516, 2023, doi: 10.1109/TIA.2023.3288503.

[51] F. Zeng, J. Zhang, G. Chen, Z. Wu, S. Huang, and Y. Liang, “Online Estimation of Power System Inertia Constant Under Normal Operating Conditions,” *IEEE Access*, vol. 8, pp. 101426–101436, 2020, doi: 10.1109/ACCESS.2020.2997728.

[52] K. Tuttelberg, J. Kilter, D. Wilson, and K. Uhlen, “Estimation of Power System Inertia From Ambient Wide Area Measurements,” *IEEE Transactions on Power Systems*, vol. 33, no. 6, pp. 7249–7257, 2018, doi: 10.1109/TPWRS.2018.2843381.

[53] T. Kerdphol, M. Watanabe, R. Nishikawa, Y. Hayashi, and Y. Mitani, “Inertia Estimation of the 60 Hz Japanese Power System From Synchrophasor Measurements,” *IEEE Transactions on Power Systems*, vol. 38, no. 1, pp. 753–766, 2023, doi: 10.1109/TPWRS.2022.3168037.

[54] J. Schiffer, P. Aristidou, and R. Ortega, “Online Estimation of Power System Inertia Using Dynamic Regressor Extension and Mixing,” *IEEE Transactions on Power Systems*, vol. 34, no. 6, pp. 4993–5001, 2019, doi: 10.1109/TPWRS.2019.2915249.

[55] W. Zhang, Y. Wen, and C. Y. Chung, “Impedance-based Online Estimation of Nodal Inertia and Primary Frequency Regulation Capability,” *IEEE Transactions on Power Systems*, pp. 1–12, 2022, doi: 10.1109/TPWRS.2022.3186525.

[56] J. Zhang and H. Xu, “Online Identification of Power System Equivalent Inertia Constant,” *IEEE Transactions on Industrial Electronics*, vol. 64, no. 10, pp. 8098–8107, 2017, doi: 10.1109/TIE.2017.2698414.

[57] F. Allella, E. Chiodo, G. M. Giannuzzi, D. Lauria, and F. Mottola, “On-Line Estimation Assessment of Power Systems Inertia With High Penetration of Renewable Generation,” *IEEE Access*, vol. 8, pp. 62689–62697, 2020, doi: 10.1109/ACCESS.2020.2983877.

[58] E. S. N. R. Paidi, H. Marzooghi, J. Yu, and V. Terzija, “Development and Validation of Artificial Neural Network-Based Tools for Forecasting of Power System Inertia With Wind Farms Penetration,” *IEEE Systems Journal*, vol. 14, no. 4, pp. 4978–4989, 2020, doi: 10.1109/JSYST.2020.3017640.

[59] E. M. Carlini, F. Del Pizzo, G. M. Giannuzzi, D. Lauria, F. Mottola, and C. Pisani, “Online analysis and prediction of the inertia in power systems with renewable power generation based on a minimum variance harmonic finite impulse response filter,” *International Journal of Electrical Power & Energy Systems*, vol. 131, p. 107042, Oct. 2021, doi: 10.1016/J.IJEPES.2021.107042.

[60] J. D. Rios Penaloza, A. Prevedi, A. Joshi, F. Napolitano, F. Tossani, and A. Borghetti, “On-line Inertia Estimation in Presence of Distributed Energy Resources,” in *2023 International Conference on Smart Energy Systems and Technologies (SEST)*, IEEE, Sep. 2023, pp. 1–6. doi: 10.1109/SEST57387.2023.10257463.

[61] J. Machowski, Z. Lubosny, J. Bialek, and J. R. Bumby, *Power System Dynamics, Stability and Control*, Third Edit. Croydon, UK: John Wiley & Sons Ltd., 2020.

[62] P. M. Anderson and M. Mirheydar, “A low-order system frequency response model,” *IEEE Transactions on Power Systems*, vol. 5, no. 3, pp. 720–729, 1990, doi: 10.1109/59.65898.

[63] E. O. Kontis, I. D. Pasiopoulou, D. A. Kirykos, T. A. Papadopoulos, and G. K. Papagiannis, “Estimation of power system inertia: A Comparative assessment of measurement-Based techniques,” *Electric Power Systems Research*, vol. 196, p. 107250, Jul. 2021, doi: 10.1016/J.EPSR.2021.107250.

[64] R. Ortega, V. Nikiforov, and D. Gerasimov, “On modified parameter estimators for identification and adaptive control. A unified framework and some new schemes,” *Annual Reviews in Control*, vol. 50, pp. 278–293, Jan. 2020, doi: 10.1016/J.ARCONTROL.2020.06.002.

[65] L. Gérin-Lajoie, “Report on the EMTP-RV 39-bus system,” 2015.

[66] S. D’Arco and J. A. Suul, “Virtual synchronous machines - Classification of implementations and analysis of equivalence to droop controllers for microgrids,” in *2013 IEEE Grenoble Conference PowerTech, POWERTECH 2013*, 2013. doi: 10.1109/PTC.2013.6652456.

[67] F. Milano, F. Dorfler, G. Hug, D. J. Hill, and G. Verbic, “Foundations and Challenges of Low-Inertia Systems (Invited Paper),” in *2018 Power Systems Computation Conference (PSCC)*, IEEE, Jun. 2018, pp. 1–25. doi: 10.23919/PSCC.2018.8450880.

[68] F. Mandrile, V. Mallemaci, E. Carpaneto, and R. Bojoi, “Lead-Lag Filter-Based Damping of Virtual Synchronous Machines,” *IEEE Transactions on Industry Applications*, vol. 59, no. 6, pp. 6900–6913, 2023, doi: 10.1109/TIA.2023.3293779.

[69] R. Ofir, U. Markovic, P. Aristidou, and G. Hug, “Droop vs. virtual inertia: Comparison from the perspective of converter operation mode,” in *2018 IEEE International Energy Conference (ENERGYCON)*, 2018, pp. 1–6. doi: 10.1109/ENERGYCON.2018.8398752.

[70] G. Han *et al.*, “A simple estimation method of grid-forming inverter inertia based on rate of change of frequency,” *IET Power Electronics*, vol. 17, no. 5, pp. 591–602, Apr. 2024, doi: 10.1049/pel2.12656.

[71] European Union, “Types of legislation.” Accessed: Aug. 20, 2024. [Online]. Available: https://european-union.europa.eu/institutions-law-budget/law/types-legislation_en

[72] European Parliament, *Directive (EU) 2018/844 of the European Parliament and of the Council of 30 May 2018 amending Directive 2010/31/EU on the energy performance of buildings and Directive 2012/27/EU on energy efficiency*. http://data.europa.eu/eli/dir/2018/844/oj, 2018.

[73] European Parliament, *Directive (EU) 2023/2413 of the European Parliament and of the Council of 18 October 2023 amending Directive (EU) 2018/2001, Regulation (EU) 2018/1999 and Directive 98/70/EC as regards the promotion of energy from renewable sources, and repealing Council Directive (EU) 2015/652*. http://data.europa.eu/eli/dir/2023/2413/oj, 2023.

[74] European Parliament, *Directive (EU) 2023/1791 of the European Parliament and of the Council of 13 September 2023 on energy efficiency and amending Regulation (EU) 2023/955*. http://data.europa.eu/eli/dir/2023/1791/oj, 2023.

[75] European Parliament, *Regulation (EU) 2018/1999 of the European Parliament and of the Council of 11 December 2018 on the Governance of the Energy Union and Climate Action*. http://data.europa.eu/eli/reg/2018/1999/oj, 2018.

[76] European Commission, *A Framework Strategy for a Resilient Energy Union with a Forward-Looking Climate Change Policy*. 2015.

[77] European Parliament, *Regulation 2019/943 of the European Parliament and of the Council of 5 June 2019 on the internal market for electricity*. http://data.europa.eu/eli/reg/2019/943/oj, 2019.

[78] European Parliament, *Regulation 2019/941 of the European Parliament and of the Council of 5 June 2019 on risk-preparedness in the electricity sector*. http://data.europa.eu/eli/reg/2019/941/oj, 2019.

[79] European Parliament, *Regulation 2019/942 of the European Parliament and of the Council of 5 June 2019 establishing a European Union Agency for the Cooperation of Energy Regulators*. http://data.europa.eu/eli/reg/2019/942/oj, 2019.

[80] International Energy Agency, "Net Zero Roadmap: A Global Pathway to Keep the 1.5 °C Goal in Reach," 2023. [Online]. Available: https://www.iea.org/reports/net-zero-roadmap-a-global-pathway-to-keep-the-15-0c-goal-in-reach

[81] European Commission Directorate-General for Energy, "Guidance on designating renewables acceleration areas," 2024. [Online]. Available: https://energy.ec.europa.eu/publications/guidance-designating-renewables-acceleration-areas_en

[82] Council of European Energy Regulators, "Regulatory Aspects of Self-Consumption and Energy Communities," 2019.

[83] J. Roberts, D. Frieden, J. Research, and Stanislas D'herbemont, "Energy Community Definitions," 2019.

[84] Energie Samen, "Smart energy sharing through energy communities," 2021.

[85] Energy Community Repository and Directorate-General for Energy, "Energy Sharing for Energy Communities - a Reference Guide," 2024. [Online]. Available: https://circabc.europa.eu/ui/group/8f5f9424-a7ef-4dbf-b914-1af1d12ff5d2/library/f221ba07-6103-43ad-bbba-df71c2de2c57/details

[86] Ricerca Sistema Elettrico (RSE), "Gli schemi di Autoconsumo Collettivo e le Comunità dell'Energia," 2020.

[87] German Federal Ministry for Economic Affairs and Climate Action, "Frequently asked questions about landlord-to-tenant electricity." Accessed: Feb. 01, 2024. [Online]. Available: https://www.bmwk.de/Redaktion/EN/FAQ/landlord-to-tenant-electricity/faq-mieterstrom.html

[88] M. Di Somma, M. Dolatabadi, A. Burgio, P. Siano, D. Cimmino, and N. Bianco, "Optimizing virtual energy sharing in renewable energy communities of residential users for incentives maximization," *Sustainable Energy, Grids and Networks*, vol. 39, p. 101492, Sep. 2024, doi: 10.1016/J.SEGAN.2024.101492.

[89] V. Z. Gjorgievski, S. Cundeva, N. Markovska, and G. E. Georghiou, "Virtual net-billing: A fair energy sharing method for collective self-consumption," *Energy*, vol. 254, p. 124246, 2022, doi: 10.1016/j.energy.2022.124246.

[90] M. E. Biresselioglu *et al.*, "Legal Provisions and Market Conditions for Energy Communities in Austria, Germany, Greece, Italy, Spain, and Turkey: A Comparative Assessment," *Sustainability*, vol. 13, no. 20, 2021, doi: 10.3390/su132011212.

[91] M. L. Di Silvestre, M. G. Ippolito, E. R. Sanseverino, G. Sciumè, and A. Vasile, “Energy self-consumers and renewable energy communities in Italy: New actors of the electric power systems,” *Renewable and Sustainable Energy Reviews*, vol. 151, p. 111565, Nov. 2021, doi: 10.1016/J.RSER.2021.111565.

[92] Energy Communities Repository, “France - Overview of the policy framework,” 2023.

[93] R. Dufo-López and J. L. Bernal-Agustín, “A comparative assessment of net metering and net billing policies. Study cases for Spain,” *Energy*, vol. 84, pp. 684–694, 2015, doi: 10.1016/j.energy.2015.03.031.

[94] G. Debizet, M. Pappalardo, and F. Wurtz, *Local Energy Communities Emergence, Places, Organizations, Decision Tools*, 1st Edition. Routledge, 2022.

[95] F. D. Minuto and A. Lanzini, “Energy-sharing mechanisms for energy community members under different asset ownership schemes and user demand profiles,” *Renewable and Sustainable Energy Reviews*, vol. 168, 2022, doi: 10.1016/j.rser.2022.112859.

[96] A. D. Mustika, R. Rigo-Mariani, V. Debusschere, and A. Pachurka, “A two-stage management strategy for the optimal operation and billing in an energy community with collective self-consumption,” *Applied Energy*, vol. 310, p. 118484, Mar. 2022, doi: 10.1016/J.APENERGY.2021.118484.

[97] A. Roy, J. C. Olivier, F. Auger, B. Auvity, S. Bourguet, and E. Schaeffer, “A comparison of energy allocation rules for a collective self-consumption operation in an industrial multi-energy microgrid,” *Journal of Cleaner Production*, vol. 389, no. January, 2023, doi: 10.1016/j.jclepro.2023.136001.

[98] Autorità di Regolazione per Energia Reti e Ambiente (ARERA), “Orientamenti per la regolazione delle partite economiche relative all’energia elettrica oggetto di autoconsumo collettivo o di condivisione nell’ambito di comunità di energia rinnovabile - DCO 112/2020,” 2020.

[99] ARERA, *Deliberazione 4 AGOSTO 2020 318/2020/R/EEL regolamentazione delle partite economiche relative all’energia condivisa da un gruppo di autoconsumatori di enregia rinnovabile che agiscono collettivamente*. 2020.

[100] Gazzetta Ufficiale della Repubblica Italiana, *Decreto Legislativo n°199/2021*. Italy, 2021.

[101] Gestore Servizi Energetici (GSE), *Regole tecniche per l’attuazione delle disposizioni relative all’integrazione di sistemi di accumulo di energia elettrica nel sistema elettrico nazionale*. Rome, 2021.

[102] Gestore Servizi Energetici (GSE), *Decreto CACER e TIAD – Regole operative per l’accesso al servizio per l’autoconsumo diffuso e al contributo PNRR*. Italy, 2024.

[103] French Government, “LAW n ° 2017-227 of February 24, 2017 ratifying the ordinances n ° 2016-1019 of July 27th, 2016 relating to the self-consumption of electricity.”

[104] French Government, “Arrêté du 21 novembre 2019 fixant le critère de proximité géographique de l’autoconsommation collective étendue.”

[105] French Government, “Arrêté du 14 octobre 2020 modifiant l’arrêté du 21 novembre 2019 fixant le critère de proximité géographique de l’autoconsommation collective étendue.”

[106] Commission de Régulation de l’énergie, “Délibération n°2021-13.”

[107] French Government, *Code de l’énergie*. France, 2023.

[108] French Government, “Ordonnance n° 2021-236 du 3 mars 2021 portant transposition de diverses dispositions de la directive (UE) 2018/2001 du Parlement européen et du Conseil du 11 décembre 2018 relative à la promotion de l’utilisation de l’énergie produite à partir de sources,” 2021, *Journal Officiel*.

[109] Spanish Government, *Real Decreto 900/2015, de 9 de octubre, por el que se regulan las condiciones administrativas, técnicas y económicas de las modalidades de suministro de energía eléctrica con autoconsumo y de producción con autoconsumo.* Spain: Boletin Oficial del Estado, 2015.

[110] J. J. Alba Ríos, V. Aragones Ahnert, J. Barquín Gil, and E. Moreda Díaz, “La regulación del autoconsumo en España: ¿un impuesto al Sol?,” *Revista de Obras Públicas: Organo profesional de los ingenieros de caminos, canales y puertos, ISSN 0034-8619, Nº. 3584, 2017, págs. 40-47*, no. 3584, pp. 40–47, 2017, Accessed: Aug. 16, 2024. [Online]. Available: https://dialnet.unirioja.es/servlet/articulo?codigo=5906915&info=resumen&idioma=ENG

[111] D. Dasí-Crespo, C. Roldán-Blay, G. Escrivá-Escrivá, and C. Roldán-Porta, “Evaluation of the Spanish regulation on self-consumption photovoltaic installations. A case study based on a rural municipality in Spain,” *Renewable Energy*, vol. 204, no. December 2022, pp. 788–802, 2023, doi: 10.1016/j.renene.2023.01.055.

[112] J. López Prol and K. W. Steininger, “Photovoltaic self-consumption is now profitable in Spain: Effects of the new regulation on prosumers’ internal rate of return,” *Energy Policy*, vol. 146, 2020, doi: 10.1016/j.enpol.2020.111793.

[113] Spanish Government, *Royal Decree 244/2019 regulating the administrative, technical and economic conditions of the self-consumption of electric energy*. Spain: Boletin Oficial del Estado, 2019.

[114] Spanish Government, *Royal Decree-Law 23/2020 which approves measures in the field of energy and in other areas for economic recovery*. Boletin Oficial del Estado, 2020.

[115] C. Inês, P. L. Guilherme, M. G. Esther, G. Swantje, H. Stephen, and H. Lars, "Regulatory challenges and opportunities for collective renewable energy prosumers in the EU," *Energy Policy*, vol. 138, 2020, doi: 10.1016/j.enpol.2019.111212.

[116] C. Gallego-Castillo, M. Heleno, and M. Victoria, "Self-consumption for energy communities in Spain: A regional analysis under the new legal framework," *Energy Policy*, vol. 150, no. January, p. 112144, 2021, doi: 10.1016/j.enpol.2021.112144.

[117] Spanish Government, *Real Decreto-ley 18/2022, de 18 de octubre, por el que se aprueban medidas de refuerzo de la protección de los consumidores de energía y de contribución a la reducción del consumo de gas natural en aplicación del "Plan + seguridad para tu energía (+SE)."* Spain: Boletin Oficial del Estado, 2022.

[118] Spanish Government, *Real Decreto-ley 20/2022, de 27 de diciembre, de medidas de respuesta a las consecuencias económicas y sociales de la Guerra de Ucrania y de apoyo a la reconstrucción de la isla de La Palma y a otras situaciones de vulnerabilidad.* Spain: Boletin Oficial del Estado, 2022.

[119] A. Ogando-Martínez, X. García-Santiago, S. Díaz García, F. Echevarría Camarero, G. Blázquez Gil, and P. Carrasco Ortega, "Optimization of Energy Allocation Strategies in Spanish Collective Self-Consumption Photovoltaic Systems," *Sustainability (Switzerland)*, vol. 15, no. 12, pp. 1–17, 2023, doi: 10.3390/su15129244.

[120] Á. Manso-Burgos, D. Ribó-Pérez, T. Gómez-Navarro, and M. Alcázar-Ortega, "Local energy communities modelling and optimisation considering storage, demand configuration and sharing strategies: A case study in Valencia (Spain)," *Energy Reports*, vol. 8, pp. 10395–10408, 2022, doi: 10.1016/j.egyr.2022.08.181.

[121] German Federal Government, *Renewable Energy Sources Act (EEG) 2017*. Germany, 2017.

[122] German Federal Government, *Reneable Energy Sources Act (EEG) 2021*. Germany, 2021.

[123] S. Benedettini, C. Stagnaro, and I. B. Leoni, "Energy communities in Europe a review of the Danish and German experiences," in *Energy Communities*, 1st ed., S. Loebbe, F. Sioshansi, and D. Robinson, Eds., Elsevier, 2022, ch. 21.

[124] P. Hälsig, F. Fit, R. Williams, and F. Fit, "Analysis of electricity sharing as modern business models for housing associations Modeling Approach," *ETG Kongress 2023*, 2023.

[125] H. Kazmi, Í. Munné-Collado, F. Mehmood, T. A. Syed, and J. Driesen, “Towards data-driven energy communities: A review of open-source datasets, models and tools,” *Renewable and Sustainable Energy Reviews*, vol. 148, p. 111290, Sep. 2021, doi: 10.1016/j.rser.2021.111290.

[126] M. Tostado-Véliz, A. Rezaee Jordehi, D. Icaza, S. A. Mansouri, and F. Jurado, “Optimal participation of prosumers in energy communities through a novel stochastic-robust day-ahead scheduling model,” *International Journal of Electrical Power and Energy Systems*, vol. 147, May 2023, doi: 10.1016/J.IJEPES.2022.108854.

[127] M. Musolino, G. Maggio, E. D’aleo, and A. Nicita, “Three case studies to explore relevant features of emerging renewable energy communities in Italy,” *Renewable Energy*, vol. 210, pp. 540–555, 2023, doi: 10.1016/j.renene.2023.04.094.

[128] R. Roversi, A. Boeri, S. Pagliula, and G. Turci, “Energy Community in Action—Energy Citizenship Contract as Tool for Climate Neutrality,” *Smart Cities*, vol. 5, no. 1, pp. 294–317, Mar. 2022, doi: 10.3390/smartcities5010018.

[129] Gestore dei Servizi Energetici - GSE, “Mappa Interattiva delle cabine primarie - manuale d’uso.” [Online]. Available: https://www.gse.it/documenti_site/Documenti%20GSE/Servizi%20per%20te/AUTOCONSUMO/Mappa%20interattiva/Manuale%20d%20uso%20della%20mappa%20interattiva%20delle%20cabine%20primarie.pdf

[130] Joint Research Centre, “Photovoltaic Geographical Information System (PVGIS).” Accessed: Sep. 13, 2024. [Online]. Available: https://joint-research-centre.ec.europa.eu/photovoltaic-geographical-information-system-pvgis_en

[131] Eurostat, “Electricity prices for household consumers - bi-annual data (from 2007 onwards).” doi: https://doi.org/10.2908/NRG_PC_204.

[132] S. Lilla, C. Orozco, A. Borghetti, F. Napolitano, and F. Tossani, “Day-Ahead Scheduling of a Local Energy Community: An Alternating Direction Method of Multipliers Approach,” *IEEE Transactions on Power Systems*, vol. 35, no. 2, pp. 1132–1142, 2020, doi: 10.1109/TPWRS.2019.2944541.

[133] C. Orozco, A. Borghetti, F. Napolitano, and F. Tossani, “Multistage day-ahead scheduling of the distributed energy sources in a local energy community,” in *2020 IEEE International Conference on Environment and Electrical Engineering and 2020 IEEE Industrial and Commercial Power Systems Europe, EEEIC / I&CPS Europe 2020*, Madrid, Spain, 2020. doi: 10.1109/EEEIC/ICPSEurope49358.2020.9160579.

[134] C. Orozco, A. Borghetti, B. De Schutter, F. Napolitano, G. Pulazza, and F. Tossani, “Intra-day scheduling of a local energy community coordinated with day-ahead multistage decisions,” *Sustainable Energy, Grids and Networks*, vol. 29, p. 100573, 2022, doi: 10.1016/J.SEGAN.2021.100573.

[135] Y. Zhou, Z. Wei, G. Sun, K. W. Cheung, H. Zang, and S. Chen, “A robust optimization approach for integrated community energy system in energy and ancillary service markets,” *Energy*, vol. 148, pp. 1–15, 2018, doi: 10.1016/j.energy.2018.01.078.

[136] M. J. Rana, F. Zaman, T. Ray, and R. Sarker, “Real-time scheduling of community microgrid,” *Journal of Cleaner Production*, vol. 286, p. 125419, 2021, doi: 10.1016/j.jclepro.2020.125419.

[137] N. Liu, Q. Tang, J. Zhang, W. Fan, and J. Liu, “A hybrid forecasting model with parameter optimization for short-term load forecasting of micro-grids,” *Applied Energy*, vol. 129, pp. 336–345, 2014, doi: https://doi.org/10.1016/j.apenergy.2014.05.023.

[138] H. S. Hippert, C. E. Pedreira, and R. C. Souza, “Neural Networks for Short-Term Load Forecasting: A Review and Evaluation,” *IEEE Transactions on Power Systems*, vol. 16, no. 1, 2001, doi: 10.1109/59.910780.

[139] F. Barroco Fontes Cunha, C. Carani, C. A. Nucci, C. Castro, M. Santana Silva, and E. Andrade Torres, “Transitioning to a low carbon society through energy communities: Lessons learned from Brazil and Italy,” *Energy Research and Social Science*, vol. 75, 2021, doi: 10.1016/j.erss.2021.101994.

[140] F. Cappellaro *et al.*, “Implementing energy transition and SDGs targets throughout energy community schemes,” *Journal of Urban Ecology*, vol. 8, no. 1, 2022, doi: 10.1093/jue/juac023.

[141] E. Commission, J. R. Centre, and L. Lyons, *Digitalisation – Opportunities for heating and cooling*. Publications Office, 2019. doi: doi/10.2760/00116.

[142] P. A. Schirmer and I. Mporas, “Non-Intrusive Load Monitoring: A Review,” *IEEE Transactions on Smart Grid*, vol. 14, no. 1, pp. 769–784, Jan. 2023, doi: 10.1109/TSG.2022.3189598.

[143] European Parliament, *Directive 2014/32/EU of the European Parliament and of the Council of 26 February 2014 on the harmonisation of the laws of the Member States relating to the making available on the market of measuring instruments*. http://data.europa.eu/eli/dir/2014/32/oj, 2014.

[144] E-distribuzione, “Presentazione dei risultati del monitoraggio delle prestazioni di comunicazione PLC tra misuratori 2G e dispositivi di utenza,” 2019.

[145] H. J. El-Khozondar *et al.*, “A smart energy monitoring system using ESP32 microcontroller,” *e-Prime - Advances in Electrical Engineering, Electronics and Energy*, vol. 9, p. 100666, Sep. 2024, doi: 10.1016/J.PRIME.2024.100666.

[146] “Emoncms.” Accessed: Sep. 13, 2024. [Online]. Available: https://emoncms.org/

[147] “ForecastSolar.” [Online]. Available: https://forecast.solar/

[148] “Gestore Mercati Energetici (GME).” [Online]. Available: https://www.mercatoelettrico.org/en/

[149] T. Pontecorvo, “Stability and operation of power systems with a high share of renewable energy sources and storage systems at the transmission and distribution level,” PhD thesis, University of Bologna, 2023.

[150] P. G. McLaren, R. Kuffel, R. Wierckx, J. Giesbrecht, and L. Arendt, “A real time digital simulator for testing relays,” *IEEE Transactions on Power Delivery*, vol. 7, no. 1, pp. 207–213, 1992, doi: 10.1109/61.108909.

[151] Opal-RT Technologies Inc., “RT-LAB User Guide,” 2015, *Canada*.

[152] M. O. Faruque *et al.*, “Real-Time Simulation Technologies for Power Systems Design, Testing, and Analysis,” *IEEE Power and Energy Technology Systems Journal*, 2015, doi: 10.1109/JPETS.2015.2427370.

[153] I. Richardson, M. Thomson, D. Infield, and C. Clifford, “Domestic electricity use: A high-resolution energy demand model,” *Energy and Buildings*, vol. 42, no. 10, pp. 1878–1887, 2010, doi: https://doi.org/10.1016/j.enbuild.2010.05.023.

[154] S. Dash and N. C. Sahoo, “Electric energy disaggregation via non-intrusive load monitoring: A state-of-the-art systematic review,” *Electric Power Systems Research*, vol. 213, p. 108673, Dec. 2022, doi: 10.1016/J.EPSR.2022.108673.

[155] A. Alberini, G. Prettico, C. Shen, and J. Torriti, “Hot weather and residential hourly electricity demand in Italy,” *Energy*, vol. 177, pp. 44–56, Jun. 2019, doi: 10.1016/j.energy.2019.04.051.

[156] Gestore Servizi Energetici, “Gruppi di Autoconsumatori di Energia Rinnovabile che Agiscono Collettivamente e Comunità di Energia Rinnovabile - Modalità di profilazione dei dati di misura e relative modalità di utilizzo ai sensi dell’articolo 9 dell’Allegato A alla Delibera 318/2020/R/eel,” Apr. 2022. [Online]. Available: https://www.gse.it/documenti_site/Documenti%20GSE/Servizi%20per%20te/AUTOCONSUMO/Gruppi%20di%20autoconsumatori%20e%20comunita%20di%20energia%20rinnovabile/Regole%20e%20procedure/Autoconsumatori.pdf

[157] Gestore Servizi Energetici, “Modalità di profilazione dei dati di misura profili standard GSE 2023 in prelievo e immissione,” 2023. [Online]. Available: https://www.gse.it/documenti_site/Documenti%20GSE/Servizi%20per%20te/AUTOCONSUMO/Gruppi%20di%20autoconsumatori%20e%20comunita%20di%20energia%20rinnovabile/Regole%20e%20procedure/profili%20GSE_prelievo%20e%20immissione_2023.zip

[158] Gestore Servizi Energetici, “Modalità di profilazione dei dati di misura profili standard GSE 2024 in prelievo e immissione,” 2024. [Online]. Available: Modalità di profilazione dei dati di misura profili standard GSE 2024 in prelievo e immissione

[159] “nPro - District Energy Planning Tool.” Accessed: Jun. 21, 2024. [Online]. Available: https://www.npro.energy

[160] U. B. Tayab, A. Zia, F. Yang, J. Lu, and M. Kashif, “Short-term load forecasting for microgrid energy management system using hybrid HHO-FNN model with best-basis stationary wavelet packet transform,” *Energy*, vol. 203, p. 117857, 2020, doi: https://doi.org/10.1016/j.energy.2020.117857.

[161] S. Haben, S. Arora, G. Giasemidis, M. Voss, and D. Vukadinović Greetham, “Review of low voltage load forecasting: Methods, applications, and recommendations,” *Applied Energy*, vol. 304, p. 117798, 2021, doi: https://doi.org/10.1016/j.apenergy.2021.117798.

[162] S. Wang, X. Wang, S. Wang, and D. Wang, “Bi-directional long short-term memory method based on attention mechanism and rolling update for short-term load forecasting,” *International Journal of Electrical Power & Energy Systems*, vol. 109, pp. 470–479, 2019, doi: https://doi.org/10.1016/j.ijepes.2019.02.022.

[163] J. C. Lopez, M. J. Rider, and Q. Wu, “Parsimonious Short-Term Load Forecasting for Optimal Operation Planning of Electrical Distribution Systems,” *IEEE Transactions on Power Systems*, vol. 34, no. 2, pp. 1427–1437, 2019, doi: 10.1109/TPWRS.2018.2872388.

[164] H. Musbah and M. El-Hawary, “SARIMA Model Forecasting of Short-Term Electrical Load Data Augmented by Fast Fourier Transform Seasonality Detection,” *2019 IEEE Canadian Conference of Electrical and Computer Engineering, CCECE 2019*, pp. 1–4, 2019, doi: 10.1109/CCECE.2019.8861542.

[165] R. Weron, *Modeling and Forecasting Electricity Loads and Prices*. 2006.

[166] H. Musbah and M. El-Hawary, “SARIMA Model Forecasting of Short-Term Electrical Load Data Augmented by Fast Fourier Transform Seasonality Detection,” in *2019 IEEE Canadian Conference of Electrical and Computer Engineering (CCECE)*, IEEE, May 2019, pp. 1–4. doi: 10.1109/CCECE.2019.8861542.

[167] V. Kotu and B. Deshpande, “Time Series Forecasting,” *Data Science*, pp. 395–445, Jan. 2019, doi: 10.1016/B978-0-12-814761-0.00012-5.

[168] G. Box, G. Reinsel, and G. Jenkins, *Time Series Analysis : Forecasting and Control, Fourth Edition*. John Wiley & Sons, 2008.

[169] A. Prevedi *et al.*, “Optimal Operation of Renewable Energy Communities Through Battery Energy Systems: A Field Data-Driven Real-Time Simulation Study,” in *2023 International Conference on Smart Energy Systems and Technologies (SEST)*, 2023, pp. 1–6. doi: 10.1109/SEST57387.2023.10257402.

[170] Comitato Elettrotecnico Italiano - CEI, *Reference technical rules for the connection of active and passive users to the LV electrical Utilities*. Italy, 2019.

[171] B. Heymann, J. F. Bonnans, P. Martinon, F. J. Silva, F. Lanas, and G. Jiménez-Estévez, "Continuous optimal control approaches to microgrid energy management," *Energy Systems*, vol. 9, no. 1, pp. 59–77, Feb. 2018, doi: 10.1007/S12667-016-0228-2/TABLES/3.

[172] H. C. Gao, J. H. Choi, S. Y. Yun, H. J. Lee, and S. J. Ahn, "Optimal scheduling and real-time control schemes of battery energy storage system for microgrids considering contract demand and forecast uncertainty," *Energies*, vol. 11, no. 6, Jun. 2018, doi: 10.3390/en11061371.

[173] Gestore Servizi Energetici, "Regole tecniche per l'attuazione delle disposizioni relative all'integrazione di sistemi di accumulo di energia elettrica nel sistema elettrico nazionale," 2021.

[174] G. P. McCormick, "Computability of Global Solutions To Factorable Nonconvex Solutions: Part I: Convex Underestimating Problems," *Mathematical Programming*, vol. 10, pp. 147–175, 1976.

[175] M. L. Bergamini, P. Aguirre, and I. Grossmann, "Logic-based outer approximation for globally optimal synthesis of process networks," *Computers and Chemical Engineering*, vol. 29, no. 9, pp. 1914–1933, 2005, doi: 10.1016/j.compchemeng.2005.04.003.

[176] S. S. Reddy, V. Sandeep, and C. M. Jung, "Review of stochastic optimization methods for smart grid," *Frontiers in Energy*, vol. 11, no. 2, pp. 197–209, Jun. 2017, doi: 10.1007/S11708-017-0457-7/METRICS.

[177] A. Bhattacharya, J. P. Kharoufeh, and B. Zeng, "Managing energy storage in microgrids: A multistage stochastic programming approach," *IEEE Transactions on Smart Grid*, vol. 9, no. 1, pp. 483–496, Jan. 2018, doi: 10.1109/TSG.2016.2618621.

[178] S. Wang, H. Gangammanavar, S. D. Eksioglu, and S. J. Mason, "Stochastic Optimization for Energy Management in Power Systems with Multiple Microgrids," *IEEE Transactions on Smart Grid*, vol. 10, no. 1, pp. 1068–1079, Jan. 2019, doi: 10.1109/TSG.2017.2759159.

[179] P. Samui, D. T. Bui, S. Chakraborty, and R. C. Deo, Eds., *Handbook of Probabilistic Models*. Elsevier, 2020. doi: 10.1016/C2017-0-04723-7.

[180] H. Heitsch and W. Römisch, "Scenario tree modeling for multistage stochastic programs," *Mathematical Programming*, vol. 118, no. 2, pp. 371–406, May 2009, doi: 10.1007/S10107-007-0197-2/METRICS.

[181] J. A. Hartigan and M. A. Wong, "Algorithm AS 136: A K-Means Clustering Algorithm," *Applied Statistics*, vol. 28, no. 1, p. 100, 1979, doi: 10.2307/2346830.

[182] A. P. Prudnikov, Yu. A. Brychkov, and O. I. Marichev, *Integrals and Series*. Routledge, 1992. doi: 10.1201/9780203750643.

[183] P. A. Ioannou and J. Sun, *Robust Adaptive Control*. Prentice Hall, 1995.

[184] S. Aranovskiy, A. Bobtsov, R. Ortega, and A. Pyrkin, “Performance Enhancement of Parameter Estimators via Dynamic Regressor Extension and Mixing,” *IEEE Transactions on Automatic Control*, vol. 62, no. 7, pp. 3546–3550, 2017, doi: 10.1109/TAC.2016.2614889.